Development of Low Cytotoxic and High Efficient Disulfide-based Polyethylenimine Non-viral Vectors for In-vitro Gene Transfection

by

DENG, Rui

A Thesis Submitted in Partial Fulfilment

of the Requirement for the Degree of

Doctor of Philosophy

in

Chemistry

The Chinese University of Hong Kong

June 2010

DOCTOR OF PHILOSOPHY (June 2010) The Chinese University of Hong Kong
(Chemistry)

TITLE: Development of Low Cytotoxic and High Efficient Disulfide-based Polyethylenimine Non-viral Vectors for In-vitro Gene Transfection

AUTHOR: Deng Rui

SUPERVISOR: Prof. Chi Wu

NO. OF PAGES: xiii, 113

Thesis Committee:

Prof. Steve C.F. Au-Yeung (Chairman)

Prof. Chi Wu (Supervisor)

Prof. Jimmy C. Yu

Prof. Marie C.M. Lin (External examiner)

Prof. Leaf Huang (Additional external examiner)

摘　要

分子生物學和基因組學的迅速發展，使得基因治療成爲可能。然而，缺乏有效基因載體是目前這項技術取得進一步發展的最大的瓶頸。聚乙烯亞胺（PEI）因其具有良好的 DNA 複合和 pH 緩衝能力，而被認爲是目前最有效的聚陽離子型非病毒載體。虽然 PEI 及其衍生物被廣泛應用在體內和體外的基因轉染實驗中，但由于缺乏對細胞內轉染機制的深入瞭解而限制了其進一步的发展和應用。到目前爲止，其較高的細胞毒性和仍顯不足的基因轉染效率使我们仍需對其做進一步的修飾和改性。已知短鏈 PEI 毒性較低，但長鏈 PEI 有更高的基因轉染效率。因此，本論文將短鏈 PEI 以二硫鍵擴鏈以增加轉染效率，同時利用其可在還原性細胞質環境中被降解的性質來降低細胞毒性。

我們首先用激光光散射（LLS）原位監控低分子量的 PEI（$M_w = 2\times10^3$ g/mol）與 dithiobis(succinimidyl propionate) (DSP)的交聯反應。通過調整加入交聯劑 DSP 的量及速度來控制交聯 PEI 鏈的長度和交聯度。通過比較兩種通過交聯得到的 PEI 樣品（PEI-7K-L, $M_w = 6.5\times10^3$ g/mol 和 PEI-400K-L, $M_w = 3.8\times10^5$ g/mol），我們發現轉染效率和細胞毒性與交聯 PEI 鏈的鏈長和結構均有關係。具有較伸展構象的 PEI-7K-L 胞毒性較低，并且基因轉染效率是常用轉染試劑 PEI25K（PEI, $M_w = 2.5\times10^4$ g/mol）的 2-10 倍以及另一種商業化試劑 Lipofectamine 2000®的 10-30 倍。相反，具有微凝膠構象的 PEI-400K-L（$M_w = 3.8\times10^5$ g/mol）雖然沒有細胞毒性，但也不具備轉染效率。我們的結果表明，在交聯反應中控制鏈長與鏈結構均對提高轉染效率至關重要。

此外，我們將聚乙二醇（PEG, $M_w = 2\times10^3$ g/mol）分別通過可還原降解的二硫鍵-S-S-和不可降解的碳碳鍵-C-C-接枝到 PEI25K，得到兩種嵌段共聚物。通過與未改性的 PEI 比較證明在生理鹽溶液環境中，由于親水 PEG 殼層的保护作用，共聚物可與質粒 DNA 形成更穩定的複合物，然而同時也導致細胞對此複合物的內吞有所減少。但血清對 PEG 保護的複合物的不良影響也同時降低。PEG-SS-PEI 顯示出比 PEG-CC-PEI 高出 2-8 倍的基因轉染效率。通過肝磷脂置換實驗表明，二硫鍵的降解導致 PEG 鏈從複合物上脫去使被包載的 DNA 分子

在胞內更容易釋放，從而提高了 PEG-SS-PEI 的基因轉染效率。因此，二硫鍵的引入可降低毒性幷提高轉染效率，而且是一個解決接枝 PEG 後所帶來副作用的很好的方案。

最後我們用光散射、凝膠電泳以及 zeta 電位儀研究了不同 PEI 分子與 DNA 的複合過程，發現 PEI 與 DNA 的複合过程在氮磷比爲 3 的時候已基本完成，而一般情況下氮磷比爲 10 時複合物具有最高轉染效率。當更多的 PEI 分子加入到複合物溶液中，幷不顯著改變複合物的物理性質。由此，我們認爲 PEI 除與 DNA 複合提供壓縮保護的功能外，在溶液中游離的 PEI 分子亦對提高基因轉染效率有至關重要的作用。雖然具體的增進機理有待進一步的研究，但我們的結論爲設計和合成更好的非病毒載體提供了新的思路。

ABSTRACT

Due to recent advances in molecular biology and genomic research, numerous diseases have been given their genetic identities for which gene therapy may be a possible prescription. Gradually, the development of viral and non-viral vectors to translocate genes has become a bottleneck. For non-viral vectors, polyethylenimine (PEI) is considered as a potential vector candidate for gene delivery because of its ability to compact DNA and its intrinsic pH buffering capacity. PEI and its derivates have been widely tested in both *in-vitro* and *in-vivo* gene transfection experiments. The progress is limited due to the lack of a better understanding of the intracellular mechanism. So far, their cytotoxicity is relatively high and gene transfection efficiency is low. This study was designed to modify PEI and optimize its cytotoxicity and gene transfection efficiency.

It has been known that short PEI chains are less toxic, but long chains are more effective in gene transfection. Therefore, we decide to use the disulfide bond (-S-S-) to extend short PEI chains to increase efficiency and also utilize the reductive cytosol environment to cleave such extended PEI chains to reduce their cytotoxicity inside the cell. Laser light scattering (LLS) was used to in-situ monitor the linking reaction between short PEI chains (M_w = 2000 g/mol) and dithiobis(succinimidyl propionate) (DSP). The molar mass and crosslinking degree of the extended PEI chains was controlled by either the amounts or the adding rate of DSP. A comparative study of two linked PEI samples (PEI-7K-L and PEI-400K-L, respectively with $M_w = 6.5 \times 10^3$ and 3.8×10^5 g/mol) reveals that cytotoxicity and gene transfection efficiency of such extended PEI chains are related to the chain length and structure. Namely, PEI-7K-L with an extended chain structure is less cytotoxic and 2-10 times more effective in the gene transfection than the "golden standard" (PEI25K) and the widely used commercial vector, Lipofectamine 2000®. Comparatively, PEI-400K-L with a spherical microgel structure is ineffective in spite of its non-toxicity. Our

study clearly demonstrates that a proper control of the chain length and structure is important.

Further, we grafted PEI with polyethylene glycol (PEG), respectively via a reductive disulfide -S-S- and a non-degradable -C-C- bond to form two copolymer vectors. A comparative study shows that the polyplexes formed between the two copolymers and DNA are more stable than that formed between unmodified PEI and DNA under the physiological condition, presumably because the grated PEG chains form a protective hydrophilic shell on the PEI/DNA polyplexes. However, PEGylation reduces the internalization of the copolymer/DNA polyplexes in *in-vitro* experiments. For the two copolymer vectors, PEG-SS-PEI is 2-8 times more effective than its counterpart (PEG-CC-PEI) in the gene transfection, presumably due to the cleavage of the grafted PEG chains inside the reductive cytosol, which promotes the release and translocation of DNA. Our results demonstrate that using the disulfide as a linker is a promising approach to overcome the PEGylation dilemma in the development of low cytotoxic and high efficient non-viral polymeric vectors.

During the complexes formation, both LLS and zeta-potential were used to follow the process. The results showed that most of anionic DNA are complexed by cationic PEI-based polymers when the molar ratio of nitrogen from PEI to phosphate from DNA (N:P) reaches ~3, but the gene transfection reaches the highest efficiency when N:P ~10. When N:P > 3, there exist two population of PEI chains in the solution mixture: bound to DNA and free in the solution. The bound PEI chains condense and protect DNA. Our current study confirms that it is those free PEI chains that play a vital role in promoting the gene transfection. Our preliminary data shows that the promotion mainly occurs in the intracellular space. The detailed mechanism is still lacking at this moment. Nevertheless, our finding leads to a totally different way in the development of non-viral vectors.

Table of Contents

Acknowledgement

First of all, I would like to express my deep and sincere gratitude to my supervisor, Prof. Wu Chi, for his insightful guidance and encouragement during the entire period of my study at CUHK. I joined the *Polymer & Colloid Laboratory* in 2006 and during the last four years in this group, I always feel warm and gratefulness since he has spent much time to give me his excellent guidance and considerations. Not only I have learned a lot from him, but also been inspired by his dedicatory attitude to the scientific research. I believe the strict trainings, precious experiences and especially the attitude to work I gained from him should be great helpful in my whole life.

I am also very grateful to Prof. Ngai To for his kind encouragement and invaluable advices. My sincere thanks are also given to my dear group members in *Polymer & Colloid Laboratory*, their friendship and assistance during the last four years left me many happy and unforgettable memories. They are Dr. Chen Gaojian, Dr. He Ning, Dr. Hong Liangzhi, Dr. Huo Hong, Dr. Jin Fan, Dr. Li Junfang, Dr. Li Wei, Dr. Luo Shizhong, Dr. Ye Xiaodong, Ms. Cai Jinge, Ms. Dai Zhuojun, Ms. Diao Shu, Ms. Ge Hui, Ms. Gong Xiangjun, Ms. Yue Yanan, Mr. Chen Qianjin, Mr. Ma Yongzheng, Mr. Wang weimao, Mr. Zhao Hong.

Thanks are also given to those visiting Professors and scholars, Prof. Zhang Mei, Prof. Lu Zaijun and Dr. So Ying H. for their kind help and fruitful discussions.

My sincerely thanks are also extended to all the staff members in the Department of Chemistry, CUHK for the active academic atmosphere and the service they offered. The financial support of the Hong Kong Special Administration Region Earmarked Grants and the Special Funds for Major State Basic Research Projects are also gratefully acknowledged.

Last but not the least, I am forever indebted to my parents and my wife Hu Chu for their endless love and strong moral support during my pursuit of a higher degree. I owe them a lot.

DENG Rui

Hong Kong, April, 2010

Chapter 1

Introduction and Background

1.1 Gene Therapy — Car rier Is the Bottleneck

Gene therapy can be defined as treatment of human diseases by the transfer of exogenous, therapeutic genes into specific cells of the patient (*1*). Due to the recent advances in molecular biology and genomic research, numerous diseases (e.g., sickle cell anemia, HIV, Parkinson's disease, Huntington's disease, Alzheimer's disease) have been given a genetic identity for which gene therapy may be a possible prescription (*2-5*). The strategy include replacing the errant gene in genetic disease, augmenting naturally occurring proteins, altering the expression of existing genes, and producing cytotoxic proteins or prodrug-activating enzymes.

For a perfect gene therapy treatment, the target gene should be specifically delivered to the targeting cells with high transfection efficiency and low toxicity, which means that the gene carrier is of vital importance to fulfill such an exciting goal. However, there still remains a long way to go due to the challenges in finding or designing an ideal gene vector (*6*).

Recombinant viruses were the first delivery agent employed as the gene carrier because of their ability inbred (*7*). The viruses, including retrovirus, adenovirus, adeno-associated virus, herpes simplex virus, pox virus and lentivirus (for example, HIV) (*8*), can either be genetically rendered to be replication defective or gutted of their genetic material and replaced with therapeutic genes. The virus vectors gradually evolved as sophisticated gene delivery vehicles because of their high gene transfection efficiency. They have been used in the majority of gene delivery studies reported in the literature and 66% of ongoing clinical trials (Figure 1.1) (*9*). Because of some early promising results since the first clinical trial in 1990, virus vectors were regarded as the most hopeful carriers to achieve the goal of successful gene therapy (*10*). However, early before the first clinical trial, some people warned that

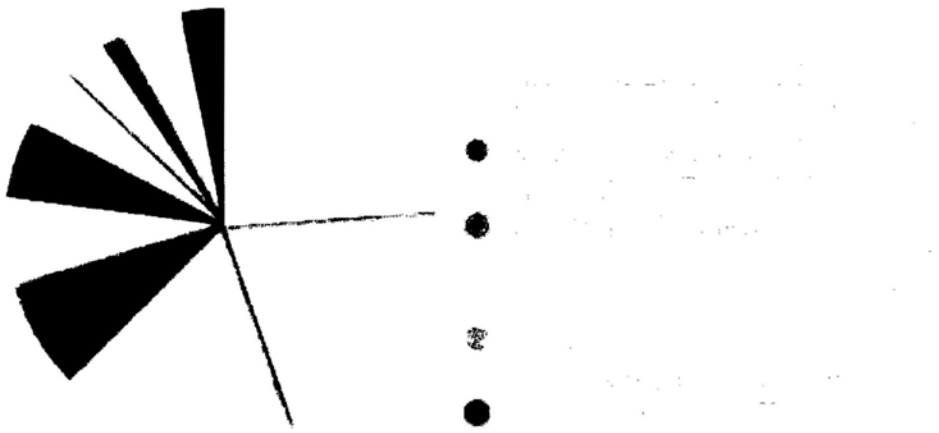

Figure 1.1. Pie chart of vectors used in gene therapy clinical trials. (9)

viral vectors could induce cancer via insertional mutagenesis, namely, random transgenic may insert into the host chromosome disrupting the normal expression of a critical gene that ordinarily regulates cell growth and division. Unfortunately, this prediction partially came true when three clinical trial participants developed leukemia-like complications post retroviral-based gene therapy (*11, 12*). Furthermore, the viral vectors themselves are inherently immunogenic, leading to difficulty with repeat administrations and the possibility of dangerous immune reactions. The immunogenic response caused by virus vector, in at least one reported incident, has led to a fatal outcome (*13*). Other problems with viral gene delivery include limitations in target-cell specificity and the costs of manufacturing.

As a result, people are motivated to seek for safer, less pathogenic and immunogenic gene delivery alternatives based on non-viral materials. The candidates include lipid-based vectors (*14*), chemically modified viruses (*15*), inorganic materials (*16, 17*), and cationic polymer-based gene delivery systems (*6, 18-20*), where the last one offer greater structural and chemical versatility for manipulating physicochemical properties, vector stability upon storage and reconstitution, and a

larger gene capacity compared to their viral counterparts.

The basic principle for the polymer utilized as a gene carrier is that the cationic polymer backbone or pendant can electrostatically interact with anionic nucleic acid, and condense the micrometer-sized nucleic acid into a particle with the diameter of tens to hundreds nanometer. This complexation process is entropically driven due to the release of counter-ions (*21*). Such obtained particles, also called polyplexes, are positive in the surface charge, which is beneficial for the approach to the negatively-charged cell membrane and internalization. Furthermore, the steric shielding provided by the polymers can protect the nucleic acid from both extracellular and intracellular nuclease degradation (*22*).

Although polymeric vectors exhibit great potential in gene therapy, their relatively poor efficiency, due to the difficulties in overcome some of the extra- and intra-cellular barriers, has limited their successful application in clinical trials, while virus vectors have sophisticatedly evolved functions to overcoming most of extra- and intra-cellular barriers to achieve satisfactory gene delivery efficiency. Therefore, consideration of the barriers in gene delivery is necessary to understand the limitations of non-viral vectors and important for the rational design of more effective vectors.

1.2 Extracellular and Intracellular Barriers

1.2.1 Nucleic Acid Packaging

The primary function for a gene delivery carrier is to envelope the target gene and protects it from the nuclease degradation. The naked nucleic acid will be degraded quickly in the presence of nuclease, whereas plasmid DNA in polyplexes can be stable for hours (*23*). Generally, the negatively-charged nucleic acids are believed to be condensed and surrounded by the polycationic polymers, which results in the positively-charged surface of the polyplexes. Although some efforts have been made in order to understand the kinetics of polyplexes formation and the final structure (*21,*

24-27), the exact process and structure of the final polyplexes is still misty. Further detailed experimental and theoretical studies on the formation of the complexes are needed in order to better understand the structure-function relationship between the polyplexes and gene transfection efficiency.

Molecular weight and structure of the polycations, in other words, the charge number, distribution and charge density have significant effect on the condensation and protection ability of nucleic acid (*28-31*). However, better nucleic acid binding affinity does not directly correlate to higher gene transfection efficiency, probably because that tight binding leads to difficulties in nucleic acid release once the polyplexes arrive at the site of action and higher charge density always accompany with the higher cytotoxicity (*32*).

1.2.2 Salt and Serum Stability

The polyplexes are stable in salt-free or low salt concentration condition because of the electrostatic repulsion. However, the polyplexes are readily to aggregate under the physiological condition (*33*), because the like-charge repulsion is screened by the salt ions and cannot balance the Van der Waals attraction. The large polyplexes aggregates are generally ineffective and can even be toxic due to embolization of the aggregates in the lung (*19*). Furthermore, the positively-charged polyplexes can be opsonized with plasma proteins such as immunoglobulin M, complement C3 and proteins of the coagulation cascade (*34*), leading to their rapid clearance by phagocytic cells of MPS in the liver, spleen, lungs, and bone marrow (*35*). The clearance rate of these particles from the circulatory system depends on their surface physicochemical characteristics. In order to gain undetectable ability against macrophages, also called the 'stealthy' ability, vectors have to be as small and neutral as possible (*36, 37*).

1.2.3 Specific Cell Targeting

Unmodified polycation/nucleic acid polyplexes usually interact with membrane-bound negatively-charged proteoglycans to facilitate cellular internalization (*38*). The proteoglycans are believed to play a central role in the endocytosis of non-targeted positively-charged polyplexes, while their exact mechanism is still unclear. However, such an interaction results in indiscriminate uptake and undesirable gene expression by unanticipated cell types. In most case, gene delivery to a very specific site is of great importance for an efficient transfection, sometimes is even of safety concern. Although "naked" polyplexes do not possess such a specific selectivity to cell types, active polymer groups on the polyplexes provide possibility for chemical modification to gain such ability by conjugating cell specific targeting ligands. The targeting ligands can be divided into four main categories, namely, endogenous ligands, carbohydrates, antibodies and cell penetrating peptides (*6*). These ligands can interact with membrane-bond receptors to accomplish cell selectivity and internalized by cell via receptor-mediate endocytosis. However, the ligand selection should be carefully considered to optimize the gene delivery efficiency, since the appropriate targeting ligand can be influenced by a myriad of factors; for example, different ligands will lead to totally different endocytic pathways.

1.2.4 Endocytic Pathway and Transport through Cytoplasm

Endocytosis refers to the cellular uptake of macromolecules and solutes into membrane-bound vesicles derived by invagination and pinching from the plasma membrane (*39*). The clathrin-mediated endocytosis (CME) was the first discovered and best characterized pathway since it was observed by electronic microscopy in 1960's, and has been regarded as the exclusive uptake pathway of exogenous biomacromolecules for a long time (*40*). Till now, other three morphologically distinct endocytic pathways have been discovered and characterized: caveolae-mediated pathway, macropinocytosis, and phagocytosis (Figure 1.2) (*40*).

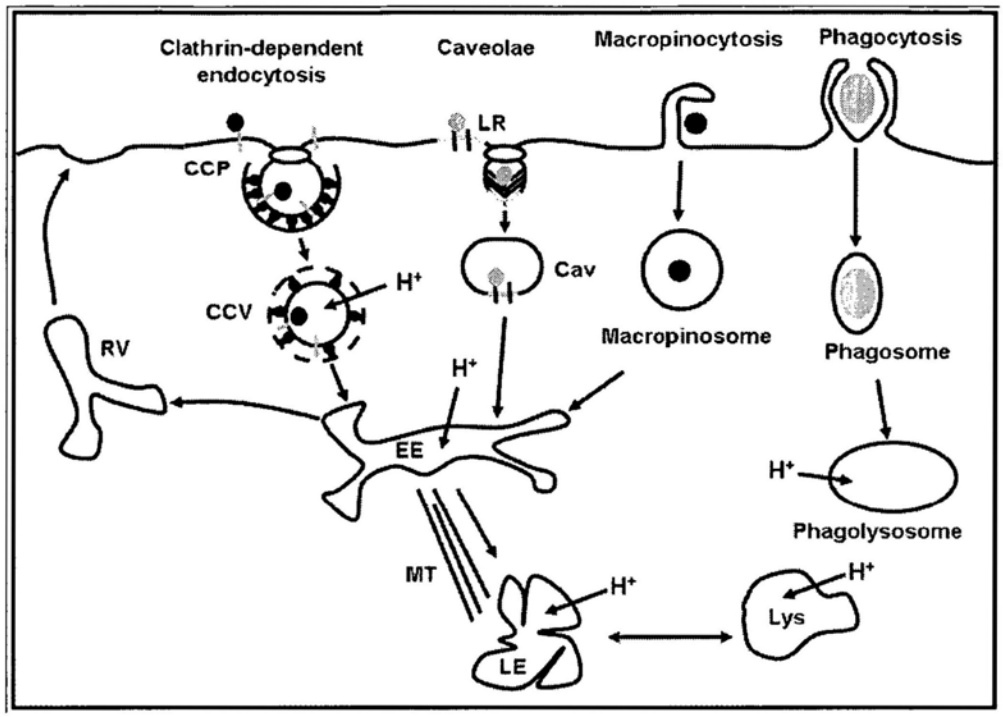

Figure 1.2. Scheme of the endocytosis pathways. CCP: clathrin-coated pit; CCV: clathrin-coated vesicle; EE: early/sorting endosome; LE: late endosome; Lys: lysosome; Cav: caveosome; LR: lipid raft; RV: recycling vesicle; MT: microtubules (40).

These four pathways differ in the coating composition, size of the detached vesicles and fate of the internalized particles.

1.2.4.1 Clathrin-Mediated Endocytosis

CME occurs in all mammalian cells and carries out the continuous uptake of essential nutrients, antigens, growth factors, and pathogens (*41*). For the polyplexes, CME can be triggered by using certain ligands, such as transferring and low-density lipoprotein (LDL) (*42, 43*), which can specifically recognize their receptors protein on the cell membrane domains called clathrin-coated pits (CCPs) (*41*). The CCPs are invaginated and then pinched off from the plasma membrane by dynamin to form intracellular clathrin-coated vesicles (CCVs) ranging in size from 100 to 150 nm in diameter. The CCVs fuse with each other to form early endosomes with pH drop from 7.4 to 6.0. Then early endosomes are transported through microtubules to late

endosomes and further fuse with more acidic lysosomes (pH ~ 4.5-5), which contain degradative enzymes ready to digest exogenous materials (*44*). CME has been regarded as the most kinetically effective mechanism for endocytosis, because it is an energy-dependent process (*41, 45*).

1.2.4.2 Caveolae-Mediated Endocytosis

Membrane microdomains rich in hydrophobic cholesterol and sphingolipids, termed lipid rafts, characterize the caveolae system (*46*). Caveolae are small flask-shaped invaginations vesicles (ca. 50 nm in diameter) on the plasma membrane. The caveolae-mediated endocytosis has been mainly elucidated by visualizing the infectious pathway of the SV40 virus (*47*). The SV40 virus is found to leave the plasma membrane in small, caveolin-1-containing vesicles and enters large peripheral organelles without acidification of their lumen. After several hours, the virus is contained into tubular caveolin-free membrane vesicles and moves rapidly along the microtubules to smooth endoplasmic reticulum. Compared to CME, the endocytosis via caveolae avoid the acidification of the endocytic vehicles (caveosomes) and degradation by lysosome (*47, 48*). Therefore, this pathway seems to be advantageous in terms of non-viral gene delivery and has been paid more and more attention gradually in recent years.

Joanna et al. (*49*) and Gabrielson et al. (*50*) investigated the endocytosis pathway of the polyplexes formed by PEI/pDNA recently. They demonstrated that the polyplexes are internalized by cell via both clathrin- and caveolae-mediated endocytosis, but only caveolae-mediated internalized polyplexes showed efficient gene transfection. Joanna et al. (*51*) also found that the pathway is particle-size dependent. Namely, internalization of microspheres with a diameter <200 nm involved clathrin-coated pits. And with increasing size, a shift to the mechanism that relied on caveolae-mediated internalization became apparent, which became the predominant pathway of entry for particles of 500 nm in size.

However, caveolae-mediated process is slow and the vehicles are small in size with low fluid phase volume. It is also greatly dependent on the cell type. So, it is unlikely that they contribute significantly to constitutive endocytosis in most cases, except for the endothelial cells in which caveolae constitute 10 to 20% of the cell surface (*52*). Meanwile, the exact mechanism and fate of caveosome are less understood than the CME counterparts. Nevertheless, caveolae-mediated endocytosis is still a promising strategy for gene delivery especially if the internalization can be increased, possibly through the use of specific and highly efficient receptors for caveolae.

1.2.4.3 Macropinocytosis

In most cells, stimulation by growth factor triggers ruffling and protrusion of the cell membrane (Figure 1.2). The actin-driven protrusions collapse onto and fuse with the cell membrane to generate large (up to 5 μm) endocytic vesicles, called macropinosomes, with irregular size and shape (*53*). The intracellular fate of the macropinosomes differs depending on the cell type. Due to their large size, macropinosomes contain large volumes of extracellular medium and is regarded as an efficient vehicle for the nonselective endocytosis of macromolecules solute (*52*).

1.2.4.4 Phagocytosis

Phagocytosis in mammalian cells is conducted primarily by specialized cells, including macrophages, monocytes, and neutrophiles, that functions to clear large (>0.5 μm) pathogens such as bacteria, yeast or large debris such as dead cells and arterial fat deposits (*54*). Large particles internalization is initiated by specific receptors on the phagocyte and ligands on the surface of the particles. This triggers actin assembly and formation of cell surface extensions that zip around the particle to engulf them. After that, actin is shed from phagosomes, which then mature by a series of fusion and fission events involving the components of the endocytic

pathway, resulting in the formation of mature phagolysosomes where internalized particles are degraded (*54*). Phagosomes trafficking occurs primarily in association with microtubules, and its maturation requires a coordinated interaction between actin-based and tubulin-based cytoskeletons (*52*). Because of its limitation in cell type, phagocytosis is not considered to be an efficient pathway in gene delivery (*39*).

1.2.5 Endo/lysosome Escape

As mentioned above, in most cases, endosomes from CME pathway ultimately fuse with lysosomes or recycle back to the cell surface. In order to avoid degradation or exocytosis, nucleic acid should escape from the endo/lysosome quickly. Several strategies have been used to overcome this barrier. Cationic lipid/nucleic acid complexes (lipoplexes) can triggers endosome release via the ion-pair mechanism, which has been proposed by Szoka *et al.* (*55*). After endocytosis, cationic lipids form ion pairs with the anionic lipids in the endosome membrane and thus destabilize the endosomal membrane by excluding the surface bound water. They also report that some cationic lipid containing pH-sensitive fusiogenic lipid DOPE can release the associated nucleic acid int o cytosol (*55*). DOPE forms a stable lipid bilayer at physiological pH, however, at lower pH value, it undergoes a transition from bilayer to an inverted hexagonal structure, whic h fuses and destabilizes the endosomal membrane resulting the release of its contents to the cytosol.

Unlike the structure transformation caused by fusiogenic lipid, some small molecules known as the lysosomotropic reagent (*56*) promote the endo/lysosome release through a different mechanism. As the name suggests, lysosomotropic reagents are taken up selectively into lysosomes. They may either inhibit the acidification of the lysosome because of its basic nature such as chloroquine (*57*), or cause the swelling and rupture of the lysosome by non-digestible sugar, such as sucrose (*58*). The addition of lysosomotropic reagent to the transfection medium usually favors transfection, such as in the PLL/DNA transfection system (*59*), but

their different pharmacokinetics with the polyplexes hinder the application in the *in vivo* application.

However, in some other polymeric delivery systems, the addition of lysosomotropic reagent or fusiogenic lipid does not improve their transgene

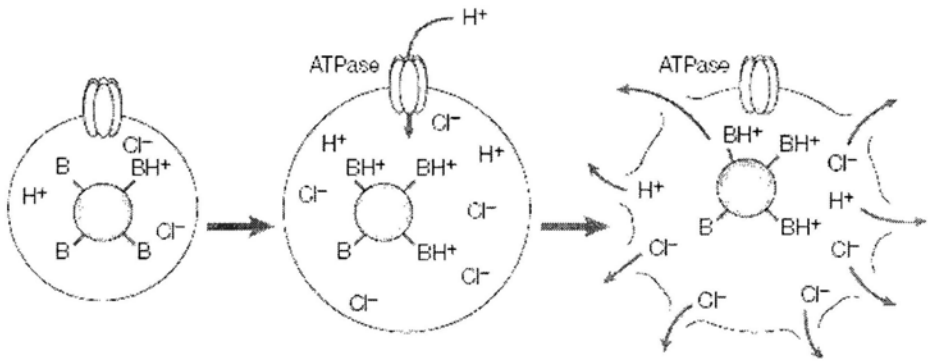

Figure 1.3 Schematic of the proton-sponge mechanism. Protonation of the proton-sponge polymer causes increased influx of protons (and counter-ions) into endocytic vesicles. Increasing osmotic pressure causes the vesicle to swell and rupture. (18)

efficiency (*60*). These polymer, such as poly(ethylene imine) (PEI) and polyamidoamine (PAMAM) dendrimers, known as "proton sponge" polymer, are believed to possess the intrinsic ability to escape from endo/lysosome (*61*). These polymers contain a large number of secondary and tertiary amines, exhibit buffer capacity during the influx of the actively transported protons by ATPase, thus prevent the acidification of endocytic vesicles and cause the accumulation of the Cl^- counter ions. The increased ion concentration ultimately causes osmotic swelling and rupture of the endo/lysosome membrane, which releases the polyplexes into the cytosol. This unique mechanism is believed to be the reason of the high gene transfection efficiency of these polymers.

1.2.6 Transport through Cytoplasm

Endocytic vehicles can be actively transported toward the nucleus through the microtubules in the cytoplasm (*62*). However, after the escape from these vehicles, the diffusion of the polyplexes or the naked nucleic acids seems extremely difficult

due to their large size and high viscosity of the cytosol (*63*). Although Suh, J. et al. demonstrated that the polyplexes can be actively transported by the microtubules through nonspecific interaction with the motor proteins (*64*), the detailed mechanisms of polyplexes transport in cytosol need to be better characterized in order to complete the whole trafficking route.

1.2.7 Nuclear Entry

How the polyplexes enter cell nucleus remains to be the most poorly understood step in the whole intracellular trafficking chain, although in cases of siRNA delivery this step could be neglected since the interference mechanism arises in the cytoplasm. Nucleus is protected by a bi-layer membrane to isolate it from other organelles and cytosol. The nuclear pore complexes (NPC) with a passive transport limit of 70 kDa molecular mass or ~10 nm diameter (~30 nm under the inclusion of a nuclear localization signal/sequence) on the nucleus envelope regulate the substance import and export from the nucleus (*65*). Obviously, the NPC are much smaller than DNA even when condensed in lipoplexes or polyplexes. Therefore, the most widely accepted mechanism for nuclear import is cell division. During mitosis, the integrity of the nuclear membrane is temporarily impaired, which allows the nuclear entry of targeting genes. However, in most *in vivo* transfection, non-dividing ("postmitotic") cells are always the destination. In this case, some gene transfection are still successful, suggesting other different mechanism for nuclear entry.

Naked nucleic acids combined with short cationic peptide sequences, known as nuclear localization signals (NLS), which can be recognized by importins facilitate the nuclear import process in the non-dividing cells (*66, 67*). Polyplexes are believed to mimic NLS to some extent due to the positively-charged surface, but they are very inefficient to serve as NLS because few vectors can reach the nucleus (*18*). In addition, Kamiya et al. proposed another mechanism that lipoplexes can fuse with the nuclear membrane, thus releasing DNA to the nucleus (*68*).

1.2.8 Polyplexes Unpackaging

In order to access by the transcription machinery, the delivered DNA must be released from the complexes upon arriving at the nucleus (*30*). However, what is the best time and location for the complexes disassociation is another important question in rational vector design. Higher binding affinity of polycations towards the nucleic acids provides better protection, however, on the other hand, too tight binding and condensation is thought to impede the timely release of the nucleic acids (*30, 69*). It is not difficult to speculate that an optimal balance between the binding and release is the key parameter for the polycations. Some studies demonstrated that polymer/nucleic acid binding strength can be adjusted by changing the number of positive charges (*70*), conjugation of PEG chains (*71*), altering the polymer molar mass (*30*), all finally leading to enhanced gene expression. And disassociation of the polyplexes can be controlled by employing some environment sensitive polymeric vectors such as thermoresponsive (*72*), hydrolytic degradable (*73-75*) and reductive degradable (*76-78*) polymers.

1.2.9 Cytotoxicity

Cytotoxicity is one of the major hurdles for the application of the polycations in successful g ene delivery. Although the exact mechanism remains uncertain, the prevailing opinion suggests that the ionic interaction between polycations and anionic surface domains of cell severely impairs membrane function and ultimately leads to cell death (*79*). Moghimi et al. proposed a two-stage mechanism for the PEI-mediated cytotoxicity. The first type of toxicity originates from compromised plasma membrane integrity and occurs in the early stages of incubating the cells with PEI. The first phase of the cytotoxic activity of PEI is then followed by apoptosis caused by PEI-induced channel formation in the mitochondrial membrane (*80*).

The cytotoxicity of the polycations is dependent on the molecular weight (MW),

structure and charge density of the polymers or size and surface charge of the polyplexes (*29, 81, 82*). Among these parameters, MW is directly proportional to both cell toxicity and transfection efficiency, which has been shown in numerous studies. This is the most significant catch-22 problem in designing a successful gene carrier. To circumvent such a problem, coinciding with the strategies used to facilitate nucleic acid release, low MW polycations were linked by degradable linkers (e.g., disulfide bonds, ester bonds) to form a high MW polymer that can eventually degrade to its lower MW counterparts after finishing their delivery duty (*83-87*). These lower MW components can then be easily cleared either via renal elimination for those MW less than 30 kDa or through natural metabolic pathways for low MW polymers that are endogenous metabolites (*88, 89*).

1.3 PEI as Gene Delivery Carrier

Cationic polymers, including off-the-shelf polymers and designed polymers, usually have protonable groups such as primary, secondary, tertiary amines or amidines. Figure 1.4 summarizes some commonly used polymers in current non-viral gene transfection.

Among these polycations, poly(ethylene imine) (PEI) emerged as the most promising candidate because its gene transfection efficiency is close to that of virus vectors (*90*). Such high efficiency is believed to derive from the unique structure of PEI, namely, every third atom of PEI is nitrogen, which makes PEI possesses very high density of amines. At physiological pH, only 15–20% of amines are protonated (*91*), and the large number of unprotonated amines can be served as the proton sponge when experience pH drop in the endo/lysosome.

As an off-the-shelf polymer, branched PEI (bPEI) has been commonly used in wastewater treatment and paper industry before it was found to be an effective carrier in gene therapy (*92*). After that, its linear form has also been applied in this field and finally commercialized (e.g. ExGen500®, jetPEI®) (*93*). Branched PEI shows a

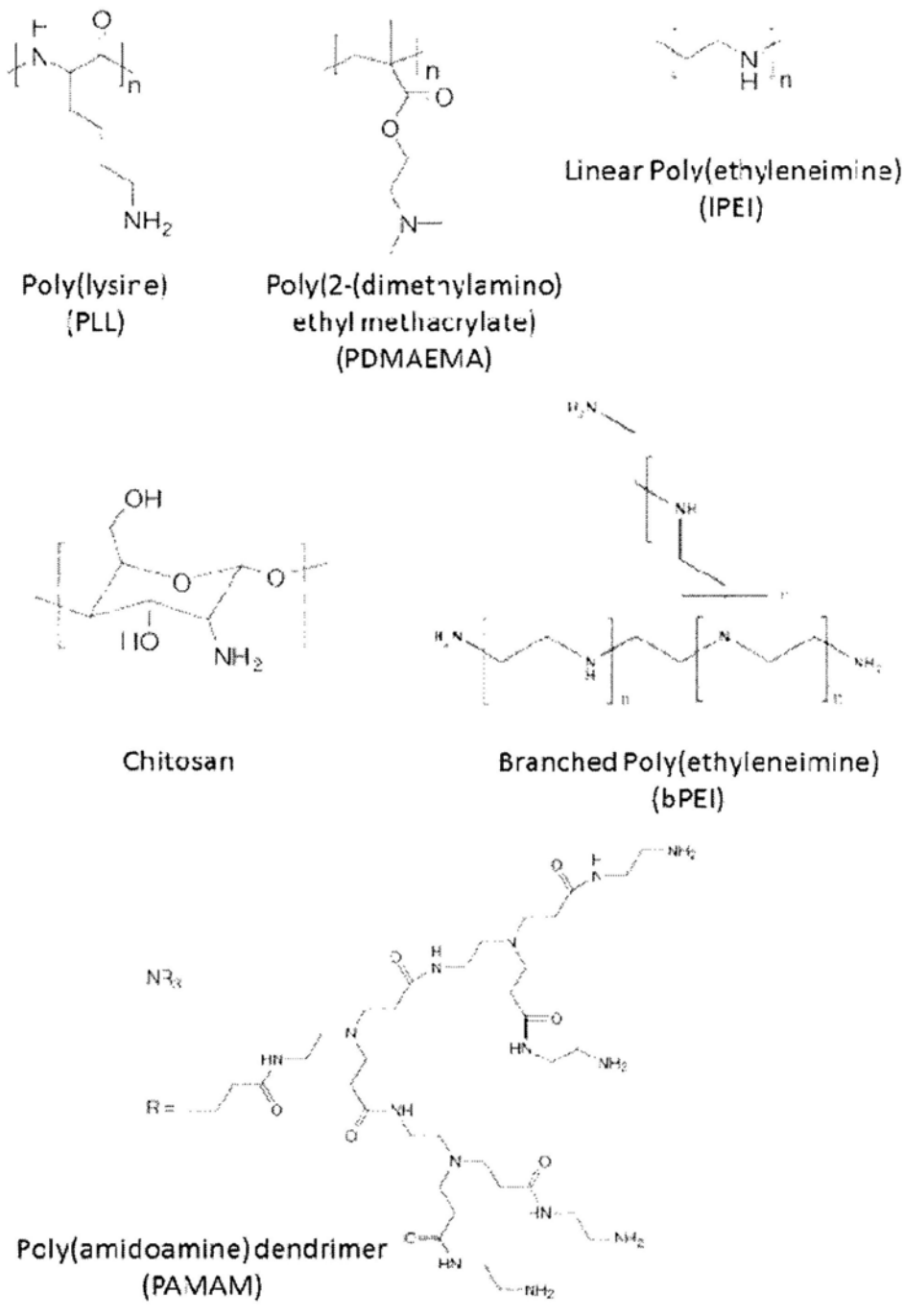

Figure 1.4. Structures of current cationic polymers used in gene therapy.

theoretical ratio of primary to secondary to tertiary nitrogen atoms of 1:2:1, while von Harpe et al. found that the degree of branching was actually 1:1:1 for commercially available bPEI, suggesting a more branched structure (*94*). In contrast,

all of the amines on linear PEI (lPEI) are secondary amine, and 90% are protonated at physiological pH (*95*).

It is commonly accepted that the best MW range for PEI, in both linear and branched form, is 5,000 – 25,000 g/mol. Lower MW PEI, despite its less cytotoxicity, has lower transfection ef ficiency presumably due to the poor DNA compacting ability. Meanwhile higher MW PEI is believed to protect the nucleic acids more effectively, but exhibit high cytotoxicity at the same time (*92*). bPEI with MW 25,000 g/mol is always regarded as the "golden standard" in most transfection experiments (*86*), because of its best balance between efficiency and cytotoxicity as well as its robustness and facile manufacturing.

1.3.1 Complexation between PEI and Nucleic Acid

PEI is capable of condensing large plasmid DNA and RNA molecules into stable polyplexes with typical size of 100-150 nm under low salt concentration conditions. In general, increase in the MW results in the decrease of polyplexes size. When MW is higher than 25 kDa, no further decrease of complex size was observed (*92*). However, in the physiological buffer, small polyplexes are prone to aggregate to form large particles with radius up to 600 nm (*29*). For the low MW PEI, the aggregation size further increase to 900 nm (*96*). In contrast, the size of polyplexes made up of PEI 48 kDa/DNA remain stable in the 150 mM NaCl buffer solution (*97*), indicating the MW dependence of aggregation behavior. Although many reports suggest that larger aggregates, due to their fast precipitation, might be favorable for *in vitro* transfection (*29, 33*), the *in vivo* application of such large aggregates may not be feasible.

Generally, the optimum gene transfection efficiency is achieved at N:P ratio 10 (nitrogen on PEI to phosphor on nucleic acid ratio) for bEI25K (*98, 99*). However, some studies showed that polyplexes prepared at N:P 10 could be purified by a SEC column, and the remaining polyplexes had the final N:P ratio of 2.5 (*100*). Thus the

other portion of PEI is believed to exist as the free form or loosely attached to the polyplexes. The removal of excess PEI led to a decrease in transfection efficiency as well a decrease in cytotoxicity. The transfection efficiency could be recovered by addition of free PEI even 4 hrs after the administration of the purified polyplexes. By using a fluorescence correlation spectroscopy, Clamme et al. also confirmed the existence of free PEI up to 86% of the total PEI amount (*101*). Therefore, these findings imply that free PEI also plays a significant role in the gene transfection besides its DNA compacting and protecting effect.

1.3.2 Systemic and Local Application of PEI/DNA Polyplexes

After intravenous injection, both unmodified lPEI- and bPEI-mediated expression could be observed in the heart, spleen, liver and kidney, however, the highest gene expression levels is predominantly found in the vascular endothelial cells of lung, due to accumulation within the lung capillary beds (*102*). Expression level in all organs can be enhanced by increasing N:P ratios. While bPEI25 and bPEI800/DNA polyplexes administrated at higher doses showed no obvious sign of severe cytotoxicity, lung embolism and death of laboratory animals were observed after intravenous i njection (*29*), due to the aggregation of the polyplexes with blood components.

Some studies reported the local applications such as lung (*103*), tumor (*104*), brain (*90*) and intranasal applications (*105*), by using the unmodified PEI-based polyplexes. In addition, a more convenient aerosol delivery of unmodified bPEI25/DNA polyplexes was found to be able to transfect most of the epithelial cells in the conducting and peripheral airways, suggesting that aerosol delivery of PEI/DNA complexes could be effective for the treatment of pulmonary diseases such as cystic fibrosis and alpha-1 anti-trypsin deficiency (*106*). Altogether, when applied locally to the tumor or organ, although problems in the systemic blood circulation can be bypassed, polyplexes trafficking through the extracellular matrix still have to

be considered (*107*).

1.4 PEI modification

Although PEIs show their potential in gene delivery, chemists are still trying to modify PEI, because the current efficiency of PEI is not satisfying enough, especially for an *in vivo* application. Large quantities of studies have been focused on the modification of PEI in the last two decades trying to overcome some of the aforementioned extra- and intra-cellular barriers.

1.4.1 Stealth Property from PEGylation

As mentioned previously, "naked" positively-charged polyplexes are not suitable for *in vivo* application. Hydrophilic polymers, in most cases polyethylene glycol (PEG), have been attached to the surface of polyplexes, in order to shield the surface charge, decrease undesired interaction with serum proteins and prolong the circulation time in blood. Furthermore, the PEG shielding also increases the stability against free-thawing (*108*).

Generally, PEGylation involves two strategies, namely, post-PEGylation and pre-PEGylation. For the post-PEGylation, polyplexes formation is finished prior to the coupling of PEG chains. However, this strategy seems troublesome in clinical application. Furthermore, considering the free PEI issue mentioned in section 1.3.1, some reported protocols regarding the post-PEGylation method (*34, 104, 109*) should be reconsidered, due to the reactivity of activated PEG toward the free PEI and the polyplexes.

The main concern about th e pre -PEGylation m ethod is that the hydrophilic copolymer may impact the formation of the polyplexes. Despite extensive investigations no consensus on the optimal degree of PEG substitution and PEG chain length has been reached, both of which contribute to the formation of the polyplexes (*92*). Generally speaking, high substitution degree and long PEG chain

length may hinder the complexation, while low substitution degree and short PEG chain cannot afford the stabilization and charge-shielding effect.

Sung et al. reported that short side PEG chains did not cause a significant effect on the complexation behavior when PEG molecular weight ranged from 350 – 1900 g/mol (*110*). While complexation was slightly hindered when grafting density were 2, 6 and 15 for PEG 5,000 g/mol, copolymers with few but long PEG blocks (MW = 20,000 g/mol) self-assembled to small and compact condensates wiht low surface charge and copolymers with many long PEG blocks generated complexes of ill-defined shape with almost no surface charge (*111*). In terms of stability in salt buffer, higher molecular weight PEG chains resulted in a decreased sensitivity of the complexes to salt-induced aggregation (*110-112*). Molecular weight of at least 2,000 - 5,000 g/mol seems to be necessary to achieve a stabilizing effect (*92*). Briefly, the structure of PEG-g-PEI copolymer has significant impact on the properties of the resulting polyplexes. PEGylation, therefore, might be considered as one method for tailoring the polyplexes with adjustable characters.

1.4.2 Ligand-PEI Conjugates for Cell Targeting

Numerous cell targeting ligands have been incorporated into polyplexes by chemical conjugation on cationic polymers, in order to be specifically internalized by certain targeting cells, such as transferrin recognized by transferrin receptor (*113, 114*), cyclic RGD peptide recognized by integrins (*115, 116*), sugar residues recognized by cell surface membrane lectines (*117*), and metabolites such as folate (*118, 119*). After the ligands incorporation on the polyplexes, uptake rate is increased compared to the unspecific uptake of polyplexes without ligand (*40*). Moreover, as discussed before, the binding of ligands to their receptors may affect the endocytosis pathway of the polyplexes as well as their intracellular rate, routing and fate. Successful targeting in cell culture has been described demonstrating up to 1000-fold enhanced gene expression in target cells in comparison with ligand-free complexes (*120*).

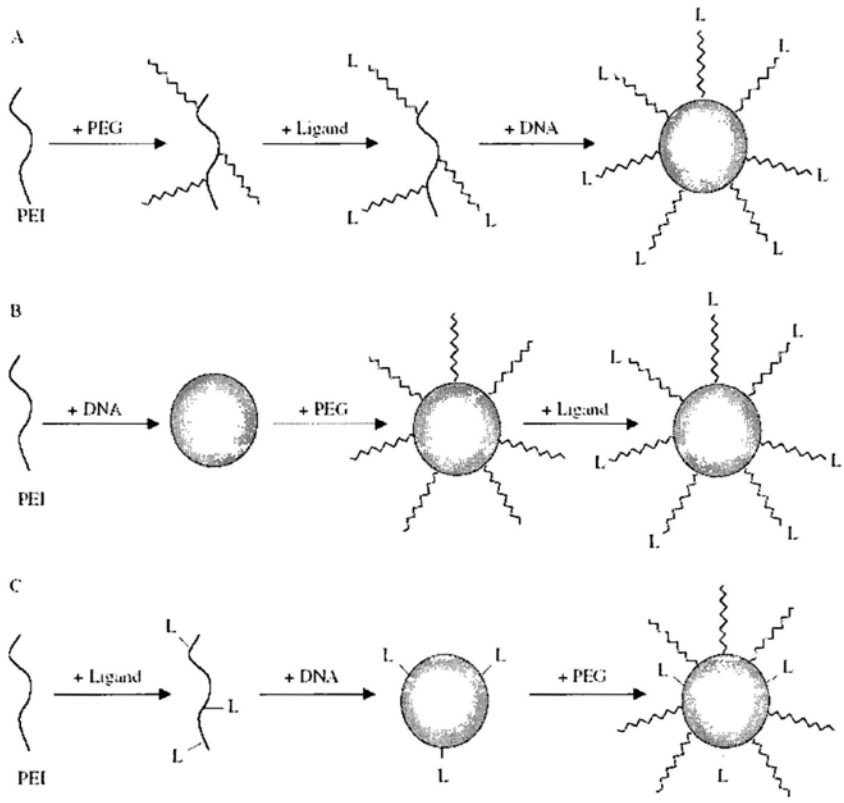

Figure 1.5. Schematic representation of three strategies used for the formation of PEGylated ligand-containing PEI/DNA complexes. (A) After PEGylation of PEI, the ligand reacts with the functionalized distal end of the hydrophilic arm. The last step then consists of condensing the DNA with the ligand-PEG-PEI conjugate. (B) PEI/DNA complexes are first generated. The resulting polyplexes are modified by a heterobifunctional PEG which reacts with amino groups of PEI. Ligands are finally incorporated into the complexes by conjugation with the distal end of the PEG. (C) The first step consists of covalently coupling the ligand to PEI. Addition of plasmid DNA leads to the formation of ligand-PEI/DNA complexes which are subsequently modified with PEG chains. (121)

However, only target ligands surrounding the polyplexes cannot provide shielding effect. Therefore, combination of stealth technology and cell targeting approaches has been developed. There are three different strategies in regard to this approach shown in Figure 1.5 (*121*). In the first strategy, activated PEG chains are first grafted to PEI, followed by coupling the ligand to the other end of the PEG chain and then complexation between copolymer and nucleic acids. The problem arising in this approach is similar to that of the pre-PEGylation method, namely, too many PEG chains will result in poor condensation ability (*122, 123*). Therefore, the

second approach is developed, where the polyplexes are generated prior to the PEGylation, and the ligands are conjugated to the PEG chain end as the last step (*109*). The last strategy refers to the ligand conjugation as the first step followed by the complexation and then PEGylation. In this method, the ligand might be masked by PEG, thus leading to difficulty for the receptor recognition.

1.4.3 Degradable Polymers

1.4.3.1 Hydrolysis sensitive degradation

One of the main problems for PEI in gene delivery is the high cytotoxicity with an effective molecular weight. Thus, it is not hard to image that crosslink low MW PEI by using degradable linker may lead to decreasing cytotoxicity. Forrest et al. synthesized a crosslinked PEI from low MW PEI 800 Da by using a diacrylate linker (*124*). The *in vitro* experiment found that the hydrolysis degradable PEI exhibited low toxicity and can be 4-8 times more effective than commercially available PEI-25K. However, water molecules are the cleaving agents and hydrolysis can occur upon first exposure to physiological environments for an *in vivo* application. Therefore, it becomes hard to know and to control where and when the degradation of these polymers takes place.

Another problem is steric shielding may impede the release of nucleic acids in the PEGylation approach. Because the dissociation process is believed to rely on the displacement by other polyanion *in vivo*, such as RNA and glycosaminoglycans (*125, 126*), but the hydrophilic corona may keep the polyanion away, hence make such a process more difficult. Based on the same concept, this problem could be circumvented by grafting PEG chains to PEI via a pH sensitive hydrolysis bond. Walker et al. synthesized the PEG-g-PEI copolymer via pH sensitive p-piperazinobenzaldehyde acetal linkage (*127*). The gene expression results showed that the reversibly shielded polyplexes exhibited up to 10 times higher gene expression *in vitro*, compared to the stably shielded control polyplexes.

1.4.3.2 Redox sensitive degradation

Disulfide-based polymeric gene delivery systems have attracted more and more attention in past decade, because unlike hydrolysis sensitive bonds, the disulfide bond is relatively stable in extracellular environment and could be quickly degraded in the reductive intracellular environment (*128*). The high concentration of glutathione (GSH) (0.5 – 10 mM) in the cytosol is responsible for the cleavage of the disulfide bond (*129*). Disulfide bonds can be incorporated into gene delivery systems in a variety of ways. The first strategy, still concerning the high cytotoxicity of the PEI, is to crosslink low MW PEI to higher MW PEI via disulfide bond. Gosselin et al. used dithiobis(succinimidylpropionate) (DSP) and dimethyl-3,3'-dithiobispropionimidate (DTBP), two disulfide linker, to crosslink low MW PEI (MW = 800 Da). The results showed that crosslinked polymers are nearly non-toxic, but their *in vitro* gene transfection efficiency was slightly lower than that of bPEI25K (*99*).

The second approach is post-crosslinking PEI chain after the polyplexes formation on the purpose of enhancing the stability of the polyplexes. Neu et al. used such a method by using DSP to crosslink the surface of the PEI/DNA polyplexes (*130*). Although the in vitro gene transfection efficiency was reduced after the crosslinking, the *in vivo* results in mice revealed increased blood concentrations depending on the stabilization degree and altered organ distribution, and the luciferase expression patterns demonstrated enhanced liver expression while unwanted lung transfection could be reduced. Another post-crosslinking method deals with the in-situ oxidation of thiolated-PEI/DNA polyplexes. However, by using this method, the *in vitro* gene transfection efficiency was not satisfying (*98*). These results may imply that the condensation-release property should be carefully balanced in gene vector design.

The last approach is to graft cationic ligands to the polymer backbone via a

disulfide linkage to afford electrostatically-mediated DNA packaging with bond cleavage and subsequent DNA release upon exposure to reductive environment in the cytosol (*77, 78*).

References and Notes

(1) Mulligan, R. C. *Science* **1993**, *260*, 926.

(2) Pawliuk, R., Westerman, K. A., Fabry, M. E., *et al. Science* **2001**, *294*, 2368.

(3) von Laer, D., Hasselmann, S., and Hasselmann, K. *J. Gene Med.* **2006**, *8*, 658.

(4) Wong, L. F., Goodhead, L., Prat, C., *et al. Hum. Gene Ther.* **2006**, *17*, 1.

(5) Burton, E. A., Glorioso, J. C., and Fink, D. J. *Gene Ther.* **2003**, *10*, 1721.

(6) Wong, S. Y., Pelet, J. M., and Putnam, D. *Prog. Polym. Sci.* **2007**, *32*, 799.

(7) Miller, A. D. *Nature* **1992**, *357*, 455.

(8) Escors, D., and Breckpot, K. *Arch. Immunol. Ther. Exp. (Warsz). 58*, 107.

(9) http://www.wiley.co.uk/genetherapy/clinical/.

(10) Cavazzana-Calvo, M., Hacein-Bey, S., Basile, C. D., *et al. Science* **2000**, *288*, 669.

(11) Check, E. *Nature* **2002**, *420*, 116.

(12) Hacein-Bey-Abina, S., Von Kalle, C., Schmidt, M., *et al. Science* **2003**, *302*, 415.

(13) Marshall, E. *Science* **2000**, *288*, 951.

(14) Ilies, M. A., Seitz, W. A., and Balaban, A. T. *Curr. Pharm. Des.* **2002**, *8*, 2441.

(15) Boeckle, S., and Wagner, E. *Aaps Journal* **2006**, *8*, E731.

(16) Sokolova, V., and Epple, M. *Angewandte Chemie-International Edition* **2008**, *47*, 1382.

(17) Son, S. J., Bai, X., and Lee, S. B. *Drug Discov. Today* **2007**, *12*, 650.

(18) Pack, D. W., Hoffman, A. S., Pun, S., *et al. Nature Reviews Drug Discovery* **2005**, *4*, 581.

(19) Morille, M., Passirani, C., Vonarbourg, A., *et al. Biomaterials* **2008**, *29*, 3477.

(20) El-Aneed, A. *J. Controlled Release* **2004**, *94*, 1.

(21) Bloomfield, V. A. *Biopolymers* **1997**, *44*, 269.

(22) Lechardeur, D., Sohn, K. J., Haardt, M., *et al. Gene Ther.* **1999**, *6*, 482.

(23) Abdelhady, H. G., Allen, S., Davies, M. C., *et al. Nucleic Acids Res.* **2003**, *31*, 4001.

(24) Bronich, T. K., Nguyen, H. K., Eisenberg, A., *et al. J. Am. Chem. Soc.* **2000**, *122*, 8339.

(25) Nguyen, T. T., and Shklovskii, B. I. *Physica a-Statistical Mechanics and Its Applications* **2001**, *293*, 324.

(26) Tang, M. X., and Szoka, F. C. *Gene Ther.* **1997**, *4*, 823.

(27) Lai, E., and van Zanten, J. H. *Biophys. J.* **2001**, *80*, 864.

(28) Godbey, W. T., Wu, K. K., and Mikos, A. G. *J. Biomed. Mater. Res.* **1999**, *45*, 268.

(29) Wightman, L., Kircheis, R., Rossler, V., *et al. J. Gene Med.* **2001**, *3*, 362.

(30) Schaffer, D. V., Fidelman, N. A., Dan, N., *et al. Biotechnol. Bioeng.* **2000**, *67*, 598.

(31) Wadhwa, M. S., Collard, W. T., Adami, R. C., *et al. Bioconj. Chem.* **1997**, *8*, 81.

(32) Fischer, D., Bieber, T., Li, Y. X., *et al. Pharm. Res.* **1999**, *16*, 1273.

(33) Ogris, M., Steinlein, P., Kursa, M., *et al. Gene Ther.* **1998**, *5*, 1425.

(34) Ogris, M., Brunner, S., Schuller, S., *et al. Gene Ther.* **1999**, *6*, 595.

(35) Brigger, I., Dubernet, C., and Couvreur, P. *Adv. Drug Del. Rev.* **2002**, *54*, 631.

(36) Gref, R., Minamitake, Y., Peracchia, M. T., *et al. Science* **1994**, *263*, 1600.

(37) Vonarbourg, A., Passirani, C., Saulnier, P., *et al. Biomaterials* **2006**, *27*, 4356.

(38) Mislick, K. A., and Baldeschwieler, J. D. *Proc. Natl. Acad. Sci. U. S. A.* **1996**, *93*, 12349.

(39) Khalil, I. A., Kogure, K., Akita, H., *et al. Pharmacol. Rev.* **2006**, *58*, 32.

(40) Midoux, P., Breuzard, G., Gomez, J. P., *et al. Curr. Gene Ther.* **2008**, *8*, 335.

(41) Takei, K., and Haucke, V. *Trends Cell Biol.* **2001**, *11*, 385.

(42) Schmid, S. L. *Annu. Rev. Biochem* **1997**, *66*, 511.

(43) Brodsky, F. M., Chen, C. Y., Knuehl, C., *et al. Annu. Rev. Cell Dev. Biol.* **2001**, *17*, 517.

(44) Maxfield, F. R., and McGraw, T. E. *Nature Reviews Molecular Cell Biology* **2004**, *5*, 121.

(45) Goncalves, C., Mennesson, E., Fuchs, R., *et al. Mol. Ther.* **2004**, *9*, 835.

(46) Matveev, S., Li, X. G., Everson, W., *et al. Adv. Drug Del. Rev.* **2001**, *49*, 237.

(47) Pelkmans, L., Kartenbeck, J., and Helenius, A. *Nat. Cell Biol.* **2001**, *3*, 473.

(48) Ferrari, A., Pellegrini, V., Arcangeli, C., *et al. Mol. Ther.* **2003**, *8*, 284.

(49) Rejman, J., Bragonzi, A., and Conese, M. *Mol. Ther.* **2005**, *12*, 468.

(50) Gabrielson, N. P., and Pack, D. W. *J. Controlled Release* **2009**, *136*, 54.

(51) Rejman, J., Oberle, V., Zuhorn, I. S., *et al. Biochem. J* **2004**, *377*, 159.

(52) Conner, S. D., and Schmid, S. L. *Nature* **2003**, *422*, 37.

(53) Swanson, J. A., and Watts, C. *Trends Cell Biol.* **1995**, *5*, 424.

(54) Allen, L. A. H., and Aderem, A. *Curr. Opin. Immunol.* **1996**, *8*, 36.

(55) Farhood, H., Serbina, N., and Huang, L. *Biochimica Et Biophysica Acta-Biomembranes* **1995**, *1235*, 289.

(56) Deduve, C., Debarsy, T., Poole, B., *et al. Biochem. Pharmacol.* **1974**, *23*, 2495.

(57) Neukamm, B., Weimann, A., Wu, S. L., *et al. J. Gene Med.* **2006**, *8*, 745.

(58) Ciftci, K., and Levy, R. J. *Int. J. Pharm.* **2001**, *218*, 81.

(59) Erbacher, P., Roche, A. C., Monsigny, M., *et al. Exp. Cell Res.* **1996**, *225*, 186.

(60) Kichler, A., Leborgne, C., Coeytaux, E., *et al. J. Gene Med.* **2001**, *3*, 135.

(61) Boussif, O., Lezoualch, F., Zanta, M. A., *et al. Proc. Natl. Acad. Sci. U. S. A.*

1995, *92*, 7297.

(62) Forrest, M. L., and Pack, D. W. *Mol. Ther.* **2002**, *6*, 57.

(63) Lukacs, G. L., Haggie, P., Seksek, O., *et al. J. Biol. Chem.* **2000**, *275*, 1625.

(64) Suh, J., Wirtz, D., and Hanes, J. *Proc. Natl. Acad. Sci. U. S. A.* **2003**, *100*, 3878.

(65) Melchior, F., and Gerace, L. *Curr. Opin. Cell Biol.* **1995**, *7*, 310.

(66) Dean, D. A., Dean, B. S., Muller, S., *et al. Exp. Cell Res.* **1999**, *253*, 713.

(67) Gasiorowski, J. Z., and Dean, D. A. *Adv. Drug Del. Rev.* **2003**, *55*, 703.

(68) Kamiya, H., Fujimura, Y., Matsuoka, I., *et al. Biochem. Biophys. Res. Commun.* **2002**, *298*, 591.

(69) Honore, I., Grosse, S., Frison, N., *et al. J. Controlled Release* **2005**, *107*, 537.

(70) Erbacher, P., Roche, A. C., Monsigny, M., *et al. Biochimica Et Biophysica Acta-Biomembranes* **1997**, *1324*, 27.

(71) Banaszczyk, M. G., Lollo, C. P., Kwoh, D. Y., *et al. Journal of Macromolecular Science-Pure and Applied Chemistry* **1999**, *A36*, 1061.

(72) Yokoyama, M. *Drug Discov. Today* **2002**, *7*, 426.

(73) Liu, X. H., Yang, J. W., Miller, A. D., *et al. Macromolecules* **2005**, *38*, 7907.

(74) Zhong, Z. Y., Song, Y., Engbersen, J. F. J., *et al. J. Controlled Release* **2005**, *109*, 317.

(75) Li, Z. H., and Huang, L. *J. Controlled Release* **2004**, *98*, 437.

(76) El-Sayed, M. E. H., Hoffman, A. S., and Stayton, P. S. *J. Controlled Release* **2005**, *101*, 47.

(77) Pichon, C., LeCam, E., Guerin, B., *et al. Bioconj. Chem.* **2002**, *13*, 76.

(78) Zugates, G. T., Anderson, D. G., Little, S. R., *et al. J. Am. Chem. Soc.* **2006**, *128*, 12726.

(79) Ryser, H. J. P. *Nature* **1967**, *215*, 934.

(80) Moghimi, S. M., Symonds, P., Murray, J. C., *et al. Mol. Ther.* **2005**, *11*, 990.

(81) Lv, H. T., Zhang, S. B., Wang, B., *et al. J. Controlled Release* **2006**, *114*,

100.

(82) Hill, I. R. C., Garnett, M. C., Bignotti, F., *et al. Biochimica Et Biophysica Acta-General Subjects* **1999**, *1427*, 161.

(83) Thomas, M., Ge, Q., Lu, J. J., *et al. Pharm. Res.* **2005**, *22*, 373.

(84) Breunig, M., Lungwitz, U., Liebl, R., *et al. Proc. Natl. Acad. Sci. U. S. A.* **2007**, *104*, 14454.

(85) Manickam, D. S., and Oupicky, D. *Bioconjugate Chem.* **2006**, *17*, 1395.

(86) Kloeckner, J., Wagner, E., and Ogris, M. *Eur. J. Pharm. Sci.* **2006**, *29*, 414.

(87) Kim, Y. H., Park, J. H., Lee, M., *et al. J. Controlled Release* **2005**, *103*, 209.

(88) Pack, D. W., Putnam, D., and Langer, R. *Biotechnol. Bioeng.* **2000**, *67*, 217.

(89) Putnam, D., and Langer, R. *Macromolecules* **1999**, *32*, 3658.

(90) Abdallah, B., Hassan, A., Benoist, C., *et al. Hum. Gene Ther.* **1996**, *7*, 1947.

(91) Suh, J., Paik, H. J., and Hwang, B. K. *Bioorg. Chem.* **1994**, *22*, 318.

(92) Neu, M., Fischer, D., and Kissel, T. *J. Gene Med.* **2005**, *7*, 992.

(93) Ferrari, S., Moro, E., Pettenazzo, A., *et al. Gene Ther.* **1997**, *4*, 1100.

(94) von Harpe, A., Petersen, H., Li, Y. X., *et al. J. Controlled Release* **2000**, *69*, 309.

(95) Lungwitz, U., Breunig, M., Blunk, T., *et al. Eur. J. Pharm. Biopharm.* **2005**, *60*, 247.

(96) Petersen, H., Kunath, K., Martin, A. L., *et al. Biomacromolecules* **2002**, *3*, 926.

(97) Kunath, K., von Harpe, A., Fischer, D., *et al. J. Controlled Release* **2003**, *89*, 113.

(98) Peng, Q., Zhong, Z. L., and Zhuo, R. X. *Bioconjugate Chem.* **2008**, *19*, 499.

(99) Gosselin, M. A., Guo, W. J., and Lee, R. J. *Bioconjugate Chem.* **2001**, *12*, 989.

(100) Boeckle, S., von Gersdorff, K., van der Piepen, S., *et al. J. Gene Med.* **2004**, *6*, 1102.

(101) Clamme, J. P., Azoulay, J., and Mely, Y. *Biophys. J.* **2003**, *84*, 1960.

(102) Goula, D., Benoist, C., Mantero, S., *et al. Gene Ther.* **1998**, *5*, 1291.

(103) Ernst, N., Ulrichskotter, S., Schmalix, W. A., *et al. J. Gene Med.* **1999**, *1*, 331.

(104) Kircheis, R., Schuller, S., Brunner, S., *et al. J. Gene Med.* **1999**, *1*, 111.

(105) Wiseman, J. W., Goddard, C. A., McLelland, D., *et al. Gene Therpay* **2003**, *10*, 1654.

(106) Gautam, A., Densmore, C. L., Golunski, E., *et al. Mol. Ther.* **2001**, *3*, 551.

(107) Ruponen, M., Honkakoski, P., Ronkko, S., *et al. J. Controlled Release* **2003**, *93*, 213.

(108) Ogris, M., Walker, G., Blessing, T., *et al. J. Controlled Release* **2003**, *91*, 173.

(109) Blessing, T., Kursa, M., Holzhauser, R., *et al. Bioconj. Chem.* **2001**, *12*, 529.

(110) Sung, S. J., Min, S. H., Cho, K. Y., *et al. Biol. Pharm. Bull.* **2003**, *26*, 492.

(111) Petersen, H., Fechner, P. M., Martin, A. L., *et al. Bioconjugate Chem.* **2002**, *13*, 845.

(112) Nguyen, H. K., Lemieux, P., Vinogradov, S. V., *et al. Gene Ther.* **2000**, *7*, 126.

(113) Wagner, E., Zenke, M., Cotten, M., *et al. Proc. Natl. Acad. Sci. U. S. A.* **1990**, *87*, 3410.

(114) Kursa, M., Walker, G. F., Roessler, V., *et al. Bioconjugate Chem.* **2003**, *14*, 222.

(115) Erbacher, P., Remy, J. S., and Behr, J. P. *Gene Ther.* **1999**, *6*, 138.

(116) Temming, K., Schiffelers, R. M., Molema, G., *et al. Drug Resistance Updates* **2005**, *8*, 381.

(117) Roche, A. C., Fajac, I., Grosse, S., *et al. Cell. Mol. Life Sci.* **2003**, *60*, 288.

(118) Aronov, O., Horowitz, A. T., Gabizon, A., *et al. Bioconjugate Chem.* **2003**, *14*, 563.

(119) Zhao, X. B. B., and Lee, R. J. *Adv. Drug Del. Rev.* **2004**, *56*, 1193.

(120) Wagner, E., and Kloeckner, J. (2006) Gene delivery using polymer therapeutics, in *Polymer Therapeutics I: Polymers as Drugs, Conjugates and Gene Delivery Systems* pp 135.

(121) Kichler, A. (2002) in *Meeting on Gene Therapy Vectors* pp S3, Evry, FRANCE.

(122) Erbacher, P., Bettinger, T., Belguise-Valladier, P., *et al. J. Gene Med.* **1999**, *1*, 210.

(123) Sagara, K., and Kim, S. W. *J. Controlled Release* **2002**, *79*, 271.

(124) Forrest, M. L., Koerber, J. T., and Pack, D. W. *Bioconjugate Chem.* **2003**, *14*, 934.

(125) Ruponen, M., Ronkko, S., Honkakoski, P., *et al. J. Biol. Chem.* **2001**, *276*, 33875.

(126) Oliver Germershaus, Shirui Mao, Johannes Sitterberg, *et al. J. Controlled Release* **2008**, *125*, 145.

(127) Knorr, V., Allmendinger, L., Walker, G. F., *et al. Bioconjugate Chem.* **2007**, *18*, 1218.

(128) Manickam, D. S., and Oupicky, D. *J. Drug Targeting* **2006**, *14*, 519.

(129) Chao Lin, J. F. J. E. *Expert opinion on drug delivery* **2009**, *6*, 421.

(130) Neu, M., Germershaus, O., Mao, S., *et al. J. Controlled Release* **2007**, *118*, 370.

Chapter 2

Fundamentals of Laser Light Scattering and Instrumentation

2.1 Introduction

The phenomenon of light scattering is encountered widely in daily life. The first recorded observation of the light scattering phenomenon can be traced back to 1802 when the light path of the gold colloid was observed by J. B. Richard. However, the first man made experimental investigation on light scattering was Tyndall who observed the scattering of the natural light passed through a colloid dispersion. Based on Maxwell theory of electromagnetic field, in 1881, Rayleigh first put forward the theory of light scattering, and pointed that the intensity of the scattered light by the non-absorption, non-interaction and isotropic small particles is reversely proportional to the fourth power of the incident wavelength. In 1944, Debye further developed the theory by measuring the molecular weight of macromolecules from dilute solution using light scattering method. Later, Zimm proposed the Zimm plot by extrapolating both angular angle and concentration to zero at a single coordinate (*1*). Since then, SLS has been widely used in the field of polymer characterization as a classical and absolute method. However, at that time light scattering was limited by measuring the scattered intensity at different angles, until the invention of laser in the 1960s. In 1964, Cummins first reported using lasers as the source of incident light for the study of poly(styrene) solutions (*2*). During the last two decades, thanks to the advance of stable laser source, ultrafast electronics and personal computers, LLS, especially DLS has evolved from a very special instrument to a routine analytical tool in polymer laboratories or even to a daily quality-control device in production lines (*3, 4*).

In principle, when a light beam is incident on a suspension of particles and the refractive index of the medium is different from that of the particles, the incident

light is scattered by each illuminated particle in all directions (*5, 6*). The scattered light from different particles mutually interfere, or combine, at a distant, fast photomultiplier tube (PMT) or avalanche-photodiode (APD) detector and result a net scattered intensity I(t) or photon counts n(t). If all of the particles are stationary, the scattered light intensity at each direction would be independent of time, however, in reality, all the scattering particles are undergoing Brownian motions, and leads to both fluctuations of the scattered intensity on the detection plane and the fluctuations of I(t) with time if the detection zone is sufficiently small. The fluctuation rates are related to different relaxation processes, for example, translational diffusions, rotational diffusions or internal motions of the scattering particles.

Generally, laser light scattering (LLS) could be divided to inelastic (e.g., Raman, fluorescence, and phosphorescence) and elastic (no absorption) light scattering. While in colloid and polymer science, light scattering is often referred to static (elastic) or dynamic (quasi-elastic) measurements of the scattered light (*5*). Static light scattering (SLS) measures the angular distribution of time averaged scattered intensity. On the other hand, dynamic light scattering (DLS) measures the intensity fluctuations with time instead of the mean light intensity. When the incident light is scattered by a moving particle or macromolecule, the detect frequency of the scattered light will be slightly change d in comparison with that of the original incident light due to the Doppler effect. The frequency shift depends on the particle's movement direction, towards or away from the detector. As the result, the frequency distribution of the scattered light is slightly broader than that of the origin incident light. This is why DLS is also called quasi-elastic light scattering. The frequency broadening, typically ~ 10^5-10^7 Hz, is so small in comparison with the incident light frequency (~ 10^{15} Hz) to be detected directly in the frequency space. Fortunately, it can be effectively recorded in the time space through a time correlation function. For such reason, DLS is sometimes called as intensity fluctuation spectroscopy, further as photon correlation spectroscopy (PCS), if digital photons are used to measure the

intensity fluctuations.

2.2 Static Laser Light Scattering

2.2.1 Scattering by a Small Particle

The electric field of light wave acting on a particle induces in it a dipole that oscillates with the same frequency with the incident light (Figure 2.1). The oscillating dipole produces a secondary oscillating field and radiates electromagnetic energy. That is to say, as a secondary light source, the particle scatters the incident light. Considering a single, optical isotropic particle with the polarizability α at origin o (Figure 2.1) in vacuum, when the particle is much smaller than the wavelength of the incident light λ_o (in practice, smaller than $\lambda_o/20$), the electric field of the incident light

$$\vec{E} = \vec{E_0} \exp[i(2\pi\nu t - \phi)] \tag{2-1}$$

is homogeneous within the particle; it induces in it a dipole $\vec{\mu} = \alpha\vec{E}$. The electric field oscillates with frequency ν and so does the induced dipole. When the electric field is not too strong, the induced dipole is proportional to the field:

$$\vec{\mu} = \alpha\vec{E} = 4\pi\varepsilon_0\alpha'\vec{E} \tag{2-2}$$

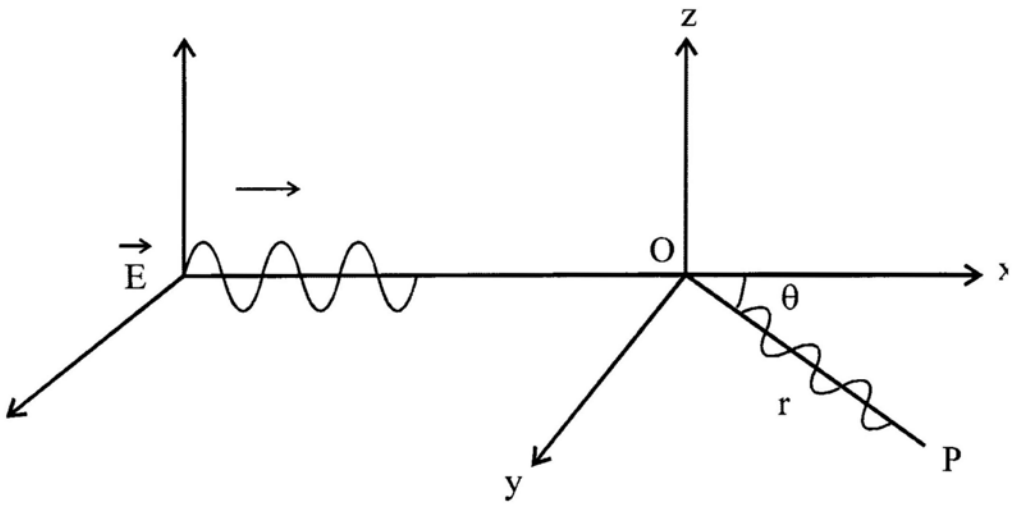

Figure 2.1. Three dimensional coordinates where origin o represents a scatter and P is observation point at xoy plane. The vertically polarized incident beam causes polarization in the scatter, which radiates into different direction.

here α' is the polarizability volume of the particle and ε is dielectric coefficient in vacuum.

According to Maxwell electromagnetic equations, the electric field generated by the oscillating dipole at point p with distance r from origin o and angle of θ from the incident light is given by

$$\overrightarrow{E_s} = \frac{d^2\vec{p}/dt^2}{4\pi\varepsilon_0 rc^2} = \frac{d^2(\overrightarrow{\mu_0}+\vec{\mu})/dt^2}{4\pi\varepsilon_0 rc^2} = -\frac{4\pi^2\alpha'}{r\lambda_0^2}\vec{E} \qquad (2\text{-}3)$$

where c is the velocity of light in vacuum and α' is the polarizability volume. $\vec{p}$ is the total dipole of the particle, i.e. the summation of the permanent $\overrightarrow{\mu_0}$ and the induced dipole $\vec{\mu}$. Since $\overrightarrow{\mu_0} << \vec{\mu}$ at room temperature and $\overrightarrow{\mu_0}$ is independent of high frequency electromagnetic field, we have adopted $\mathrm{d}^2\vec{p}/dt^2 = \mathrm{d}^2\vec{\mu}/dt^2$ in equation (2-3). Thus, the time-average scattered intensity i ($kJ \cdot m^{-2} \cdot s^{-1}$) of the particle at point p is

$$i = \varepsilon_o c\langle E_s^2\rangle = \frac{16\pi^4\alpha'^2}{\lambda_0^4 r^2}(\varepsilon_o c < E^2 >) = \frac{16\pi^4\alpha'^2}{\lambda_0^4 r^2} I_o \qquad (2\text{-}4)$$

where I_o is the intensity of primary light. Equation (2-4) shows that the scattered intensity is proportional to the square of molecular weight since for particles made from a given isotropic material, α' is proportional to their molecular weight. On the other hand, i / $I_0 \propto \lambda_0^{-4}$, means that the scattering is much stronger for light with a shorter wavelength.

2.2.2 Scattering by Many Small-Particle System

When there are N independent same small particles in volume V, the total scattered intensity per unit scattering volume I is the simple summation of the scattered intensity of N/V particles:

$$I = i(N/V) = \frac{16\pi^4 N\alpha'^2}{V\lambda_0^4 r^2} I_o \qquad (2\text{-}5)$$

Define Rayleigh ratio $R = Ir^2/I_o$, we have

$$R = \frac{16\pi^4 N\alpha'^2}{V\lambda_0^4} \tag{2-6}$$

where R is dependent on the concentration, the size and the nature of the particles.

2.2.3 Scattering by Real Systems

For a real case, two kinds of interference must be considered. One is the intra-particle interference. When the particle is not small enough, i.e. dimension $>\lambda/20$, the light scattered from two scattering points within the volume of the same particle has a significant phase difference. The other one is the inter-particle interference. In the former situation, we can assume that a larger particle with volume V' is composed of N' scattering units each with equivalent volume and polarizability α_o'. For each scattering unit, the scattered intensity at observation point p can still be expressed by equation (2-3). Therefore, the scattered electric field of the whole particle at point p is the superposition of the electric field of all N' units:

$$\overrightarrow{E_s} = \sum_{l=1}^{N'} \overrightarrow{E_{s,l}} = -\frac{4\pi^2}{\lambda_0^2 r}\alpha'_o \overrightarrow{E_0} \sum_{l=1}^{N'} \exp[i(2\pi\nu t - \phi_l)] \tag{2-7}$$

Further, the time-average scattered intensity at point p is

$$i = \varepsilon_o c\left\langle E_s^2 \right\rangle = \frac{16\pi^4 \alpha'^2_o}{\lambda_0^4 r^2} I_o \left\langle \sum_{l=1}^{N'}\sum_{m=1}^{N'} \exp[i(\vec{q}\cdot\overrightarrow{r_{lm}})] \right\rangle \tag{2-8}$$

where $\Delta\phi_{lm} = \phi_l - \phi_m$ is phase difference between scattering unit l and m at point p. As can be seen from Figure 2.2,

$$\Delta\phi_{lm} = \vec{q}\cdot\overrightarrow{r_{lm}} \tag{2-9}$$

where $\overrightarrow{r_{lm}} = \overrightarrow{r_m} - \overrightarrow{r_l}$ and $\vec{q} = \vec{r_i} - \overrightarrow{r_f}$ is called scattering vector which is the difference of the unit vector in the direction of the incident beam ($\vec{r_i}$) and the one along the scattered beam ($\overrightarrow{r_f}$), and the vector module is given by

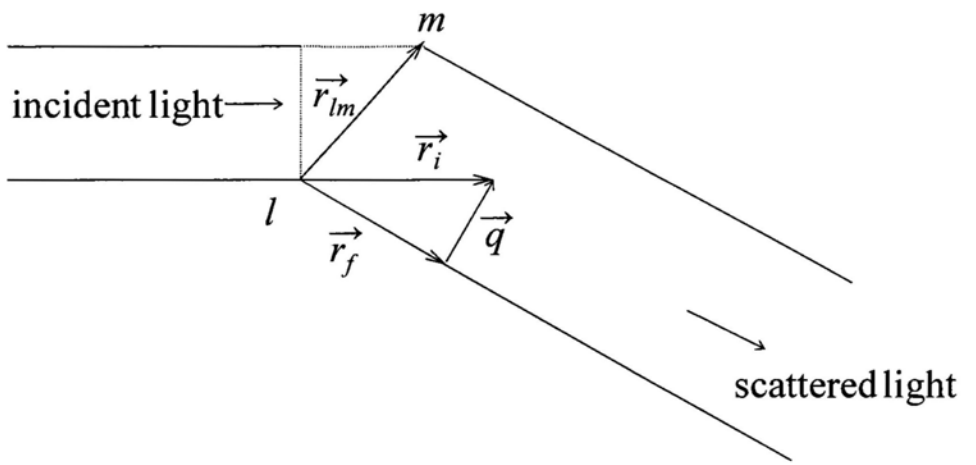

Figure 2.2. Schematic of the scattering vector and the interference of scattered light inside a larger particle.

$$q = \left|\vec{q}\right| = \frac{4\pi n}{\lambda_o}\sin\left(\frac{\theta}{2}\right) \tag{2-10}$$

where n is the refractive index of the medium. With an increasing θ, q increases and 1/q has been used as a spatial resolution ruler with which SLS is able to probe the size of colloidal particles or macromolecules at a finite angle. By averaging over all possible orientations ($\vec{r_{lm}}$) of the particle, we have

$$i(\theta) = \frac{16\pi^4}{r^2\lambda_0^4} I_o \alpha'^2_o \sum_{l=1}^{N'}\sum_{m=1}^{N'} \frac{\sin(q\, r_{lm})}{q\, r_{lm}} \tag{2-11}$$

where θ is the inclined angle from direction of primary beam to that of line op in Figure 2.1. When θ approaches to 0,

$$i(\theta \to 0) = \frac{16\pi^4}{r^2\lambda_0^4} I_o \alpha'^2_o N'^2 \tag{2-12}$$

Note $N'\alpha_o' = \alpha'$ so that equation (2-12) is the same as equation (2-4). We then define an angular scattering function $P(\theta)$ as

$$P(\theta) = \frac{R(\theta)}{R(0)} = \frac{1}{N'^2}\sum_{l=1}^{N'}\sum_{m=1}^{N'} \frac{\sin(q\, r_{lm})}{q\, r_{lm}} \tag{2-13}$$

After developing $\sin(q\, r_{lm})$ into a Taylor series and retain the two leading terms, the result reads

$$P(\theta) = 1 - \frac{q^2}{6N'^2}\sum_{l=1}^{N'}\sum_{m=1}^{N'} r_{lm}^2 + \cdots \tag{2-14}$$

where $\frac{1}{2N'^2}\sum_{l=1}^{N'}\sum_{m=1}^{N'} r_{lm}^{\ 2}$ is defined as the mean square of radius of gyration $R_g^{\ 2}$. Thus

$$P(\theta) = 1 - (1/3)q^2 R_g^{\ 2} + \cdots \tag{2-15}$$

which is related to the conformation of the larger particles and that is why it is also called the structure factor (or form factor). For N independent larger particles in volume V, equation (2-11) can be re-written as

$$R(\theta) = \frac{16\pi^4 N}{V\lambda_0^4}\alpha' P(\theta) \tag{2-16}$$

Interestingly, it is noted that when the above discussion is applied to a homogeneous pure gas or liquid, one will find that the scattered intensity is zero in all directions except in the direction of incident beam. It is because for any selected small scattering element in the scattered volume we can always find another one whose electric field at point p is counterweight of the former by interference. Then the scattered waves will exactly cancel each other. All the volume elements can be paired up in this way. However, in a real case, light scattering does exist, even for pure gas and liquid of small molecules. It is because the all of the small molecules move randomly all the time and cause a density fluctuate for an individual volume element from the average property. The light waves scattered by individual elements will have different amplitudes and thus they will not canceled completely by interference. Thus, polarization volume α_l' of a scattering unit l will also more or less deviate its most probable value α_o' as $\alpha_l' = \alpha_o' + \delta\alpha_o'$, and the existence of $\delta\alpha_o'$ leads to the light scattering of pure gas and liquid.

Followed the above treatment, we can divide scattering volume V into N scattering units and substitute α_o' in equation (2-7) with $\alpha_o' + \delta\alpha_o'$. The term α_o' will not make any contribution to scattered intensity, so that only the term $\delta\alpha_o'$ needs to be considered. Then equation (2-7) can be re-written as

$$\overrightarrow{E_s} = \sum_{l=1}^{N}\overrightarrow{E_{s,l}} = -\frac{4\pi^2}{\lambda_0^2 r}\overrightarrow{E_0}\sum_{l=1}^{N}\delta\alpha'_l \exp[i(2\pi\nu t - \phi_l)] \tag{2-17}$$

Similar to equation (2-8), taking time-average scattered intensity and following the definition of Rayleigh ratio, we can rewrite the equation (2-17) as

$$R(\theta) = \frac{16\pi^4}{V\lambda_0^4} \sum_{l=1}^{N}\sum_{m=1}^{N} \delta\alpha'_l \, \delta\alpha'_m \exp[i\vec{q}(\vec{r_m} - \vec{r_l})] \tag{2-18}$$

where $\delta\alpha_l'$ and $\delta\alpha_m'$ are random functions of time and space. To further average equation (2-18) over time, we could separate the terms in the double sum into terms for which $l = j$ and $l \neq j$, and we have

$$R(\theta) = \frac{16\pi^4}{V\lambda_0^4}\left[\sum_{l=1}^{N}\sum_{m=1}^{N} <(\delta\alpha'_l)^2> + \sum_{l\neq m}^{N}\sum_{m=1}^{N} <\delta\alpha'_l \, \delta\alpha'_m> \exp[i\vec{q}(\vec{r_m} - \vec{r_l})]\right] \tag{2-19}$$

The fluctuation of $\delta\alpha_l'$ and $\delta\alpha_m'$ are independent of each other and $<\delta\alpha> = 0$. Therefore, $<\delta\alpha_l'\delta\alpha_m'> = <\delta\alpha_l'><\delta\alpha_m'> = 0$ and equation (2-19) turns to be

$$R(\theta) = \frac{16\pi^4}{V\lambda_0^4}\left[\sum_{l=1}^{N}\sum_{m=1}^{N} <(\delta\alpha'_l)^2>\right] \tag{2-20}$$

The time-average fluctuation of polarization volume of the small scattering unit, $<(\delta\alpha_l')^2>$ should be a constant and is written as $<(\delta\alpha_o')^2>$. Thus, $\sum_{l=1}^{N}\sum_{m=1}^{N} <(\delta\alpha'_l)^2> = N^2<(\delta\alpha_l')^2>$ and equation (2-20) turns to be

$$R = \frac{16\pi^4}{V\lambda_o^4} N^2 \cdot <(\delta\alpha'_o)^2> = \frac{16\pi^4}{V\lambda_o^4} \cdot <(\delta\alpha')^2> \tag{2-21}$$

where we have used the relation $\delta\alpha' = N\delta\alpha_o'$. Next we need to find the expression of $<(\delta\alpha')^2>$. For a macromolecule solution or a colloid dispersion, α' is a function of concentration C and density ρ. $\delta\alpha' = (\partial\alpha'/\partial C)\,\partial C + (\partial\alpha'/\partial\rho)\partial\rho$. Since C and ρ are independent of each other, we have

$$<(\delta\alpha')^2> = (\frac{\partial\alpha'}{\partial C})^2 <(\delta C)^2> + (\frac{\partial\alpha'}{\partial\rho})^2 <(\delta\rho)^2> \tag{2-22}$$

So, for a dilute solution, equation (2-21) becomes

$$R_{\text{solution}} = \frac{16\pi^4}{V\lambda_o^4}(\frac{\partial\alpha'}{\partial C})^2 <(\delta C)^2> + \frac{16\pi^4}{V\lambda_o^4}(\frac{\partial\alpha'}{\partial\rho})^2 <(\delta\rho)^2> \tag{2-23}$$

where $\frac{16\pi^4}{\lambda_0^4}(\frac{\partial\alpha'}{\partial C})^2 <(\partial C)^2>$ and $\frac{16\pi^4}{\lambda_0^4}(\frac{\partial\alpha'}{\partial\rho})^2 <(\partial\rho)^2>$ are the excess Rayleigh ratio of the solution (R_{excess}) and that of the solvent (R_{solvent}), respectively. R_{excess} is the net scattering intensity of the solute by subtracting the intensity of solvent from that of

the solution. According to Clausius-Mossotti equation (7), ε_r -1 = $4\pi\alpha'/V$ and $\varepsilon_r = n^2$, we obtain

$$(\frac{\partial\alpha'}{\partial C}) = (\frac{\partial\alpha'}{\partial\varepsilon_r})(\frac{\partial\varepsilon_r}{\partial n})(\frac{\partial n}{\partial C}) = \frac{n}{2\pi}(\frac{dn}{dc}) \tag{2-24}$$

On the other hand, we know from thermodynamics that the concentration fluctuation can be expressed as $<(\delta C)^2> = \frac{k_B T}{(\partial^2 A/\partial C^2)_{T,V}}$ and $(\frac{\partial^2 A}{\partial C^2})_{T,V} = -\frac{1}{CV_m}(\frac{\partial\mu}{\partial C})_{T,V}$, where V_m and μ are respectively the partial volume and chemical potential of the solvent. And the change in concentration can cause the change in osmotic pressure, namely,

$$(\frac{\partial\mu}{\partial C})_{T,V} = (\frac{\partial\mu}{\partial\pi})_{T,V}(\frac{\partial\pi}{\partial C})_{T,V} = -(\frac{\partial\mu}{\partial P})_{T,V}(\frac{\partial\pi}{\partial C})_{T,V} = -V_m(\frac{\partial\pi}{\partial C})_{T,V}.$$

In dilute macromolecular solution, $\frac{\pi}{C} = \frac{RT}{M}(1 + A_2CM + \cdots)$ where A_2 is the second-order virial coefficient. Thus

$(\frac{\partial\pi}{\partial C})_{T,V} = \frac{RT}{M}(1 + 2A_2CM + \cdots)$ and $<(\delta C)^2> = \frac{CM}{N_A V(1 + 2A_2CM + \cdots)}$

Now substitute $<(\delta C)^2>$ and equation (2-24) into the expression of R_{excess}, we have

$$R_{\text{excess}} = \frac{4\pi^2 n^2}{\lambda_o^4 N_A}(\frac{dn}{dC})^2 \frac{CM}{1 + 2A_2CM + \cdots} \tag{2-25}$$

Rearrange equation (2-25) by defining $K = 4\pi^2 n^2 (dn/dC)^2 / (N_A \lambda_0^4)$, we get

$$\frac{KC}{R} = \frac{1}{M} + 2A_2C + \cdots \tag{2-26}$$

where we omit the footnote "excess" in R_{excess}. For larger macromolecules, construction factor must be introduced, thus

$$\frac{KC}{R(\theta)} = \frac{1}{MP(\theta)} + 2A_2C \tag{2-27}$$

The last question in deriving basic equation of SLS is the polydispersity in real cases. From equation (2-15) we know $P(\theta)$ = 1-(1/3)$q^2R_g^2$ + ···. Thus, in the limit of vanishing concentration $C \to 0$,

$$R(\theta) = KCMP(\theta) = KCM[1-(1/3)\, q^2R_g^2 + \cdots] \tag{2-28}$$

Considering the additive nature of the excess Rayleigh ratio, for a polydispersed polymer solution at $C \to 0$

$$R(\theta) = \sum_i R(\theta)_i = \sum_i KC_i M_i [1 - (1/3) q^2 R_{g,i}{}^2 + \cdots] \tag{2-29}$$

If we divide equation (2-29) by the total polymer concentration $C = \sum_i C_i$, we can get

$$\frac{R(\theta)}{KC} = \frac{\sum_i C_i M_i}{\sum_i C_i} \left(1 - \frac{q^2 \sum_i C_i M_i R_{g,i}{}^2}{3 \sum_i C_i M_i} + \cdots \right) \tag{2-30}$$

or

$$\frac{R(\theta)}{KC} = M_w [1 - (1/3) q^2 < R_g{}^2 >_z + \cdots] \tag{2-31}$$

When $q^2 R_g{}^2 << 1$, omitting the higher order terms in series in equation (2-27), we get

$$\frac{KC}{R(\theta)} = \frac{1}{M_w} [1 + \frac{1}{3} q^2 < R_g{}^2 >_z] + 2A_2 C \tag{2-32}$$

This is the basic equation of SLS. The molecular weight in the equation, $M_w = \sum_i C_i M_i / \sum_i C_i$, is weight-average; and the mean square radius of gyration, $< R_g{}^2 >_z = \sum_i C_i M_i R_{g,i}{}^2 / \sum_i C_i M_i$, is z-average. It is shown that with $R(\theta)$ measured at a series of C and q, we are able to determine $<R_g{}^2>_z$ from the slope of $[KC/R(\theta)]_{C \to 0}$ versus q^2; A_2 from the slope of $[KC/R(\theta)]_{\theta \to 0}$ versus C; and M_w from $[KC/R(\theta)]_{C \to 0, K \to 0}$. The Zimm plot, i.e., $KC/R(\theta)$ versus (q^2 + kC) with k being an adjustable constant, allows both q and C extrapolations to be made on a single coordinate plane (*8, 9*). It should be noted that Equation (2-32) is valid under restrict condition, namely, the polymer solution exhibits no adsorption, no fluorescence, and no depolarized scattering. For branched structures, the Berry plot ($[KC/R(\theta)]^{1/2}$ vs q^2 + kC) is more adequately used because it often removes much of the curvature observed in the angular dependence of the Zimm plot (*10*). If the structure is expected to be large and globular, the Berry plot is not linearized but still shows upturn. In these cases, it is often appropriate to apply a modified Guinier plot, i.e., $\ln[KC/R(\theta)]$ vs q^2 + kC that

removes the upturn even more efficiently (*11, 12*).

In practice, the Rayleigh ratio is determined by a relative method, namely, by measuring the scattering intensity of a standard such as benzene or toluene, we can calculate the Rayleigh ratio of a give solution by

$$R_{vv}(\theta) = R^{o}_{vv}(\theta)\frac{I(\theta)_{solution} - I(\theta)_{solvent}}{I(\theta)_{standard}}\left(\frac{n_{solvent}}{n_{standard}}\right)^{\gamma} \qquad (3\text{-}33)$$

where the subscript "*vv*" means both the incident and the scattered light are vertically (z-axis direction in Figure 2.1) polarized; I and n are the time-average scattered light intensity and the refractive index, respectively. The term $(n_{solvent}/n_{standard})^{\gamma}$ is a refraction correction for the scattering volume and γ is a constant between 1 and 2, depending on the detection geometry of the light scattering instrument. If we take the incident light as the x-direction and the scattered light as the y-direction (i.e., $\theta = 90^{o}$), we only need to have a linear correction of the refraction in the x-direction if a slit is used to determine the scattering volume, i.e., $\gamma = 1$ because we have already seen all the scattered lights in the z-direction (vertical). On the other hand, if a pinhole with a size much smaller than the diameter of the incident beam at the center of the scattering cell, we have to correct the refraction in both the x- and z-directions, i.e., $\gamma = 2$. However, $1 < \gamma < 2$, if the pinhole size is comparable to the beam diameter. In practice, we should avoid this situation by choosing either a slit or a smaller pinhole (*6*).

2.3 Dynamic Laser Light Scattering

Motions (translational, rotational or internal motion) of colloidal particles or macromolecules in solution can be studied conveniently by using dynamic laser light scattering (DLS). Measurement at a single scattering angle gives information on the dimension of colloidal particle or macromolecules in the solution with reasonable accuracy. Unlike the static LLS version, DLS does not measure the excess scattering intensity between the pure solvent and the solution. The signal from the moving

macromolecule or particle is unambiguously separated from the signal that originates from the rest of the solution. The basic principle of DLS has been utilized in some commercial particle-sizing systems for many years. The measurement and data analysis are automated. Users only need to prepare a c lean solution simply by filtration. In recent years, DLS has also been used as the on-line detector in size exclusion chromatography (SEC) (*13*). Nowadays, the most commonly used method in quasi-elastic light scattering (QELS) is the digital technique of photon correlation spectroscopy (or optical mixing) which measures the intensity fluctuation of scattered light in time domain. Practically, there are two basic forms of optical mixing: heterodyne and homodyne (self-beating). Heterodyne mixing refers to the mix of the scattered light with a reference beam (local oscillator) unshifted or shifted in frequency from the incident light beam. In self-beating optical mixing, the scattered wave is directly detected instead of mixed with a reference signal. Here we only consider the self-beating intensity-intensity time correlation spectroscopy.

2.3.1 Power Spectrum of Scattered Light

Now we consider again an N particle scattering system with scattering volume V. We view N particl es as N scatters. Thus, the scattered electric field as well as the scattered intensity at point p in Figure 2.1 can still be expressed using equation (2-7) and (2-8) as following,

$$\vec{E}(t) = \sum_{i=1}^{N} \vec{E_i}(t) = -\frac{4\pi^2}{\lambda_0^2 r} \alpha'_o \vec{E_0} \sum_{i=1}^{N} \exp i[2\pi\nu t - \phi_i(t)] \tag{2-34}$$

and

$$I(t) \propto \sum_{i=1}^{N} \sum_{j=1}^{N} \exp i \vec{q}[\vec{r_i}(t) - \vec{r_j}(t)] \tag{2-35}$$

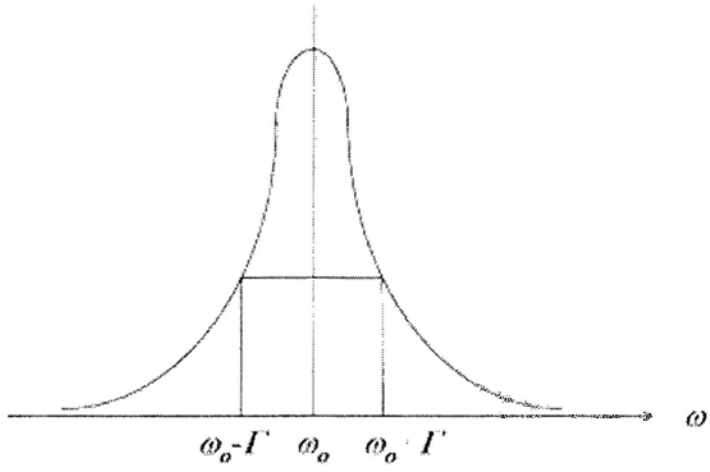

Figure 2.3 The power spectrum S(ω) of scattered light: a Lorentzian optical frequency distribution centered by the angular frequency of the incident light ω_0 with line width of Γ.

Note $\phi_i(t)$ represents the phase term of ith particle and is now a function of time due to the motion of the particles. Same situation should be applied to $I(t)$ and $\Delta\phi_{ij}(t)$ because $\Delta\phi_{ij}(t) = \vec{q}\cdot\vec{r}_{ij}(t)$ and $\vec{r}_{ij}(t)$ will have different orientation at different time t. When the scattered particles are undergoing Brownian motion, $\vec{E}(t)$ has a randomly modulated phase. The light scattered is broadened in frequency with an optical frequency distribution, or power spectrum $S(\omega)$ as shown in Figure 2.3.

Since the motion of the particles has no preferred direction, the optical spectrum of scattered light contains a continuous distribution of frequencies, i.e., Lorentzian distribution centered by ω_0, the angular frequency of the incident light:

$$S(\omega) = \frac{2\Gamma}{\Gamma^2 + (\omega - \omega_o)^2} \tag{2-36}$$

It can be seen from Figure 2.3 and equation (2-36) that when $\omega = \omega_o$, $S(\omega) = 2/\Gamma$; and when $\omega = \omega_o \pm \Gamma$, $S(\omega) = 1/\Gamma$, which means that when the scattered frequency shifts a distance of Γ from ω_o, the density function of power spectrum $S(\omega)$ is half the value that of its peak value. For this reason, Γ is called the half-width at half-height, or simply, line-width. As mentioned before, it is difficult to measure Γ (or $S(\omega)$) directly in frequency domain because $\Gamma << \omega_o$. It is known from mathematics that $S(\omega)$ and the field-field autocorrelation function $\langle E(0)E^*(t)\rangle$ are a

pair of Fourier transform and inverse Fourier transform:

$$< E(0)E^*(t) > = \int_{-\infty}^{\infty} S_x(\omega)\exp(-i\omega\, t)\mathrm{d}\omega \qquad (2\text{-}37)$$

$$S(\omega) = \frac{1}{2\pi}\int_{-\infty}^{\infty} < E(0)E^*(t) > \exp(i\omega\, t)\mathrm{d}t \qquad (2\text{-}38)$$

These two equations are known as Wiener-Khintchine theory. Thus, $S(\omega)$ and $<E(0)E^*(t)>$, two functions originally located in frequency domain and time domain respectively, are now connected with each other.

2.3.2 Siegert Relation (6)

Another important equation in DLS is Siegert relation. Without a local oscillator (i.e., a constant fraction of the incident light reaching the detector from various intentional sources, such as surface reflection or scratching), the self-beating of the scattered electric field leads to normalized intensity-intensity autocorrelation function, $g^{(2)}(q,t)$ based on the Sieget relation:

$$\mathrm{g}^{(2)}(q,t) = 1 + \left|g^{(1)}(\mathrm{q},t)\right|^2 \qquad (2\text{-}39)$$

where $g^{(2)}(q,t) \equiv [<I(q,0)I(q,t)> / <I(q,0)>^2]$ and $g^{(1)}(q,t) \equiv [<E(q,0)E^*(q,t)> / <E(q,0)E^*(q,0)>]$ is the normalized field-field time correlation functions. Thus, the intensity-intensity time correlation function

$$G^{(2)}(q,t) = <I(q,0)I(q,t)> = <I(q,0)>^2\, g^{(2)}(q,\, t) = <I(q,0)>^2[1+ \mid g^{(1)}(q,\, t)|^2] \qquad (2\text{-}40)$$

The significance of introducing $g^{(2)}(q,t)$ and $G^{(2)}(q,t)$ lies in the fact that $G^{(2)}(q,t)$ and $<I(q,0)>$ can be measured experimentally. In practice, the detection area cannot be zero. Therefore, the scattered light detected cannot be purely coherent and an instrument parameter, β (<1), is introduced in equation (2-40):

$$G^{(2)}(q,t) = A(1+\beta\left|\, g^{(1)}(q,t)\,\right|^2) \qquad (2\text{-}41)$$

where $A(\equiv< I(q,0) >^2)$ is the baseline, t is the delay time, β is a parameter depending on the coherence of the detection optics, and $I(t)$ is the detected scattered intensity or photon counts at time t, including contributions from the solvent and the solute. Therefore, $G^{(2)}(q,t) =< [I_{solvent}(q,0) + I_{solute}(q,0)][I_{solvent}(q,t) + I_{solute}(q,t)] >$ and

equation (2-41) becomes

$$G^{(2)}(q,t) = A\{1 + \beta[\frac{I_{solvent}}{I_{solution}} | g^{(1)}_{solvent}(q,t)| + \frac{I_{solute}}{I_{solution}} | g^{(1)}_{solute}(q,t)|]^2\} \quad (2\text{-}42)$$

where all the cross terms have been cancelled by assuming that the light scattered by solvent molecules and particles is not correlated. It should be noted that $|g^{(1)}_{solvent}(q,t)|$ decays much faster than $|g^{(1)}_{solute}(q,t)|$ because small solvent molecules diffuse faster than larger particles. Thus, after a very short delay time, equation (2-42) changes to

$$G^{(2)}(q,t) \cong A[1 + \beta(\frac{I_{solute}}{I_{solution}})^2 | g^{(1)}_{solute}(q,t)|^2] = A[1 + \beta_{app}\left|g^{(1)}_{solute}(q,t)\right|^2] \quad (2\text{-}43)$$

where $\beta_{app} = \beta(I_{solute}/I_{solution})^2$. For a dilute solution, the scattered intensity from solvent molecules could become appreciable (i.e., $I_{solute} \leq I_{solution}$) and thus the apparent coherence β_{app} would be lower, i.e., $G^{(2)}(q,0)$ appears to have a low value than expected. We should be aware of this situation, especially for weakly scattered dilute and low-molar-mass polymer solution. For example, if $I_{solute} = I_{solvent}$, $\beta_{app} = \beta/4$. In fact, I_{solute} can be estimated from β_{app} if the values of β at different scattering angles have been pre-calibrated with a narrowly distributed latex standard whose scattering intensity is much stronger than that of the solvent, as first demonstrated by Sun *et al.*(*14*).

2.3.3 Translational Diffusions

Next we will see how to get the information about the motion of the particles from the measured intensity-intensity time correlation function $G^{(2)}(q,t)$. For monodispersed spherical scatters, $|g^{(1)}(q,t)|$ is theoretically represented as an exponential decay function:

$$| g^{(1)}(\mathrm{q},t)| = G\exp(-\Gamma t) \quad (2\text{-}44)$$

where G and Γ are the factor of proportionality and the line-width, respectively, and $\Gamma = \tau_c^{-1}$, the characteristic decay time representing the rate of dynamic relaxation in self-beating. For a polydispersed polymer sample with a continuous distribution of

molecular weight M, equation (2-44) may be transformed to

$$|g^{(1)}(q,t)| = \int_0^\infty G(\Gamma)\exp(-\Gamma t)d\Gamma \qquad (2\text{-}45)$$

where $G(\Gamma)$ is the line width distribution and $G(\Gamma)d\Gamma$ is the statistic weight of the particles or macromolecules which possess line width Γ. For a dilute solution, Γ measured at a finite scattering angle is related to C and q by

$$\Gamma = q^2 D(1 + k_d C)(1 + f\, q^2 < R_g^2 >_z) \qquad (2\text{-}46)$$

where D is the translational diffusion coefficient of the solute at C approaching to 0, k_d is the diffusion second virial coefficient, and f is a dimensionless parameter depending on the polymer chain structure and solvent (*15*). Hence, for small C and q, $D \approx \Gamma/q^2$ and it is apparent that $|g^{(1)}(q,t)|$ decays faster at a higher scattering angle. Figure 2.4 shows the linear dependence of the line with Γ on the scattering vector q and indicates that this relaxation mode has diffusive character.

It should be noted that by the definition of $|g^{(1)}(q,t)|$, $G(D) = q^2 G(\Gamma)$, the translational diffusion coefficient distribution is an intensity distribution. And because

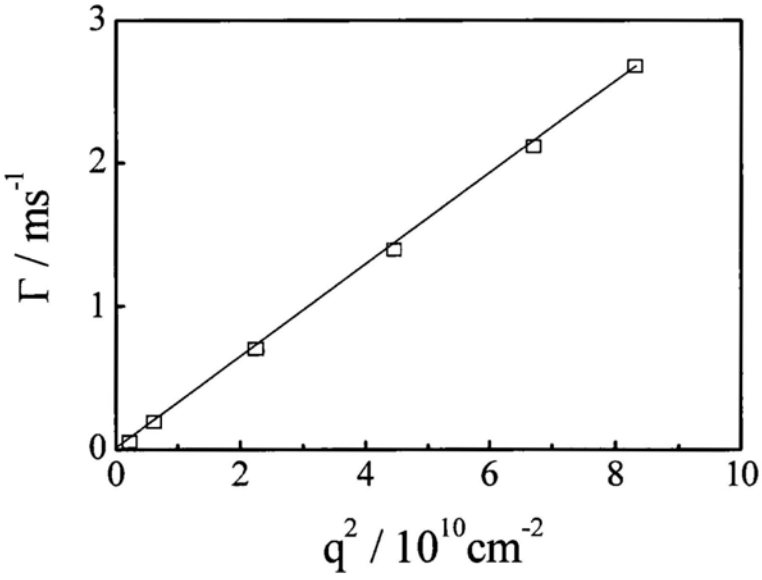

Figure 2.4. Linear dependence of the characteristic line width Γ on scattering vector q.

$|g^{(1)}(q,t)|$ approaches unity when $t \to 0$, we now have

$$|g^{(1)}(\mathrm{q} \to 0, t \to 0)| = \frac{\langle E(q,0)E^*(q,t \to 0)\rangle}{\langle \mathrm{E(q,0)E}^*(q,0)\rangle} = \int_0^\infty G(\Gamma)\mathrm{d}\Gamma = \int_0^\infty G(D)dD = 1 \qquad (2\text{-}47)$$

The average diffusion coefficient <*D*> can be defined as

$$< D >= \int_0^\infty G(D)D\ dD \qquad (2\text{-}48)$$

Further, the translational diffusion coefficient D may be related to the molecular friction factor f through the Stokes-Einstein equation

$$D = k_B T / f \qquad (2\text{-}49)$$

where k_B and T are the Boltzmann constant and the absolute temperature, respectively. For a hard sphere with a radius of R, $f = 6\pi\eta R$, where η is the viscosity of the solvent. For a polymer coil, R is replaced by its hydrodynamic radius R_h, so finally we get

$$R_h = \frac{k_B T}{6\pi\eta D} \qquad (2\text{-}50)$$

2.3.4 Analysis of the Correlation Function

Equation (2-45) shows that once $|g^{(1)}(q,t)|$ is determined from $G^{(2)}(q,t)$ through equation (2-41), $G(\Gamma)$ and then $G(D)$ can be computed from the Laplace inversion of $|g^{(1)}(q,t)|$ (*16, 17*). In the recent three decades, many computation programs were developed, among of which the CONTIN program developed by Provencher is one of the most widely used and accepted programs for the computation (*18*). However, note that equation (2-41) is one of the first kind Fredholm integral equations, whose inversion is an ill-conditioned problem because of the bandwidth limitation of photon correlation instruments, some unavoidable noises in the measured time correlation function, and a limited number of data points. That is to say the data of $g^{(1)}(q,t)$ do not always provide information necessary and sufficient to determine $G(\Gamma)$ uniquely. Thus, in practice, reducing the noise in the measurement of intensity-intensity time correlation function

becomes more important than choosing a program for data analysis. For this reason, it is crucial that the sample is cleaned (i.e., made "dust-free") very thoroughly before measurements. A common principle is to keep the relative difference between the measured and calculated baselines not exceeding 0.1%. The error analysis related to the above problem can be found elsewhere (*19, 20*).

It is worth to note that there is a temptation among the users of DLS to extract too much information from the intensity-intensity time correlation function measured. In some l iteratures, three or even four peaks in $G(D)$ were reported. Actually, it is meaningless because they were extracting "data" from experimental noises. It has to be warned that even a bimodal distribution of $G(D)$ has to be justified by pre-experimental knowledge or other physical evidence. This does not mean that the Laplace inversion programs developed in the past are useless. On the contrary, they have been quite successful in retrieving the desired information, especially in terms of the average line width $<\Gamma>$ ($\equiv \int_0^\infty \Gamma G(\Gamma)d\Gamma$) and the relative width ($\mu_2/<\Gamma>^2$) of the line-width distribution ($G(\Gamma)$) with $\mu_2 = \int_0^\infty (\Gamma - <\Gamma>)^2 G(\Gamma)d\Gamma$. Therefore, the Laplace inversion is a very helpful method in analyzing the line width distribution $G(\Gamma)$, and should be used with a full understanding of its ill-conditioned nature and limitations.

In practice, if one is only interested in the determination of $<\Gamma>$ and $\mu_2/<\Gamma>^2$, a limited but fast cumulants analysis method adopted by Koppel can be used (*21*), wherein $[G^{(2)}(q,t)$ -A]/A is expanded as

$$\ln \frac{G^{(2)}(q,t) - A}{A} = (1 + \ln \beta) - <\Gamma> t + \frac{\mu_2 t^2}{2!} - \frac{\mu_3 t^3}{3!} + \cdots \qquad (2\text{-}51)$$

where

$$\mu_m = \int_0^\infty (\Gamma - <\Gamma>)^m G(\Gamma)\mathrm{d}\Gamma \qquad (2\text{-}52)$$

is the mth moment of the line-width distribution $G(\Gamma)$. A mth order cumulants fit means that all the terms higher than t^m in equation (2-51) are terminated in the data analysis. The first cumulant Γ, also called the initial slope, is an important parameter,

because it can be calculated for many physical systems (*22, 23*). The second cumulant μ_2 is a measure of the width of the distribution. For unimodal distributions of slightly polydisperse polymers in solution, the following relation has been derived (*23*):

$$\mu_2 / \bar{\Gamma}^2 \approx (M_z / M_w - 1) / 4 \qquad (2\text{-}53)$$

It is worth noting that, in practice, the cumulants fit can be used for a relatively narrow characteristic line-width distribution. For $\mu_2/\langle\Gamma\rangle^2 < \sim 0.2$, the second order cumulants fit is normally sufficient, while when $\mu_2/\langle\Gamma\rangle^2$ is in the range ~ 0.2-0.3, the third order cumulants fit is required. For even higher values of $\mu_2/\langle\Gamma\rangle^2$, higher order expansions should be used. Generally, it is difficult, however, to find how many terms are sufficient to obtain a reliable result, since too many terms in the cumulants fit might lead to an over-fitting of experimental noises. Therefore, for a widely-distributed sample, the use of cumulants fit is tedious. By contrary, by using CONTIN fit, it may yield reliable $\langle\Gamma\rangle$ and $\mu_2/\langle\Gamma\rangle^2$ values under all conditions as long as the measured time correlation function was obtained within a proper bandwidth range and the photon counts have sufficient statistics. However, it has been warned that the line-width distribution obtained from the Laplace inversion is an estimate only. So, one should be aware of the limitations, and must realize that the Laplace inversion methods can provide useful information and distinguish between unimodal and multimodal line-width distributions.

2.4 Combination of Static and Dynamic Light Scattering

In many cases, a direct combination of z-average mean square radius of gyration ($\langle R_g \rangle$) and the average hydrodynamic radius ($\langle R_h \rangle$) leads to a very useful dimensionless parameter in determining polymer or particle structure. For example, for a uniform non-draining sphere and a linear flexible coiled polymer chain in a good solvent, the value of $\langle R_g \rangle / \langle R_h \rangle$ is ~ 0.774 and 1.5, respectively. For a normal hyper-branched polymer, such a ratio is ~ 1.0-1.3, depending on the branching degree (*24-26*).

The volume-excluding effect on the $\langle R_g \rangle / \langle R_h \rangle$ for linear chains was estimated qualitatively by Weill and des Cloiseaux (*27*) on the basis of scaling arguments. Akcasu et al. continued their study in a quantitative manner on the basis of blob model (*28*). Weill et al. showed that for a long linear chain in a good solvent, as the molecular weight increases, due to the hydrodynamic draining, $\langle R_h \rangle$ increases slower than $\langle R_g \rangle$, which induce $\langle R_g \rangle / \langle R_h \rangle \sim M^{0.05}$, i.e., $\langle R_g \rangle / \langle R_h \rangle$ increases as M_w increases. More exact calculations had been carried out by Tanaka and Stockmayer for small excluded volume based on the perturbation theory (*29*).

2.5 Practice of Laser Light Scattering

Figure 2.5 shows the layout of the modern commercial light scattering spectrometer (ALV/SP-125 equipped with an ALV-5000 multi-τ digital time correlator) used in our laboratory. Its components include the light source, the optics, the cell holder and the detector. Nowadays, a LLS instrument also should have a digital output (single photon counting) from a fast photomultiplier, i.e., the output current pulse have already

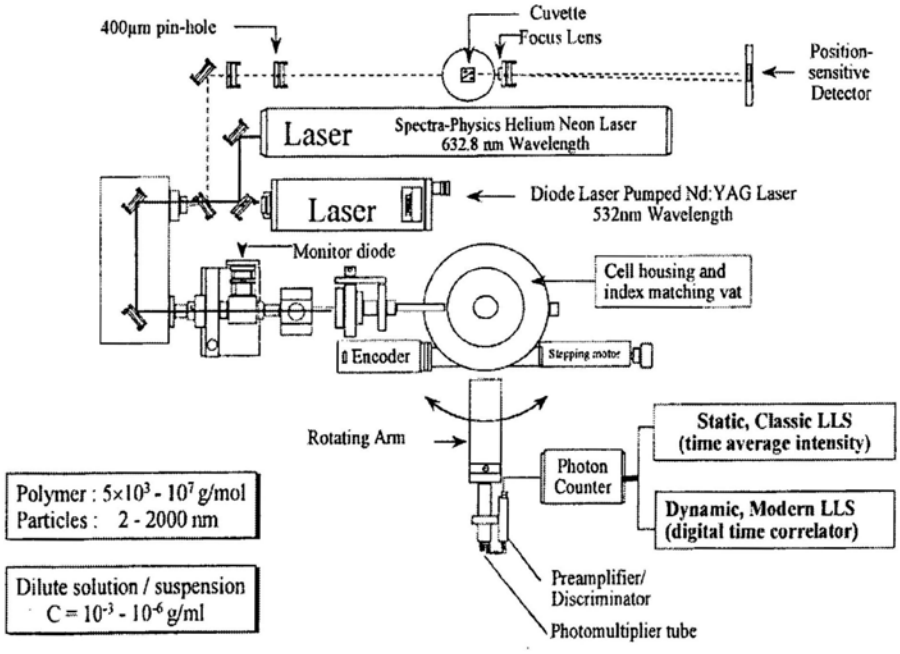

Figure 2.5. Laser Light Scattering Spectrometer incorporated with differential refractometer.

been treated by pre-amplifier/amplifier/discriminator before it is connected to a time correlator which is often a single plug-in board to a computer.

2.5.1 Light Source

Generally, the light source is a helium-neon (He-Ne) laser with a wavelength of 632.8 nm and an output power ranging from 5-50 mW or an argon-ion (Ar^+) laser with a wavelength of 488 or 514.5 nm and an output power of 50-400 mW. Krypton lasers can be also used as the source because of their longer wavelength.

The laser used in DLS should have a TEM_{00} mode with a Gaussian intensity profile make it be focused to produce a higher power density for the incident beam leading to a smaller scattering volume and a higher coherent factor in the optical mixing experiment. A laser with a beam amplitude RMS noise less than 0.5% should be chosen as the source so that the noise level of the intensity-intensity time correlation function in DLS will not be affected and long-term amplitude stability less than ±1% for the convenience of time-averaged scattered light intensity measurements. It should be noted that in DLS measurements, long-term stability is usually not very important because the maximum delay time normally is no more than minutes, typically less than one second.

2.5.2 Optics and Cell Design

The mechanical parts of Laser Light Scattering instrument is called goniometer including a cell holder, a co-axial and rotatable arm for accurate angular-controlling and the fast and sensitive avalanche photo diode (APD) detector which is installed on the arm. The conventional sample cell holder in LLS normally consists of a hollow cylindrical brass block with an outside diameter of 50-80 mm and an inside diameter of 10-20 mm which matching the outside diameter of the scattering cell. The brass block is normally placed inside a cylindrical optical glass cup filled with a refractive index matching fluid (e.g, xylene, toluene, and silica oil) with refractive index very close to that of optical glass (~1.5) to reduce surface scattering and the curvature of

the scattering cell. A water circulation from a thermostat controls the temperature of index matching vat precisely. A proper alignment of the optical path is normally judged by the constant scattered intensity for benzene or toluene after scattering volume correction by sinθ to within 1% (if the scattering volume is chosen by a slit) or 2% (if a small pinhole is used) over an angular range ~ 15-150°. In principle, the scattering cell with an optical quality should be used. However, in practice, a selected normal cylindrical sample vial can also be used as the scattering cell, which greatly reduces the experimental cost and make the scattering cell disposable.

2.5.3 Detector

An avalanche photo diode (APD) detector in Geiger mode with high quantum efficiency is used. APD detector has a higher photon count rate than a conventional photo multiplier tube (PMT), leading to a faster and more sensitive response to photon. Overall quantum efficiency of 70% at 633 nm is reachable for modern APDs, which is very suitable for the light source (λ = 632.8 nm) used, as the range of wavelength for the maximum performance of the detector lies between 600 nm to 750 nm. The output signal is then treated by an amplifier before it is connected to the multiple tau digital time correlator situated in a computer. The APDs show a very low dark count (< 30 Hz) contribution and response to signal pulse quickly enough for DLS sampling. The rotatable arm makes the APD detector able to get both dynamic and static data at variable angles.

2.5.4 Sample Preparation

If a macromolecule sample can be dissolved in more than one solvent, to choose a proper solvent for the LLS measurement, one should follow the be guidelines below: 1) no light absorption at certain wavelength to avoid the adsorption correction, 2) a higher contrast, i.e., a higher refractive index increment (*dn*/*dC*), and 3) less polar and less viscous to make the dust-free easier.

2.5.5 Differential Refractometer

To have a good accuracy in the measurements of M_w, $\langle R_g^2 \rangle_z$ and A_2, the specific refractive index increment (*dn/dC*) must be evaluated with a high accuracy because the relative error in *dn/dc* is doubled in the errors in M_w, $\langle R_g^2 \rangle_z$ and A_2. The *dn/dc* is usually measured by using a differential refractometer for the polymer solutions at different concentrations in the dilute regime. Fitting the plot of Δn as a function of c by a straight line through the origin gives the value of *dn/dc* by the slope. The measurement of *dn/dc* must be carried out at the same temperature and the same wavelength as those in the light-scattering measurement.

In a refractometer developed in our laboratory (*30*), a small pinhole with a diameter 400 μm is illuminated with laser light. The illuminated pinhole is imaged to a position sensitive detector by a lens located at an equal distance (2*f*-2*f*) form the pinhole and the detector. A temperature-controlled refractometer cuvette is placed in front of the lens. When sample was injected into the cuvette, the displaced light beam refracted at the boundary between the sample and reference liquid from the center of the detector was transferred into output voltage and measured by a digital voltmeter. Since the laser source of the set up can be changed, by choosing a laser source with the same wavelength of the source used in Laser Light Scattering experiment, correction is no needed. This novel design has made the measurement of Δn much easier and provides reliable and accurate values of *dn/dC* from the instrument's stability.

Reference and Notes

(1) Zimm, B. H. *J. Chem. Phys.* **1948**, *16*, 1099.

(2) Cummins, H. Z.; Knable, N.; Yeh, Y. *Phys. Rev. Lett.* **1964**, *12*, 150.

(3) Brown, W. Ed., *Dynamic Light Scattering: The method and some applications*, Clarendon Press: Oxford, 1993.

(4) Brown, W. Ed., *Light Scattering: Principles and Development*, Clarendon Press: Oxford, 1996.

(5) Chu, B. *Laser Light Scattering: Basic Principles and Practice*, 2nd ed.; Academic Press: New York, 1991.

(6) Berne, B. J.; Pecora, R. *Dynamic Light Scattering*, John Wiley & Sons Press: New York, 1972.

(7) Atkins, P. W. *Physical Chemistry*; 6th ed., Oxford University Press: Oxford, 1998.

(8) Zimm, B. H. *J. Chem. Phys.* **1948**, *16*, 1099.

(9) Burchard, W. *Light Scattering Techniques* In *Physical Techniques for Study of Food Biopolymers;* Ross-Murphy, S. B., Ed., Blackie Academic & Professional: London, 1995, Chapter 4.

(10) Berry, G. C. *J. Chem. Phys.* **1966**, *44*, 4550.

(11) Guinier, A. *Ann. Phys.* **1939**, *12*, 161.

(12) Guinier, A.; Fournet, G. *Small Angle Scattering of X-rays*; Wiely: New York, 1955.

(13) Wu, C.; Chu, B. *Light Scattering* In Tanaka, T. Ed., *Experimental Methods in P olymer Science*, Academic Press: San Diego, 2000. pp 1-56.

(14) Sun, S. T.; Nishio, I.; Swislow, G.; Tanaka, T. *J. Chem. Phys.* **1980**, *73*, 5971.

(15) Stockmayer, W. H.; Schmidt, M. *Macromolecules* **1984**, *17*, 509.

(16) Chu, B.; Ford, J. R.; Dhadwal, H. S. *Methods Enzymol.* **1983**, *117*, 256.

(17) Chu, B.; Wu, C.; Ford, J. R. *J. Colloid Interface Sci.* **1985**, *105*, 473.

(18) Provencher, S. W. *J. Chem. Phys.* **1976**, *64*, 2772.

(19) Raczek, J. *Eur. Polym. J.* **1983**, *19*, 607.

(20) Nordmeier, E.; Lechner, M. D. *Polym. J.* **1989**, *21*, 623.

(21) Koppel, D. E. *J. Chem. Phys.* **1972**, *57*, 4814.

(22) Akcasu, Z. *Polymer*, **1980**, *21*, 866.

(23) Akcasu, Z.; Han, C. C. *Polymer*, **1981**, *22*, 1019.

(24) Burchard, W.; Schmidt, M.; Stockmayer, W. H. *Macromolecules*, **1980**, *13*, 1265.

(25) Burchard, W.; Schmidt, M.; Stockmayer, W. H. *Macromolecules*, **1980**, *13*, 580.

(26) Douglas, J. F.; Roovers, J.; Freed, K. F. *Macromolecules*, **1990**, *23*, 4168.

(27) Weill, G.; des Cloiseaux, J. *J.Physique*, **1979**, *40*, 99.

(28) Akcasu, A. Z.; Benmouna, M. *Macromolecules*, **1978**, *11*, 1193.

(29) Tanaka, G.; Stockmayer, W. H. *Proc. Natl. Acad. Sci.*, **1982**, *79*, 6401.

(30) Wu, C., Xia, K.Q. *Review of Scientific Instruments*, **1994**, *65*, 587.

Chapter 3

Disulfide-Linked Low Molecular Weight PEI with Controllable Chain Length and Structure in Non-Viral Gene Delivery

3.1 Introduction

The development of non-viral vectors for gene transfection has attracted more and more interest in recent years because of their enhanced safety, biocompatibility, facile preparation and high flexibility to accommodate different sizes of DNAs in comparison with viral vectors (*1-4*). Non-viral vectors are mostly made of cationic surfactants or polymers. Hundreds, if not thousands, of synthetic polymers or copolymers have been prepared and tested in the last few decades, but polyethylenimine (PEI) is still regarded as one of the most effective non-viral vectors. Its high gene transfection efficiency is believed to originate from the so-called intrinsic "proton sponge" effect (*5-8*); namely, partially protonated PEI absorbs more protons inside endocytic vesicles embedded with some ATPase proton pumps, accompanied by an influx of chloride counter-ions, ultimately rupturing endocytic vesicles due to a higher osmotic pressure.

It has been known that long PEI chains are highly effective in gene transfection, but more cytotoxic (*9-11*). To circumvent such a catch-22 problem, short PEI chains are linked by some degradable linkers, i.e. ester, β-aminoester and disulfide, for the development of higher efficient and lower cytotoxic non-viral vectors in recent years (*10, 12-18*). The former two linkers have a hydrolysis half-life time ranging from hours to days. In contrast, the reduction of a disulfide is fast in the presence of glutathione (GSH) in cytosol (*19-21*). Disulfide linkers can react with primary amine groups on PEI with a neutral or a preserved cationic linkage. It has been reported that dithiobis(succinimidyl propionate) (DSP), yielding a neutral amide inking bond, leads to a higher gene transfection efficiency than those with some charge-preserved linkages (*14, 22*). It was also reported that some DSP-linked branched PEI chains are highly effective and nearly non-toxic (*13, 14*).

However, Kloeckner et al. (*14*) found that conditions of the linking reaction strongly affect the final molar mass and chain structure. Even for a given linker/PEI molar ratio, different groups obtained products with significantly different molar masses (*12, 13*). Most of previous studies only listed the linker/PEI ratio instead of the actual average molar mass. To develop a useful macromolecular biomaterial, it is important to control its molar mass and structure before we study how its biomedical properties are affected by the chain length and structure. Previously, a mixture of DMSO and water was always used to dissolve PEI (*12*) because it is apparently insoluble in pure DMSO. The shortcoming of such a mixture solvent is that water inactivates DSP because it hydrolyses both active ester terminus in the reaction mixture (*23*) or losses one proton-capture amine group on PEI by inactivating only one termini on DSP.

In the current study, we found that it is carbon dioxide in the air that ionizes PEI and makes PEI insoluble in pure DMSO. Therefore, after the complete removal of water and carbon dioxide, PEI becomes soluble in pure DMSO so that we can avoid the side reaction. Further, we developed an in-situ laser light-scattering (LLS) method to monitor the linking reaction in terms of the increase of the chain length. In this way, we can repeatedly obtain linked PEI chains with a desired molar mass. Armed with these well-defined PEI samples made of short PEI2K chains, we studied effects of the chain length and structure on their cytotoxicity and *in vitro* gene transfection efficiency.

3.2 Experimental Section

Materials and Cell Lines. Two branched PEIs (M_w = 2,000 g/mol, PEI2K; and M_w = 25,000 g/mol, PEI25K), dithiobis(succinimidyl propionate) (DSP), disuccinimidyl suberate (DSS) and D,L-dithiothreitol (DTT) were purchased from Sigma-Aldrich and used without further purification. Dimethyl sulphoxide (DMSO) was freshly dried under a reduced pressure before use. The PEI/DMSO solution was clarified by a 0.2-μm filter under the protection of N_2. Plasmid DNA pGL3 (5,256 bp) with a SV40 promoter and an enhancer sequences encoding luciferase was purchased from

Promega (Madison, USA). Plasmid DNA pLUNIG-LIGL, a lentivirus vector with an enhanced green fluorescent protein (GFP) and a luciferase reporter gene was constructed in house. Lipofectamine 2000 (Lipo) was purchased from Invitrogen. Fetal bovine serum (FBS), phosphate buffered saline (PBS) and Dulbecco's modified Eagle's medium (DMEM) were products of GIBCO (NY, USA). 3-(4, 5-dimethylthiazol-2-yl)-2, 5-diphenyltetrazolium bromide (MTT) was purchased from Sigma-Aldrich (Deutschland). Bright-Glo assay kit and DNaseI kit were purchased from Promega (Madison, USA), respectively. 293T cells were grown in DMEM supplemented with 10% FBS and 1% penicillin-streptomycin in a humidified environment with 5% CO_2 at 37 ℃.

Linking of short PEI2K chains with DSP and DSS. As shown in Figure 3.1, we developed a laser light-scattering (LLS) device to in-situ monitor the linking reaction. The dust-free DSP/DMSO solution with a concentration of 1.0×10^{-2} g/mL was slowly injected into a PEI2K/DMSO solution (4.6×10^{-2} g/mL) with a rate of 0.1 or 0.5 mL/h by a programmable syringe pump (Kd Scientific). The solution mixture was vigorously mixed. A commercial LLS spectrometer (ALV/DLS/SLS-5022F) was used to monitor the scattering intensity change during the linking reaction. Note that during each LLS measurement, the stirring was stopped. A container filled with

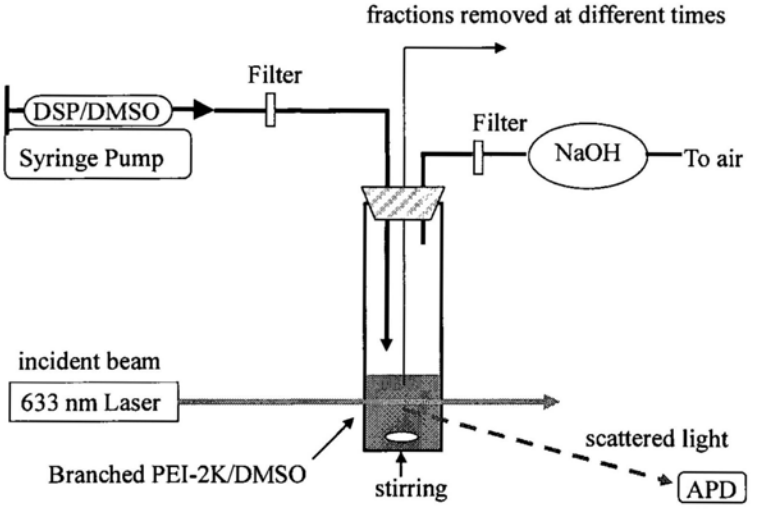

Figure 3.1. Schematic of a recently developed reaction device to link polyethyleneimine (PEI) with dithiobis(succinimidyl propionate) (DSP) with an in-situ laser light scattering monitor.

NaOH was used to keep the solution mixture away from both water and carbon dioxide. A fraction of the reaction mixture was withdrawn by a syringe at different times, i.e., different DSP/PEI ratios. Each extraction was diluted with deionized water to stop the linking reaction and then dialyzed in deionized water, where a membrane with a cut-off molar mass of 500 was used.

Transmission Electron Microscopy. The samples for the transmission el ectron microscopy (TEM) studies were prepared using negative staining with 1% uranyl acetate. Briefly, a drop of the sample solution was allowed to settle on a carbon film-coated copper grid for 1 min, the excess sample was wicked away with filter paper and a drop of staining solution was allowed to contact the sample for 1 min. The samples were analyzed using a FEI CM120 electron microscope.

Cytotoxicity Assay. The cytotoxicity assessment was carried out on 293T cells by using the MTT-assay. 293T cells were seeded in a 96-well plate at an initial density of ca. 5000 cells per well in 100 μL of the DMEM complete medium. After 24 h, the cells were treated with polymers at different chosen concentrations. The treated cells were incubated in a humidified environment with 5% CO_2 at 37 ℃ for 48 h. The MTT reagent (in 20 μL PBS, 5 mg/mL) was added to each well. The cells were further incubated for 4 h at 37 ℃. The medium in each well was then removed and replaced by 100 μL DMSO. The plate was gently agitated for 15 min before the absorbance (A) at 490 nm was recorded by a microplate reader (Bio-Rad). The cell viability was calculated by

$$\text{Cell viability (\%)} = (A_{treated} / A_{control}) \times 100\% \qquad (3\text{-}1)$$

where $A_{treated}$ and $A_{control}$ are the absorbance values of the cells cultured with and without PEI. Each experiment condition was done in quadruple. The data are shown as the mean value plus a standard deviation (± SD).

Formation of Polyplexes. The DNA/PEI polyplexes were prepared with different desired N:P ratios (ratios of nitrogen atoms on PEI to phosphorus on plasmid DNA) by adding an appropriate amount of PEI to 2 μg of plasmid DNA (plasmid pGL3) in PBS. The resultant polyplexes were incubated for 10 min at the room temperature before use.

Such prepared polyplexes were analyzed by the gel retardation assay, in which the polyplexes were mixed with a buffer and then loaded on a 0.8 % agarose gel containing EtBr in TBE buffer. The gel electrophoresis was run at 80 V for 1 h and then photographed under UV. The DNA/Lipofectamine 2000 complexes were prepared according to the supplier's protocol (*24*). In DNase assay, 2 units of DNaseI was added respectively to the plasmid DNA and the polyplexes, containing 1 μg of DNA, and incubated for 1 h at 37 °C. Before conducting the gel electrophoresis, 1 μL stop buffer was added and incubated at 65 °C for 15 min to stop the reaction.

A commercial laser light scattering (LLS) instrument (ALV5000) with a vertically polarized 22 mW He-Ne laser head (632.8 nm, Uniphase) was used to determine the particle size. In dynamic LLS (DLS), the Laplace inversion of each measured intensity-intensity time correlation function $G^{(2)}(q,t)$ in the self-beating mode can be related to a line-width distribution $G^{(2)}$. For a diffusive relaxation, Γ is related to the translational diffusion coefficient D by $(\Gamma/q^2)_{(C\rightarrow 0,q\rightarrow 0)} = D$, so that $G(\Gamma)$ can be converted into a transitional diffusion coefficient distribution G(D) or a hydrodynamic radius distribution $f(R_h)$ via the Stokes-Einstein equation, $R_h = (k_BT/6\pi\eta)/D$, where k_B, T, and η are the Boltzmann constant, the absolute temperature, and the solvent viscosity, respectively.

The zeta-potential of the polyplexes dispersed in the PBS (1×10^{-2} μg/mL pDNA) was measured by a commercial Brookhaven Zeta Plus spectrometer with two platinum-coated electrodes and one He-Ne laser as the light source. The current was fixed at 10 mA and at least 30 cycles were measured for each polyplexes dispersion at the room temperature.

***In vitro* Gene Transfection.** The *in vitro* gene transfection efficiency was quantified by using the luciferase transfection assays, in which plasmid pGL3 was used as an exogenous report gene. 293T cells were plated in a 48-well plate at an initial density of ~ 50,000 cells per well, 24 h prior to the gene transfection. The polyplexes were further diluted in a serum-free medium and then added to each well. The final plasmid DNA concentration is 0.4 μg per well in a total volume of 300 μL. The complete DMEM medium (1 mL for each well) was added 4 h after the transfection.

The gene expression was determined after 48 h by using a GloMax 96 Microplate Luminometer (Promega, USA). Meanwhile, the protein concentration in each well was determined by the Bio-Rad protein assay reagent (Bio-Rad, USA). The transfection efficiency is expressed as a relative light units (RLU) per mg protein in each well (mean ± SD, triplicates). The transfection efficiency can also be directly visualized by a fluorescent microscope when the plasmid pLUNIG-LIGL (10 kbp) is used. The transfection procedure of using the two different plasmids was identical.

3.3 Results and Discussion

After trying to use some previously reported procedures of linking short PEI chains with DSP (*13, 14*), we found that PEI is insoluble in DMSO if there exists carbon dioxide (Figure 3.2) because it reacts with PEI to form ammonium carbonate in the presence of a trace amount of H_2O. To the best of our knowledge, such a phenomenon has not been reported before. In the presence of CO_2 and a trace amount of H_2O, the reaction mixture is inhomogeneous. The addition of H_2O into DMSO can dissolve the ionized PEI chains (*12*), but some side reactions become inevitable. Therefore, we found that in order to make the linking reaction controllable, one has

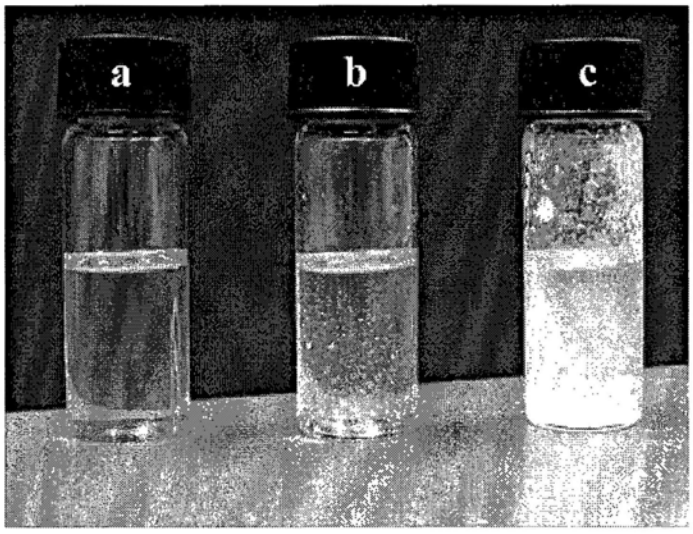

Figure 3.2. Photograph of PEI2K/DMSO solution (c = 0.01 g/mL). a) Freshly prepared solution. Note that there is already some flocculation formed in the dissolving process. b) PEI2K/DMSO solution exposed in air for 2 min. c) PEI2K/DMSO solution bubbled CO_2 for 5 seconds.

to completely remove CO_2 and H_2O from the reaction mixture.

Since branched PEI chains have more than two $-NH_2$ groups, the linking reaction can easily lead to the formation of microgels if it is not done properly. Previous work reported by Gosselin et al. (*13*) and Kloeckner et al. (*14*) used an equal or excessive amount of DSP so that their reaction mixture has to be purified by a column to remove microgels or even macrogels, which makes the process more complicate and expensive with a poorly controlled molar mass and a low yield. Particularly, for a given [linker]:[PEI] ratio, they obtained two linked PEI samples with different molar masses (2.3×10^4 and 8.0×10^3 g/mol). It is well known that a controllable molar mass is an essential requirement for a FDA approval.

Furthermore, we found that after the removal of carbon dioxide and water, it is also vitally important to control how fast DSP is added into the PEI/DMSO solution. Namely, a quick addition of DSP leads to the formation of microgels so that the reaction mixture becomes turbid even at a low [DSP]:[PEI] ratio. In the contrast, if DSP is extremely slowly introduced, the reaction mixture remains transparent even when [DSP]:[PEI] approaches 1. To make the reaction controllable and repeatable, we used a computer-controlled syringe pump to inject DSP into the PEI/DMSO solution (Figure 3.1). During the linking reaction, LLS was used to in-situ monitor the change of the scattering intensities, i.e., the weight average molar mass (M_w) of the linked PEI chains. M_w can be calculated using:

$$M_w = M_{w,PEI2K} \times \frac{< I_0 >_{PEI}}{C_{PEI}} / \frac{< I_0 >_{PEI2K}}{C_{PEI2K}} \qquad (3\text{-}2)$$

where C_{PEI} and C_{PEI2K} are the concentrations of resultant linked PEI and initial short PEI2K chains, respectively; $<I_0>_{PEI}$ and $<I_0>_{PEI2K}$ are the time-average scattering intensities of resultant linked PEI and initial short PEI2K chains at the zero scattering angle (θ), respectively. Assuming that most of PEI2K chains are linked, we have $C_{PEI} \approx C_{PEI2K}$ so that eq. 3-2 can be rewritten as $M_w \approx M_{w,PEI2K}<I_0>_{PEI}/<I_0>_{PEI2K}$. Figure 3.3A shows that $<I>_{PEI}$ at each [DSP]:[PEI2K] ratio is independent of the scattering angle, even for linked PEI with the highest molar mass, 3.8×10^5 g/mol (denoted as

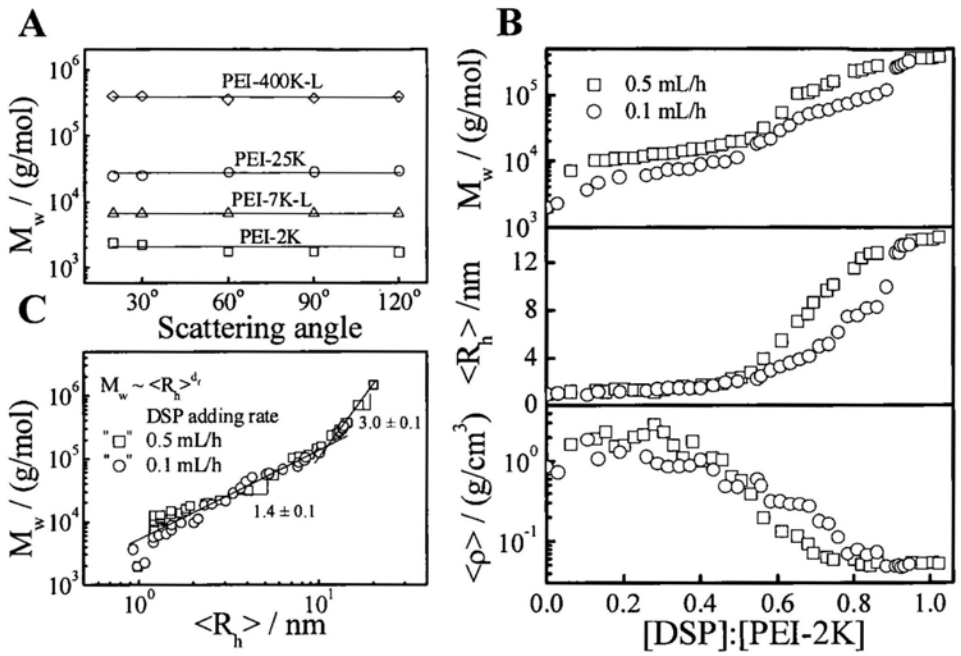

Figure 3.3. A. Angular dependence of weight average molar mass (M_w) of different polyethyleneimine (PEI) polymers in water. B. Linking reagent (DSP) content dependence of weight average molar mass (M_w), average hydrodynamic radius ($<R_h>$) and average chain density ($<\rho>$) of resultant linked PEI2K chains, where $<\rho> = M_w/[(4/3)\pi<R_h>^3]$. C. Double-logarithmic plots of weight average molar mass (M_w) vs average hydrodynamic radius ($<R_h>$) of resultant linked PEI2K chains.

PEI-400K-L), indicating that the radius of gyration ($<R_g>$) of these linked PEI chains must be smaller than 15 nm. In other words, we have $<R_g>/<R_h> < 1$ because $<R_h> = 22$ nm for PEI-400K-L in H_2O. Therefore, PEI-400K-L has a spherical microgel conformation with a more uniform chain density (*25-27*). To further testify the microgel conformation of PEI-400K-L, TEM images is taken and shown in Figure 3.4.

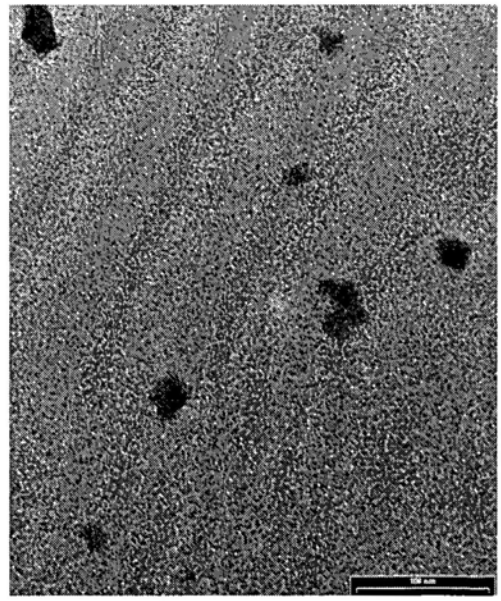

Figure 3.4. TEM image of PEI-400K-L. Bar: 100 nm.

Figure 3.3B shows how the DSP

adding rate affects the weight average molar mass (M_w), the average hydrodynamic radius ($\langle R_h \rangle$) and the average chain density ($\langle \rho \rangle$) of resultant linked PEI chains, where $\langle \rho \rangle$ is defined as $M_w/[(4/3)\pi\langle R_h \rangle^3]$. The addition of DSP at a rate of 0.5 mL/h leads to a sharp initial increase of M_w from 2×10^3 to $\sim 10^4$ g/mol even when [DSP]:[PEI2K] is only 0.1, indicating the formation of a small amount of large clusters at this initial stage. Further addition of DSP results in a gradual increase of M_w before another sharp increase of M_w from 2×10^4 to 3.8×10^5 g/mol at [DSP]:[PEI2K] ~ 1.0. Using a lower DSP adding rate of 0.1 mL/h, M_w is only 3.7×10^3 g/mol when [DSP]:[PEI2K] = 0.1, revealing that on average only two chains are linked together. In contrast, the initial increase of $\langle R_h \rangle$ is less affected by the DSP adding rate.

Figure 3.3C shows a double-logarithmic plot of M_w vs $\langle R_h \rangle$ for the linked PEI chains in DMSO. In the range of $1 < R_h < 10$ nm, $M_w \propto \langle R_h \rangle^{1.4\pm0.1}$, indicating that these linked PEI chains have a more extended linear structure with some inevitable branches. The scaling exponent (d_f) becomes 3.0 ± 0.1 when $R_h > 10$ nm, revealing that the linked PEI chains have a uniform chain density, presumably due to the formation of spherical microgels. A combination of Figures 3.3B and 3.3C shows

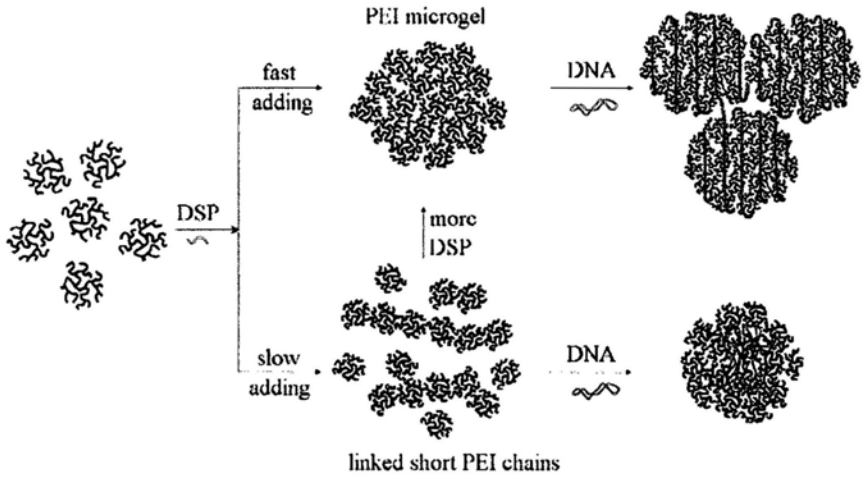

Figure 3.5. Schematic of effect of different DSP adding rates on resultant linked PEI2K chains and their corresponding complexation with plasmid DNA.

that when [DSP]:[PEI2K] ~ 0.9, spherical microgels are formed in spite of different DSP adding rates. It is worth noting that the higher DSP adding rate always results in a broader molar mass distribution. Therefore, it is better to add DSP slowly into the PEI/DMSO solution in order to obtain more linearly linked PEI chains with less branches structure, as schematically shown in Figure 3.5.

Two linked PEI samples at lower adding rate, respectively with $M_w = 7 \times 10^3$ (denoted as PEI-7K-L) and 4×10^5 g/mol (denoted as PEI-400K-L) obtained from one reaction at two different [DSP]:[PEI2K] ratios are used next. On the other hand, it is also found that the linking reaction of PEI2K by using non-degradable DSS as linker is similar to that of using DSP (data not shown). Thus a crosslinked PEI2K sample with DSS, denoted as PEI-7K-C ($M_w = 7 \times 10^3$), is also obtained for comparison in the next. Their molecular characterizations are summarized in Table 3.1.

Table 3.1. Molecular characterization of two linked PEI2K samples in different solvents.

Sample	$\frac{n_{linker}}{n_{PEI2K}}$	M_w	$\langle R_h \rangle$ / nm	
		g/mol	in DMSO	in H_2O
PEI-7K-L	2.86×10^{-1}	6.5×10^3	1.4	3.0
PEI-400K-L	1.02	3.8×10^5	14	22
PEI-7K-C	2.95×10^{-1}	7.0×10^3	1.5	3.2

Figure 3.6 shows that both M_w and $\langle R_h \rangle$ of PEI-7K-L, PEI-400K-L and PEI-7K-C remain constants in the range of pH = 7.8-4.5, revealing that disulfide bond in PEI-7K-L, PEI-400K-L and amide bond in all of the three polymers in an acidic environment are stable, which is important since the linked PEI chains should provide the same protection as long PEI25K chains in the endosomal and lysosomal compartments. In contrast, the disulfide bond can be quickly reduced by DTT under a neutral or alkaline condition. Figure 3.7 shows the reducing kinetics of the disulfide

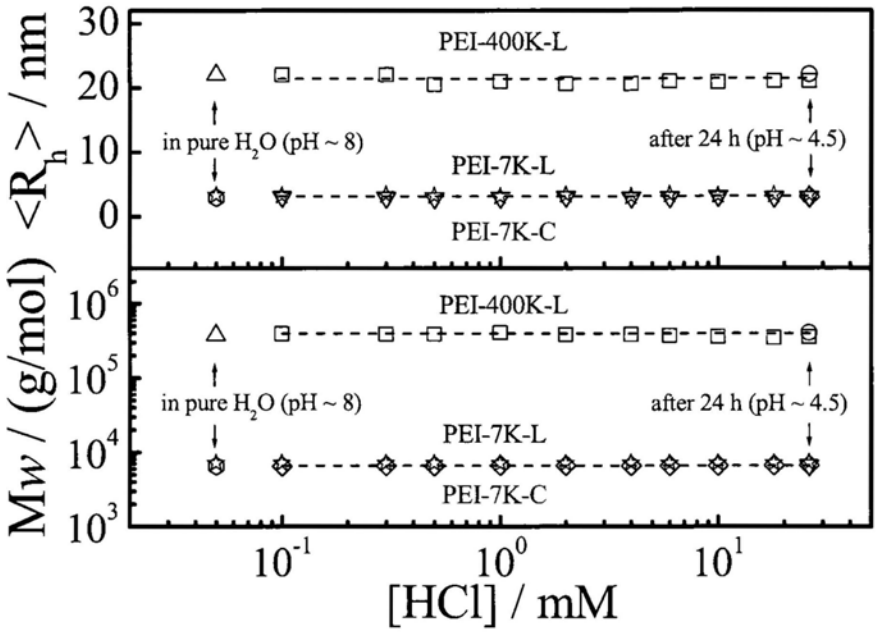

Figure 3.6. HCl concentration-dependence of stability of DSP-linked (PEI-7K-L and PEI-400K-L) and DSS-linked PEI2K chains (PEI-7K-C) in acidic solutions in terms of changes of weight average molar mass (M_w) and average hydrodynamic radius $<R_h>$.

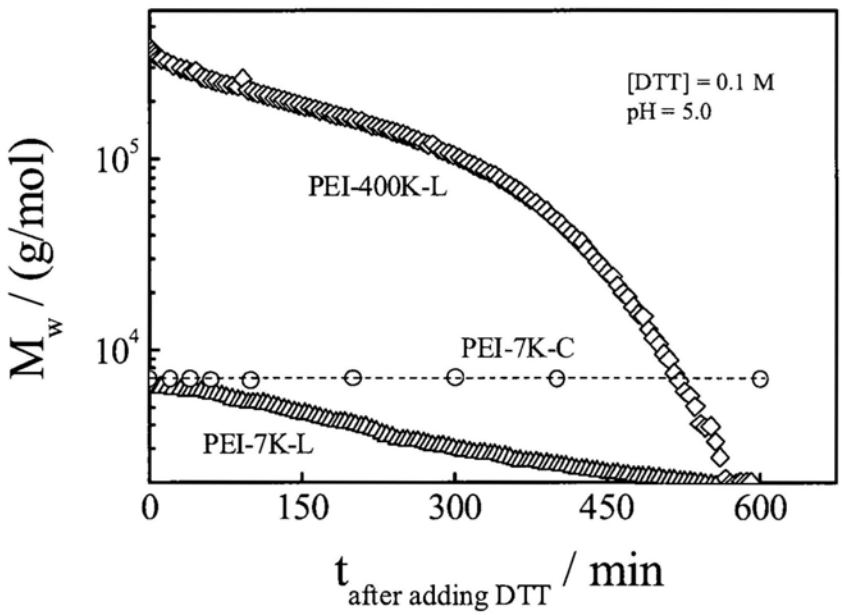

Figure 3.7. Time dependence of M_w of PEI-7K-L, PEI-400K-L and PEI-7K-C (C = 1 × 10^{-2} g/mL) with 0.1 M added D,L-dithiothreitol (DTT).

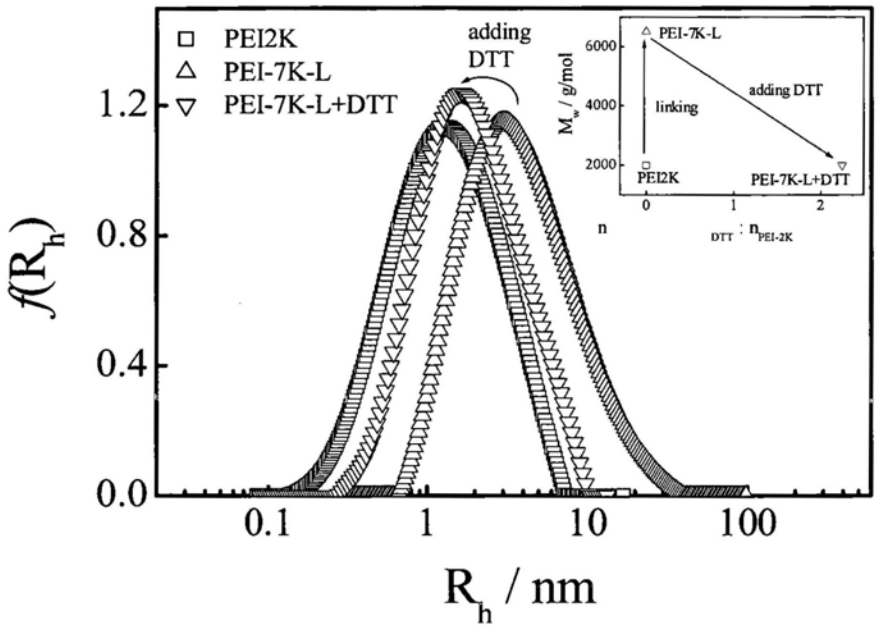

Figure 3.8. Effect of adding a reducing agent, D,L-dithiothreitol (DTT, C = 0.1 M) on hydrodynamic radius distribution ($f(R_h)$) of resultant linked PEI chains (PEI-7K-L) in water at 37 ℃. For comparison, we also plot $f(R_h)$ of initial PEI2K.

bond inside PEI-7K-L and PEI-400K-L in the presence of DTT at pH 5.0 in terms of the decrease of M_w. It is clear that the breakage of the disulfide bond takes ~10 h in both cases, revealing that the reduction of the disulfide bond in the acidic pH is a slow process. However, it should be mentioned that the disulfide degradation is nearly instantaneous at the physiological pH, which cannot be traced by LLS. On the other hand, PEI-7K-C is stable as expected in such an environment. Figure 3.8 gives a better view of the break of the disulfide bond in PEI-7K-L after the addition of a reduce agent (DTT) at pH 7.4, because both M_w and $f(R_h)$ quickly decrease to their respective values of PEI2K.

Armed with these well-characterized linked PEI chains, we studied effects of the chain length and structure on their cytotoxicity and gene transfection efficiency. The cytotoxicity was tested by using the MTT assay. Figure 3.9 shows that PEI-7K-L, PEI-400K-L and PEI-7K-C exhibit a significantly lower cytotoxicity in comparison with long PEI25K chains, but all higher than that of PEI2K. The cell viability of

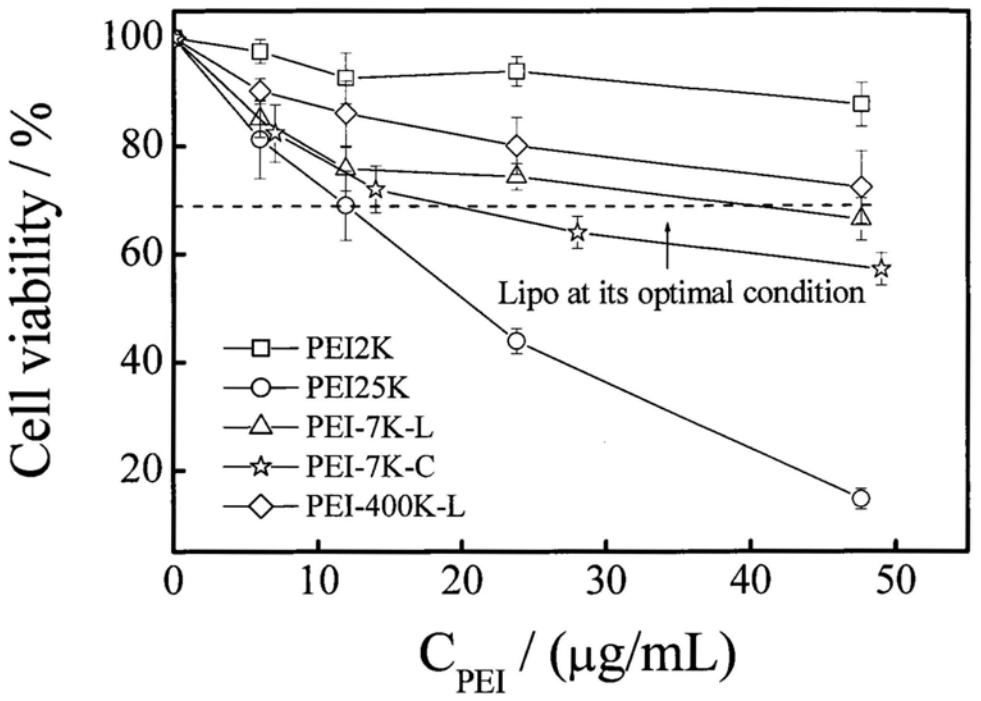

Figure 3.9. Comparison of 293T cell viability of different PEI samples.

PEI-7K-L is higher than that of PEI-7K-C, indicating that the degradation of disulfide in the cytosol could lead to the decrease of the cytotoxicity. In the working concentration range, i.e., N:P $\leq$ 120, corresponding to $C_{PEI} \leq$ 21 μg/mL, they are even less cytotoxic than or comparable to a commercial vector, Lipofectamine 2000 (Lipo), at its optimal condition based on the supplier's protocol. It is worth noting that PEI-400K-L has a much higher molar mass than PEI25K, but less cytotoxic, clearly indicating that linking short PEI chains into larger PEI molecules with disulfide bond can indeed reduce its cytotoxicity.

Further, using the gel retardation assay, we studied the condensation of DNA with different PEIs. Figure 3.10 shows that PEI25K can retard DNA at N:P = 3 and efficiently condense DNA at N:P = 5, reflecting in the disappearance of the two DNA strips. The complete complexation of DNA with PEI-7K-L occurs only when N:P > 10, indicating that PEI-7K-L is a less effective condensing agent than PEI25K. Surprisingly, PEI-400K-L is completely ineffective because the retardation appears

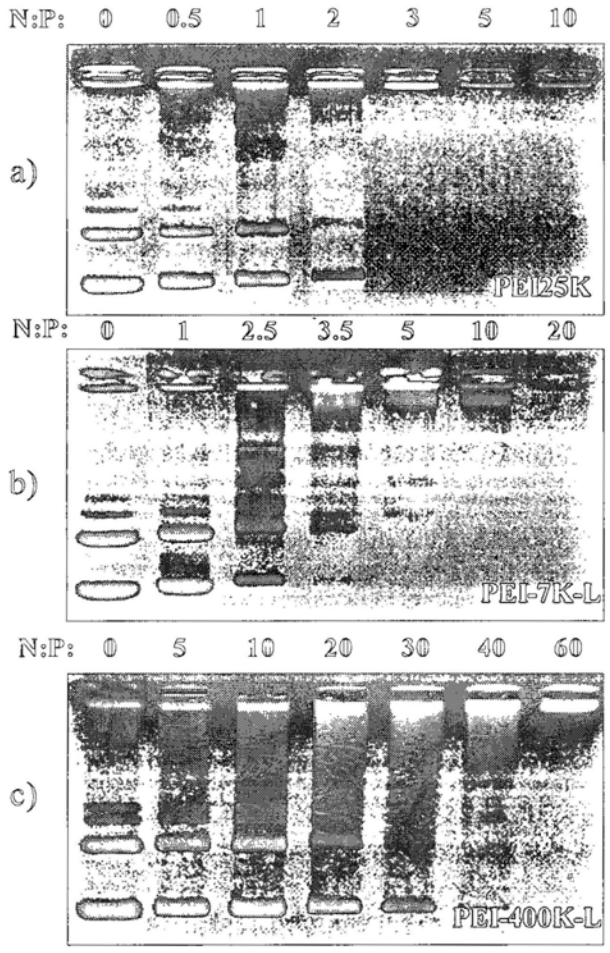

Figure 3.10. N:P ratio dependence of gel retardation assay tests of a) PEI25K, b) PEI-7K-L and c) PEI-400K-L.

only when N:P > 60. Figure 3.11 shows that the hydrodynamic radius ($\langle R_h \rangle$) of the polyplexes for each vectors measured in 30 mM NaCl. The $\langle R_h \rangle$ values of PEI25K, PEI-7K-L, PEI-7K-C and PEI-400K-L after the retardation occurs are ca. 50, 60, 60 and 80 nm, respectively. On the other hand, Figure 3.12 shows that as expected, the zeta-potential of the polyplexes in PBS changes from -55 mV to +25 mV as the N:P ratio increases. Consisting with those gel retardation results, the addition of PEI25K, PEI-7K-L or PEI-7K-C inverses the zeta-potential at N:P ~ 3 and the zeta-potential reaches a plateau at N:P ~ 5. In contrast, when PEI-400K-L is used, a much higher ratio of N:P = 30 is needed to reverse the zeta-potential. The low complexation efficiency of DNA with PEI-400K-L can be attributed to its microgel nature. It is

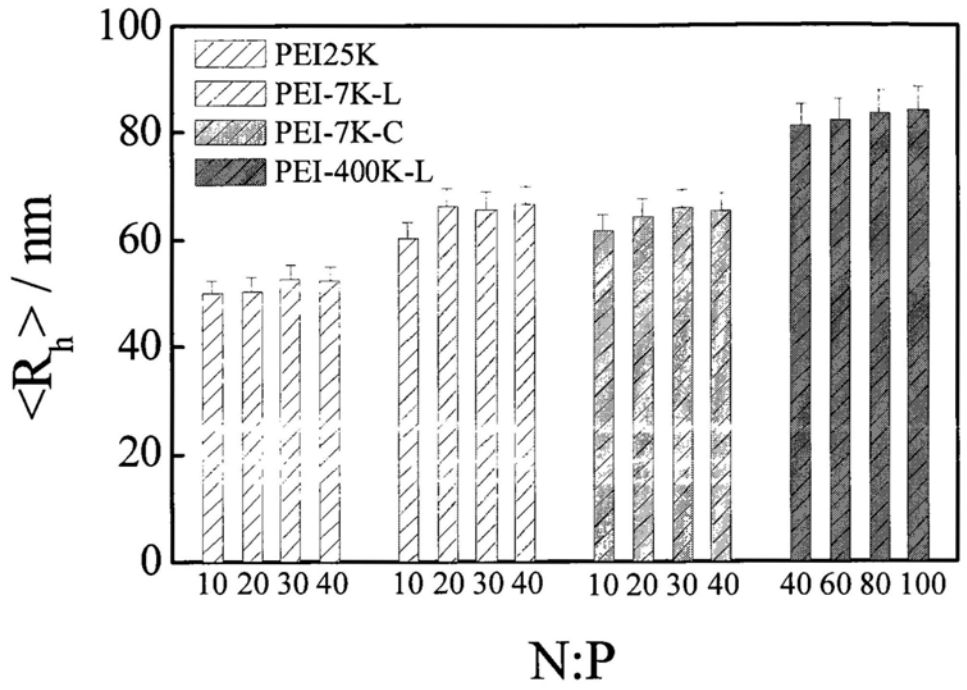

Figure 3.11. N:P ratio dependence of hydrodynamic radius (<R_h>) of different PEI/DNA polyplexes in 30 mM NaCl solution.

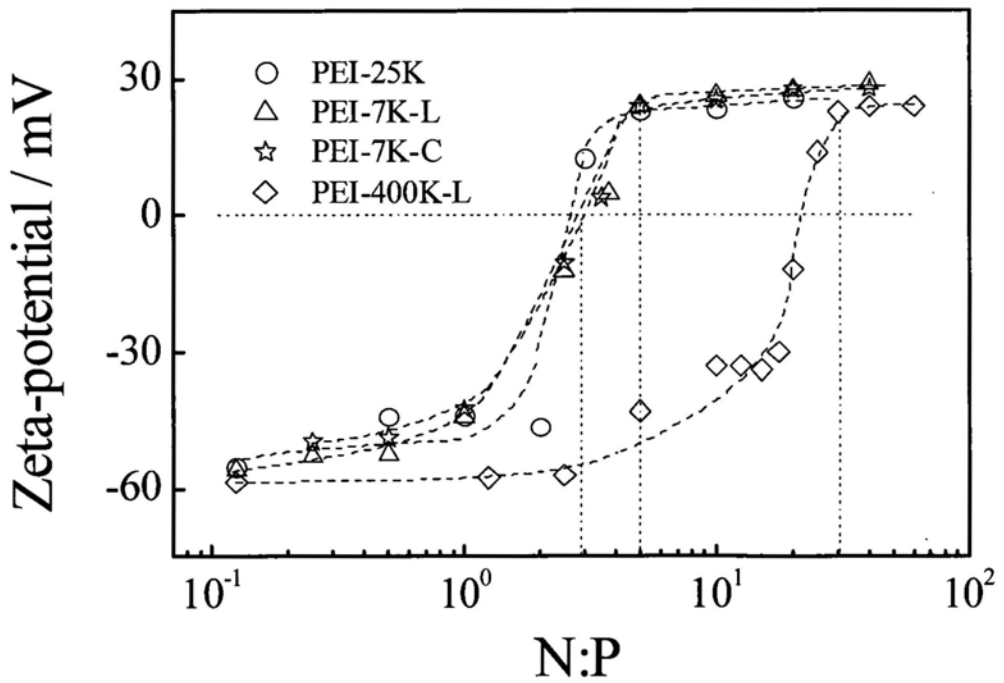

Figure 3.12. N:P ratio dependence of zeta-potential of different PEI/DNA polyplexes in PBS buffer.

supposed that, as schematically shown in Figure 3.5, DNA only wraps on the surface of the microgel, and such a DNA-winding complex is formed, resembling with the DNA chains winding around histone octamer to form nucleosome in the chromatin. With such a structure of PEI-400K-L/DNA complexes, DNA is more accessible by EtBr molecule to emit stronger fluorescence even after the DNA is retarded in gel electrophoresis test (ca. N:P > 40), while the fluorescence intensity is very weak for PEI25K or PEI-7K-L after the DNA is complexed and retarded, because the DNA is embedded by the smaller cationic PEI molecules which prevent the intercalating of EtBr into DNA helix. Such a DNA-winding structure is also proposed by some research groups through theoretic calculation and experimental results (*28, 29*). To evaluate the protection effect of the vectors against enzyme degradation, the DNaseI was added to the complexes. As shown in Figure 3.13, lane 3 shows that PEI-400K-L

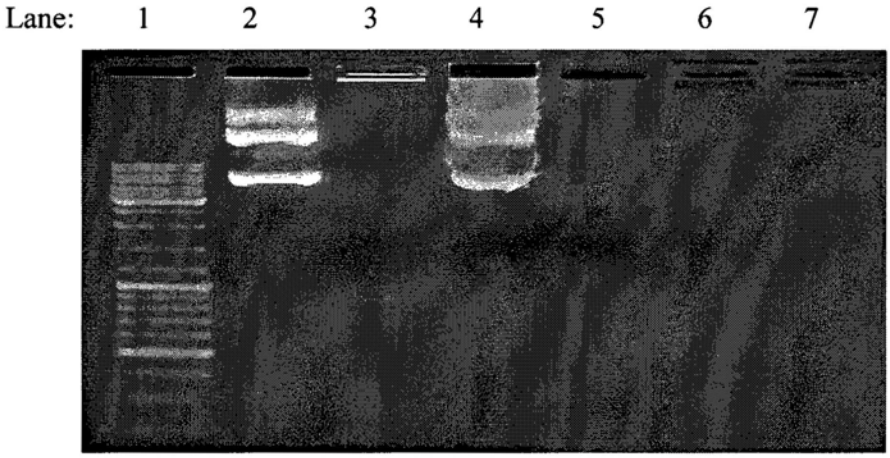

Figure 3.13. DNase assay of DNA/PEI-400K-L complexes. Lane 1 is the DNA marker; lane 2 is naked pGL3; lane 3 is PEI-400K-L/DNA complex at N:P 60; lane 4 is 2 M NaCl treated PEI-400K-L/DNA complex at N:P 60; lane 5 is digested naked pGL3 by DNaseI; lane 6 is PEI-400K-L/DNA complex at N:P 60 treated with DNaseI; and lane 7 is 2 M NaCl treated PEI-400K-L/DNA complex at N:P 60 after digested with DNaseI.

retards DNA at N:P = 60 and shows strong fluorescence in the slot. Lane 4 shows that after the addition of 2 M NaCl to the PEI-400K-L/DNA complexes, the DNA can be released again exhibiting near the same bands with naked DNA (lane 2). After the treatment of DNaseI, the naked DNA was degraded completely (lane 5). Both of the DNaseI-treated PEI-400K-L/DNA complexes before and after the addition of 2

M NaCl do not show any fluorescence (lane 6 and 7), indicating the poor DNA protection effect of PEI-400K-L comparing with PEI25K and PEI-7K-L (data not shown). Such result may prove our proposed structure of the PEI-400K-L/DNA complexes, since the DNA chains wrapping around the positively charged microgel can be easily attacked by the enzyme, while in contrast, the PEI25K and PEI-7K-L can embed and protect DNA sufficiently.

Figure 3.14 shows a comparison of *in vitro* transfection efficiencies of different PEI chains, where pGL3 is used as the report gene. PEI25K shows an optimal efficiency at N:P ~ 10, consistent with previous reports (*13, 15, 30*). Lipofectamine 2000 is ~ 6 times less efficient than PEI25K in the transfection of 293T cells. The gene transfection efficiency of PEI-7K-L is 2-10 times higher than that of PEI25K in the range of N:P = 10-60 and reaches its maximum at N:P = 30. As for PEI-7K-C, only when N:P = 30, the efficiency is marginally exceed that of PEI25K at N:P 10, implying that it is the disulfide bond rather than the molar mass resulting the enhanced gene transfection efficiency of PEI-7K-L. Such an efficiency-promoting effect of PEI-7K-L could be attributed to the quick cleavage of the disulfide bond

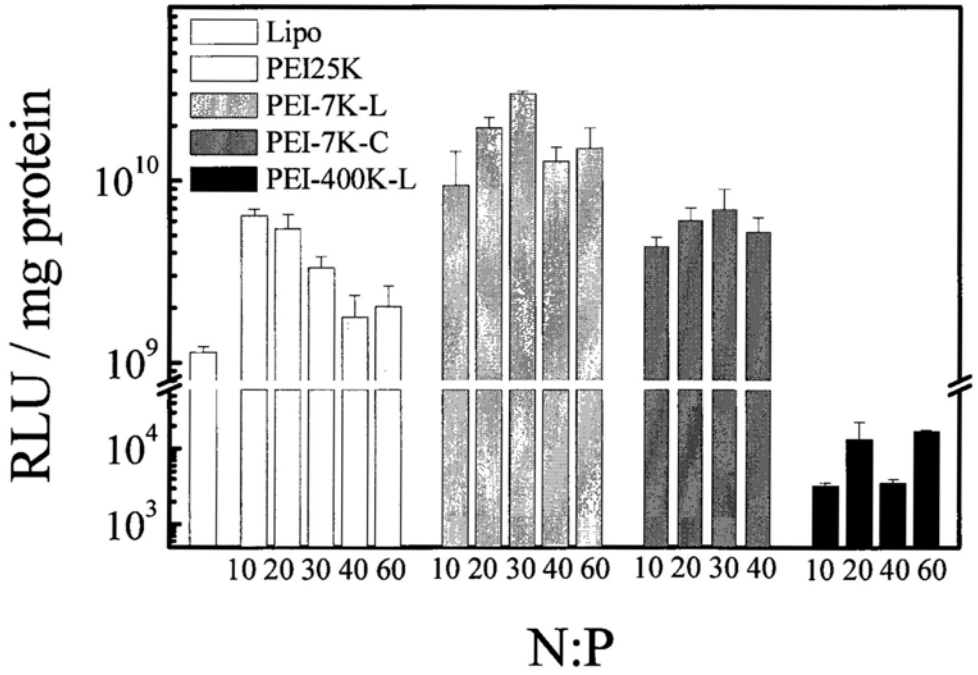

Figure 3.14. N:P ratio dependence of *in vitro* gene transfection efficiency of five different non-viral vectors.

after the endosomal escape of polyplexes and easier release of pDNA from the polyplexes. The decrease of the transfection efficiency at higher N:P ratios can be attributed to the higher cytotoxicity. These results demonstrate that the incorporation of disulfide in the linking reaction of low molar mass PEI can dramatically boost the gene transfection efficiency and lower the cytotoxicity. Again, the transfection efficiency of the DNA/PEI-400K-L polyplexes is even surprisingly lower than the naked DNA without any PEI.

The transfection efficiency can also be directly visualized with a fluorescent microscope when pLUNIG-LIGL is used as the report gene. Figure 3.15 shows that the cells transfected by the DNA/PEI-7K-L polyplexes with N:P ~ 30 express more green fluorescent proteins than those transfected by the DNA/Lipofectamine 2000

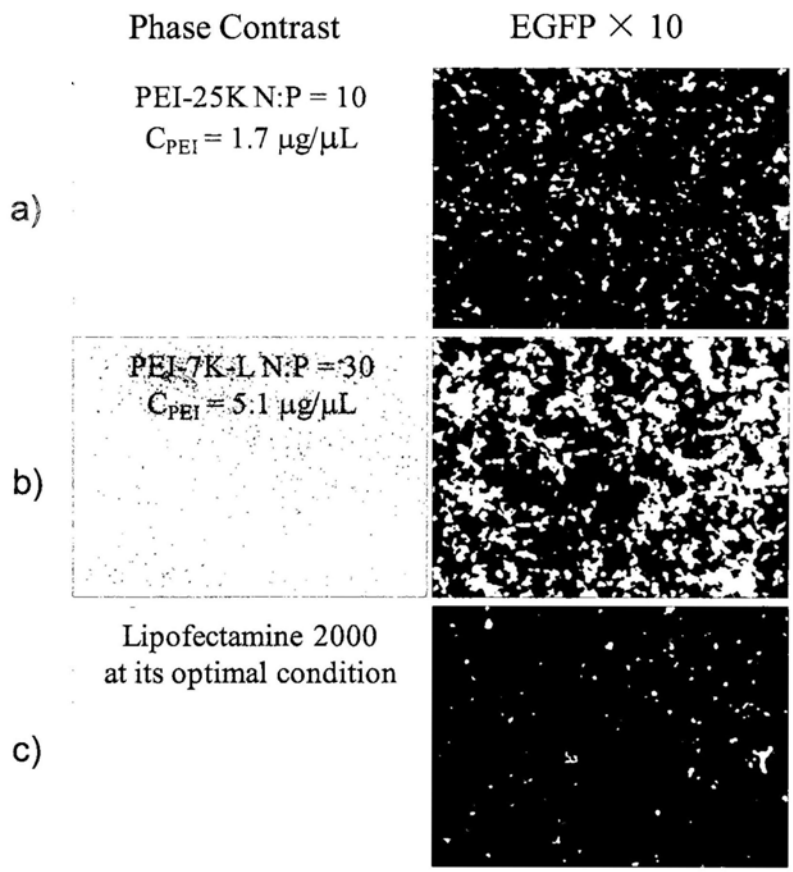

Figure 3.15. Fluorescent microscopic images of 293T cells transfected with plasmid DNA (pLUNIG-LIGL) in the presence of different PEI vectors.

and the DNA/PEI25K polyplexes, respectively, at their optimal conditions. It reveals that PEI-7K-L as an effective vector to deliver larger plasmids is much better than those reported vectors (*13, 14*). We have to reconsider previous assumption that PEI with a higher molar mass are more effective in condensing, protecting and delivering genes into a cell (*9*). Our results reveal that it is important to properly control the linking reaction to avoid the formation of a microgel structure.

3.4 Conclusion

Using a recently developed reaction device, we are able to in situ monitor the linking reaction by using in-situ laser light scattering to control the molecular parameters of the linked PEI chains. We have found that in the reaction of using dithiobis(succinimidyl propionate) (DSP) to link short polyethyleneimine (PEI) chains (M_w = 2000 g/mol), it is vitally important to remove both a trace amount of water and CO_2. The DSP adding rate as well as the amount of DSP is also vitally important for the preparation of low cytotoxic and high efficient non-viral gene transfection vectors because they affect not only the linked PEI chain length, but also the chain structure. A comparative study of the gene transfection efficiency and cytotoxicity of two such linked PEI samples (PEI-7K-L and PEI-400K-L, respectively with $M_w = 6.5 \times 10^3$ and 3.8×10^5 g/mol) reveals that PEI-7K-L with an extend linear chain structure is even less cytotoxic and 2-10 times more effective in the gene transfection of 293T cells than both the "golden standard" PEI25K and the commercially widely used Lipofectamine 2000. On the other hand, PEI-400K-L with a spherical microgel structure is ineffective in spite that it is much non-toxic. Our current study clearly demonstrates that a proper control of the chain structure is more important than that of the overall molar mass; namely, one should try to avoid the microgel formation in the linking reaction.

References and Notes

(1) Schatzlein, A. G. *Anti-Cancer Drugs* **2001**, *12*, 275.

(2) Schatzlein, A. G. *J. Biomed. Biotechnol.* **2003**, *2003*, 149.

(3) Pack, D. W., Hoffman, A. S., Pun, S., *et al. Nature Reviews Drug Discovery* **2005**, *4*, 581.

(4) Jackson, D. A., Juranek, S., and Lipps, H. J. *Mol. Ther.* **2006**, *14*, 613.

(5) Boussif, O., Zanta, M. A., and Behr, J. P. *Gene Ther.* **1996**, *3*, 1074.

(6) Baker, A., Saltik, M., Lehrmann, H., *et al. Gene Ther.* **1997**, *4*, 773.

(7) Godbey, W. T., Wu, K. K., and Mikos, A. G. *J. Controlled Release* **1999**, *60*, 149.

(8) Verkman, A. S., Sonawane, N. D., and Szoka, F. C. *J. Biol. Chem.* **2003**, *278*, 44826.

(9) Godbey, W. T., Wu, K. K., and Mikos, A. G. *J. Biomed. Mater. Res.* **1999**, *45*, 268.

(10) Fischer, D., Bieber, T., Li, Y. X., *et al. Pharm. Res.* **1999**, *16*, 1273.

(11) von Harpe, A., Petersen, H., Li, Y. X., *et al. J. Controlled Release* **2000**, *69*, 309.

(12) Thomas, M., Ge, Q., Lu, J. J., *et al. Pharm. Res.* **2005**, *22*, 373.

(13) Gosselin, M. A., Guo, W. J., and Lee, R. J. *Bioconjugate Chem.* **2001**, *12*, 989.

(14) Kloeckner, J., Wagner, E., and Ogris, M. *Eur. J. Pharm. Sci.* **2006**, *29*, 414.

(15) Peng, Q., Zhong, Z. L., and Zhuo, R. X. *Bioconjugate Chem.* **2008**, *19*, 499.

(16) Breunig, M., Lungwitz, U., Liebl, R., *et al. Proc. Natl. Acad. Sci. U. S. A.* **2007**, *104*, 14454.

(17) Ou, M., Wang, X. L., Xu, R. Z., *et al. Bioconjugate Chem.* **2008**, *19*, 626.

(18) Lin, C., Blaauboer, C. J., Timoneda, M. M., *et al. J. Controlled Release* **2008**, *126*, 166.

(19) Saito, G., Swanson, J. A., and Lee, K. D. *Advanced Drug Delivery Reviews* **2003**, *55*, 199.

(20) Schafer, F. Q., and Buettner, G. R. *Free Radical Biol. Med.* **2001**, *30*, 1191.

(21) Lee, Y., Mo, H., Koo, H., *et al. Bioconjugate Chem.* **2007**, *18*, 13.

(22) Gosselin, M. A., Guo, W. J., and Lee, R. J. *Bioconjugate Chem.* **2002**, *13*, 1044.

(23) Lomant, A. J., and Fairbanks, G. *J. Mol. Biol.* **1976**, *104*, 243.

(24) Dalby, B., Cates, S., Harris, A., *et al. Methods* **2004**, *33*, 95.

(25) Burchard, W., Schmidt, M., and Stockmayer, W. H. *Macromolecules* **1980**, *13*, 1265.

(26) Akcasu, A. Z., and Han, C. C. *Macromolecules* **1979**, *12*, 276.

(27) Brown, W. *Light Scattering - Principles and Development* Oxford Science Publication, **1996**.

(28) Nguyen, T. T., and Shklovskii, B. I. *J. Chem. Phys.* **2001**, *115*, 7298.

(29) Kabanov, V. A., Sergeyev, V. G., Pyshkina, O. A., *et al. Macromolecules* **2000**, *33*, 9587.

(30) Manickam, D. S., and Oupicky, D. *Bioconjugate Chem.* **2006**, *17*, 1395.

Chapter 4

Comparative Study of Gene Transfection Efficiency of PEI Grafted with PEG Respectively via -C-C- and -S-S- Linkage

4.1 Introduction

Nowadays, the design and preparation of effective gene delivery vectors becomes a major bottleneck in gene therapy. Besides the fast development of viral vectors, non-viral polymeric vectors as a safe and versatile alternative attracted more attention (*1*). Cationic polymers, such as poly(L-lysine) (PLL) (*2, 3*), polyethylenimine (PEI) (*4-6*), chitosan (*7*) and polyamidoamine (*8*), can condense long nucleic acid chains via electrostatic interaction to form polymer/nucleic acid complexes, termed as polyplexes, with a size of ~100 nm. The polyplexes with a slightly positively-charged surface can facilitate the cellular uptake (*9-11*). On the other hand, the positively-charged surface is problematic in *in-vivo* applications. Namely, such "naked" polypl exes tend to absorb proteins and aggregate in the physiological salt condition so that they are less effective in the gene transfection and even toxic due to their embolization in lung (*1*). The absorption of serum albumin and other negatively charged proteins can lead to a rapid clearance of them by phagocytic cells and the reticuloendothelial system (*12*).

To circumvent such problems, the surface of the polyplexes was usually modified by grafting a layer of hydrophilic polymers, such as the intensively investigated polyethylene glycol (PEG). The steric and hydrophilic shell stabilizes the polyplexes in the physiological condition, reduces their undesirable interaction with proteins, and also increases their intravenous circulation time (*1, 4, 6*). Note that the PEGylation of biological macromolecules and surfaces has been used in many pharmaceutical and biotechnical applications (*13-15*). The influences of the chain length and grafting density of PEG and the resultant structure on the condensation of DNA have been thoroughly investigated (*9, 16, 17*). The increase of the chain length and grafting density impede the DNA complexation. Short PEG chains ($M_w \leq 500$

g/mol) are not able to provide the shielding effect, while a molecular weight of at least 2,000 - 5,000 g/mol seems to be necessary to achieve such a effect (*4*). Unfortunately, to make the polyplexes "stealth" in our body via a proper PEGylation and at the same time, to increase the cell uptake create a dilemma; namely, the PEGylation normally reduces the cellular uptake, prevents the intracellular unpacking, and hampers the following release of DNA in the nuclei (*2, 9, 18-20*). The attachment of some targeting ligands at the PEG chain end can enhance the cellular uptake (*4, 17, 21, 22*). On the other hand, the pH sensitive linkages were used to promote the intracellular unpacking because of a lower pH environment inside the endolysosome (*18, 19, 23-25*). However, in a *in-vivo* app lication the hydrolysis begins when the polyplexes enter the blood circulation, and the hydrolysis rate inside the cell is normally relatively slow and difficult to control (*23, 26*). Further, the detachment of PEG from the polyplexes inside lysosomes also increases the degradation of DNA, another dilemma. In contrast, using a reductive disulfide bond to coat PEG on the surface of the polyplexes should keep the PEG shield intact in the oxidizing environment inside endo/lysosomes and promotes a fast breakage of PEG chains once the polyplex escapes from the endo/lysosomes into the cytoplasm because the disulfide is quickly reduced by glutathione (GSH) and thioredoxin (*27, 28*). To have a better understanding of the PEGylation, we prepared a pair of copolymers by linking PEG to the most extensively investigated cationic non-viral polymeric gene vectors (PEI), respectively via the -C-C- and -S-S- bonds (Figure 4.1) and conducted a comparative study of their complexation with DNA and gene transfection behavior.

4.2 Experimental Section

Materials and Cell Lines. PEI (M_w = 2.5×10^3 g/mol and M_w/M_n = 2.5) (PEI25K), N-hydroxysuccinimide (NHS) and N,N'-dicyclohexylcarbodiimide (DCC), triethylamine (TEA), methanesulfonyl chloride, 3,3'-dithiodipropionic acid (DTPA), suberic acid (SA), D,L-dithiothreitol (DTT), heparin, $NaHCO_3$, $MgSO_4$ and Et_2O were purchased from Sigma-Aldrich and used without further purification. PEG

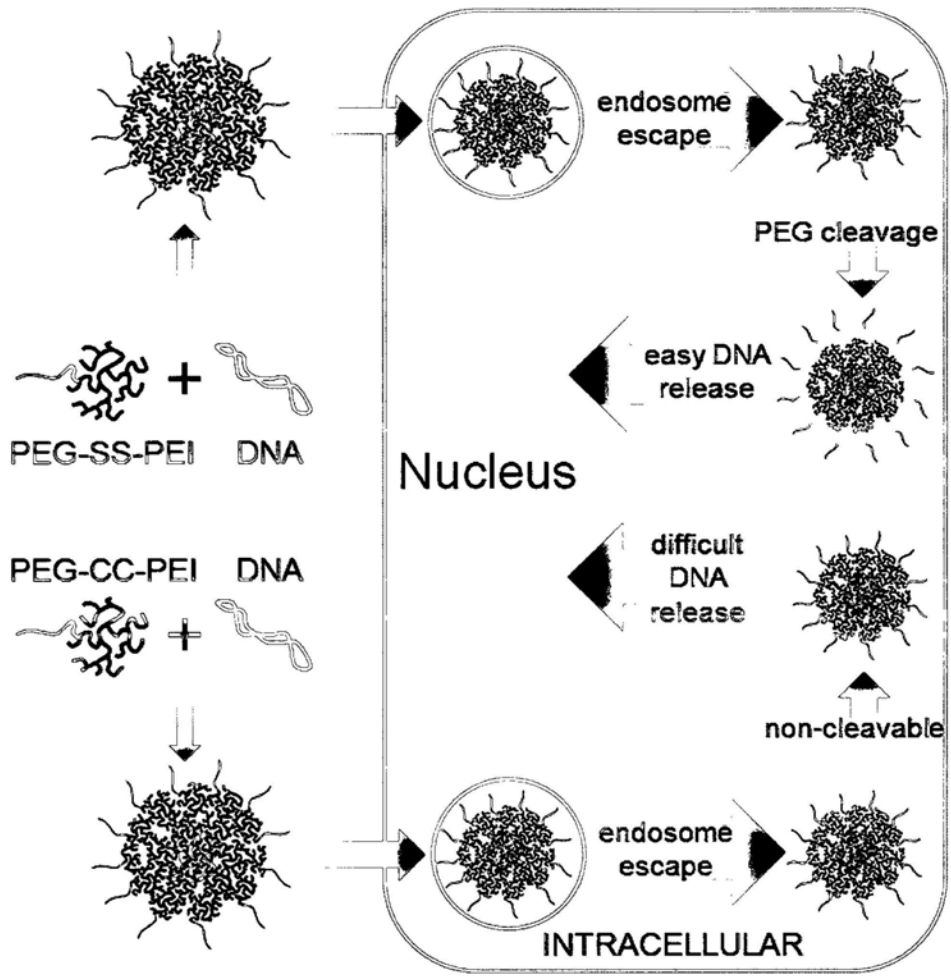

Figure 4.1. Schematic of PEG-SS-PEI/DNA and PEG-CC-PEI/DNA polyplexes formation and their respective intracellular pathway, where drawings of different components do not reflect their actual sizes.

monomethyl ether (M_w = 2.0×10^3 g/mol, M_w/M_n = 1.05) was a gift from BASF and was dried under vacuum at 110 °C for 8 hrs before use. CH_2Cl_2 and THF purchased from Merck were dried by CaH_2 and distilled before use. Dialysis membranes were purchased from Spectrum Laboratories, Inc. Plasmid DNA (pDNA) pGL3 with a SV40 promoter and an enhancer sequence encoding luciferase and Bright-Glo assay kit were purchased from Promega (Madison, USA). Fetal bovine serum (FBS), phosphate buffered saline (PBS) and Dulbecco's modified Eagle's medium (DMEM) were products of GIBCO (NY, USA). 3-(4,5-dimethylthiazol-2-yl)-2,5-diphenyltetrazolium bromide (MTT) was purchased from Sigma-Aldrich

(Deutschland). 293T cells were grown in DMEM supplemented with 10% FBS and 1% penicillin-streptomycin in a humidified environment with 5% CO_2 at 37 °C.

Synthesis of PEG-NH_2. The synthetic routes can be found elsewhere (*29*). Briefly, 10 g of PEG monomethyl ether was dissolved in 80 mL of freshly dried CH_2Cl_2, followed by the addition of 3.8 g of TEA in an ice bath. 2.3 g of methanesulfonyl chloride was added dropwise with stirring under N_2 protection. The reaction in the mixture was conducted under N_2 atmosphere at the room temperature for 12 hrs. The reaction mixture was washed with 120 mL of 50 mM $NaHCO_3$. The organic fraction was dried over $MgSO_4$ and filtered, and the solvent was evaporated to give methanesulfonylated PEG.

^1H NMR spectra were recorded on a Bruker SpectroSpin 400 MHz spectrometer, and chemical shifts for ^1H NMR spectra were reported relative to tetramethylsilane (TMS) signal in the deuterated solvent (TMS, d = 0.00 ppm). Integration of the characteristic signals in ^1H NMR spectra was used to calculate the conversation ratio and the composition of the resultant copolymers. ^1H NMR of methanesulfonylated PEG ($CDCl_3$) δ(ppm): 4.37 (t, 2H, $CH_3SO_3CH_2CH_2$), 3.6 (bs, 170H, CH_2CH_2O), 3.36 (s, 3H,OCH_3), 3.07 (s, 3H, CH_3SO_3). Then the product was immediately dissolved in 100 mL concentrated solution of aqueous ammonia and was left to stir for 48 hrs in a sealed flask. The mixture was extracted twice with CH_2Cl_2, and the organic layers were combined, dried over $MgSO_4$ and filtered. The solution was concentrated and was added to Et_2O to precipitate PEG-NH_2. ^1H NMR ($CDCl_3$) δ(ppm): 3.60 (bs, 170H, CH_2CH_2O), 3.36 (s, 3H,OCH_3), 2.90 (t, 2H, $CH_2CH_2NH_2$), 2.65(br, NH_2).

Synthesis of PEG-DTPA and PEG-SA. 3.8 g of DPTA (or SA) and 4.4 g of NHS were dissolved is 50 mL of dry THF in ice bath, 8 g of DCC in dry THF was added dropwise under N_2 protection. After stirring for 1 hr under N_2 protection, the mixture was reacted at the room temperature for 24 hrs. Further, after 4 g of PEG-NH_2 was dissolved in 40 mL of dry THF, it was added to the reaction mixture dropwise with vigorous stirring. The reaction continued for another 24 hrs, followed by the addition of 100 mL of D.I. water. Finally, THF in the reaction mixture was removed by rotary

evaporation; the insoluble by-products were removed by filtration; and the remaining solution was dialyzed against D.I. water with a membrane ($M_{cut\text{-}off}$ 500) for 24 hrs. PEG-DTPA and PEG-SA were recovered by lyophilization. ^{1}H NMR of PEG-DTPA ($CDCl_3$) δ(ppm): 6.70 (br, N*H*CO), 3.60 (bs, 170H, C*H*$_2$C*H*$_2$O), 3.37 (s, 3H,OC*H*$_3$), 2.98 (m, 4H, C*H*$_2$SSC*H*$_2$), 2.70 (t, 2H, C*H*$_2$COOH), 2.61 (t, 2H, NHCOC*H*$_2$). ^{1}H NMR of PEG-SA ($CDCl_3$) δ(ppm): 6.55 (br, N*H*CO), 3.60 (bs, 170H, C*H*$_2$C*H*$_2$O), 3.38 (s, 3H,OC*H*$_3$), 2.30 (t, 2H, C*H*$_2$COOH), 2.18 (t, 2H, NHCOC*H*$_2$), 1.65 (m, 4H, NHCOCH$_2$C*H*$_2$(CH$_2$)$_2$C*H*$_2$CH$_2$COOH), 1.36 (m, 4H, NHCO(CH$_2$)$_2$C*H*$_2$C*H*$_2$(CH$_2$)$_2$COOH).

Synthesis of PEG-g-PEI Copolymer. 2.0 g of PEG-DTPA (or PEG-SA) and 0.14 g of NHS were dissolved in 20 mL of dry THF and 0.25 g of DCC dissolved in 15 mL of dry THF was added dropwise under N_2 protection at the room temperature. The reaction was carried out for 40 hrs. The reaction mixture was filtrated under N_2 and added to anhydrous PEI/THF solution dropwise under vigorous stirring. The reaction continued for another 40 hrs, followed by the addition of 100 mL of D.I. water. Finally, THF in the reaction mixture was removed by rotary evaporation; the insoluble by-products were removed by filtration; and the remaining solution was dialyzed against D.I. water with a membrane ($M_{cut\text{-}off}$ 2000) for 24 hrs to remove unreacted PEG chains. ^{1}H NMR of PEG-g-PEI with disulfide bond (PEG-SS-PEI) (D_2O) δ(ppm): 3.68 (bs, 170H, C*H*$_2$C*H*$_2$O), 3.10-2.70 (m, 833H, C*H*$_2$C*H*$_2$NH); ^{1}H NMR of PEG-g-PEI with SA linkage (PEG-CC-PEI) (D_2O) δ(ppm): 3.67 (br, 170H, C*H*$_2$C*H*$_2$O), 3.05-2.64 (m, 931H, C*H*$_2$C*H*$_2$NH).

Laser Light Scattering (LLS). A commercial laser light-scattering spectrometer (ALV5000) with a vertically polarized 22-mW He-Ne laser (632.8 nm, Uniphase) was used to characterize the PEG-g-PEI copolymers and the DNA/PEG-g-PEI polyplexes. In static LLS (*30*), we can obtain the weight-average molar mass (M_w) and the z-average root-mean square radius of gyration ($\langle R_g \rangle_z$) of scattering objects in a dilute solution/dispersion from the angular and concentration dependence of the excess absolute scattering intensity (Rayleigh ratio $R_{vv}(q)$) as

$$\frac{KC}{R_{vv}(q)} = \frac{1}{M_w}\left(1+\frac{1}{3}q^2R_g^{\ 2}\right)+2A_2C \qquad (4\text{-}1)$$

where $K \equiv 4\pi^2n^2(dn/dC)^2/(N_A\,\lambda_0^{\ 4})$ and $q = (4\pi n\lambda_0)\sin(\theta/2)$ with N_A, dn/dC, n, and λ_0 being the Avogadro number, the specific refractive index increment, the solvent refractive index, and the wavelength of the light in a vacuum, respectively. A_2 is the second virial coefficient. $(dn/dC)_{632.8\ nm}$ of the PEI copolymer and DNA in water was determined by using the Jianke differential refractometer (*31*). $(dn/dC)_{632.8\ nm}$ of the polyplexes were calculated by using

$$(dn/dC)_{polyplex} = w_{DNA}(dn/dC)_{DNA} + w_{polymer}(dn/dC)_{polymer} \qquad (4\text{-}2)$$

where w_{DNA} and $w_{polymer}$ are two weight fractions of DNA and copolymer, respectively. The measurement angular range used was 20°-150° for the copolymers, and 20°-50° for the polyplexes. All of the measurements were carried out at 25.0 ± 0.1 °C.

In dynamic LLS (*32*), the Laplace inversion of each measured intensity-intensity time correlation function $G^{(2)}(q,t)$ in the self-beating mode can be related to a line-width distribution $G(\Gamma)$. For a diffusive relaxation, Γ is related to the translational diffusion coefficient D by $(\Gamma/q^2)_{(C\to 0,q\to 0)} = D$. Therefore, $G(\Gamma)$ can be converted into a transitional diffusion coefficient distribution G(D) or a hydrodynamic radius distribution $f(R_h)$ via the Stokes-Einstein equation, $R_h = (k_BT/6\pi\eta)/D$, where k_B, T, and η are the Boltzmann constant, the absolute temperature, and the solvent viscosity, respectively.

Formation and Characterization of Polyplexes. The polyplexes with different desired N:P ratios (ratios of nitrogen atoms on PEI to phosphorus on plasmid DNA) were prepared by adding an appropriate amount of PEI polymer solution to a plasmid DNA (plasmid pGL3, 5 kbp) solution in PBS. The incubation time was 10 min for PEI25K/DNA polyplexes and 60 min for PEG-g-PEI/DNA polyplexes before use. Such prepared polyplexes were analyzed by the gel retardation assay. Where applicable, different amounts of heparin was added and incubated with polyplexes (2 μg DNA at N:P 10) for 30 minutes at the room temperature. The polyplexes were mixed with the loading buffer and then loaded on a 0.8 % agarose gel containing

EtBr in TBE buffer. The gel electrophoresis was run at 120 V for 20 min and then photographed under UV.

The zeta-potential of the polyplexes dispersed in PBS (1×10^{-2} μg/mL pDNA) was measured by a commercial Brookhaven Zeta Plus spectrometer with two platinum-coated electrodes and a He-Ne laser as the light source. The current was fixed at 10 mA and at least 30 cycles were measured for each polyplexes dispersion. For the transmission electron microscopy (TEM) study, after incubation in the PBS for 15 min, the polyplexes were negatively stained with 1% uranyl acetate. A drop of the sample solution was allowed to settle on a carbon film-coated copper grid for 5 min, the excess sample was wicked away with a filter paper and a drop of staining solution was allowed to contact the sample for 1 min. The samples were analyzed using a FEI CM120 electron microscope.

***In vitro* Gene Transfection.** The *in vitro* gene transfection efficiency was quantified by using the luciferase transfection assays, in which plasmid pGL3 was used as an exogenous report gene. 293T cells were plated in a 48-well plate at an initial density of ~50,000 cells per well, 24 hrs prior to the gene transfection. The polyplexes were further diluted in the serum-free or 10% FBS-containing DMEM medium and then added to each well. The final plasmid DNA concentration is 0.4 μg per well in a total volume of 300 μL. 4 hrs later, the transfection medium was aspirated and 1 mL of complete DMEM medium was added int o each well. The gene expression was determined after 48-hrs incubation by using a GloMax 96 Microplate Luminometer (Promega, USA). Meanwhile, the protein concentration in each well was determined by the Bio-Rad protein assay reagent (Bio-Rad, USA). The gene transfection efficiency is expressed as a relative light units (RLU) per mg protein in each well (mean ± SD, triplicates).

Cytotoxicity Assay. The cytotoxicity assessment was carried out on 293T cells by using the MTT-assay. 293T cells were seeded in a 96-well plate at an initial density of ca. 5000 cells per well in 100 μL of the DMEM complete medium. After 24 hrs, the polymer solutions with different concentrations were added into the cells. Such treated cells were incubated in a humidified environment with 5% CO_2 at 37 °C for

48 hrs. Then, the MTT reagent (in 20 μL PBS, 5 mg/mL) was added to each well and the cells were further incubated for 4 hrs at 37 °C. Finally, the medium in each well was removed and replaced by 100 μL DMSO. The plate was gently agitated for 15 min before the absorbance (A) at 490 nm was recorded by a microplate reader (Bio-Rad). The cell viability was calculated by

$$\text{Cell viability (\%)} = (A_{treated} / A_{control}) \times 100\% \quad (4\text{-}3)$$

where $A_{treated}$ and $A_{control}$ are the absorbance values of the cells cultured with and without the PEI or copolymers. Each experiment condition was done in quadruple. The data are shown as the mean value plus a standard deviation (± SD).

Flow Cytometry. pGL3 was labeled with Cy5 fluorescent dye by using Label IT® nucleic acid labeling kits (Mirus, USA) according to the protocol. The labeling density was one label every 50 base pairs of double-stranded DNA and was proved to be unaffected to the formation of polyplexes (*33*). The labeled polyplexes were used to transfect 293T cells following the above transfection procedure. 4 hrs later, the medium was removed and the cells were washed with 150 μL of ice-cold PBS. Further, the cells were treated with 0.25% trypsin and PBS supplemented with 20 mM sodium azide to prevent further cellular uptake of the polyplexes (*34*). The trypan blue/PBS was added with a concentration of 0.04 % to quench the fluorescence of extracellularly bound polyplexes. Finally, the cells were washed twice and resuspensed by ice-cold PBS. The total preparation time was less than 30 min. A Beckman Coulter flow cytometry was used, in which Cy5 fluorescence was excited at 635 nm and detected with a 665±20 nm bandpass filter. To discriminate viable cells from dead cells and to exclude doublets, the cells were appropriately gated by the forward/side scattering and pulse width. 1×10^4 gated events per sample were collected. Experiments were performed at least in triplicate. The mean fluorescence intensity (MFI) of those cells that had taken up the polyplexes served as an indirect measurement of the average number of the internalized polyplexes. All that experimental values were normalized to the cells that received 150 mM NaCl instead of the polyplexes solution.

4.3 Results and Discussion

Synthesis and Characterization of PEG-g-PEI. Scheme 4.1 shows the preparations of the PEG-g-PEI block copolymer with a disulfide linkage (PEG-SS-PEI), and its non-degradable counterpart (PEG-CC-PEI). In step 1, the terminal hydroxyl group on the PEG monomethyl ether was first converted to an amine group via a two-step reaction: a) the hydroxyl to a methanesulfonyl intermediate group; and b) further to an amine by using aqueous ammonia, with a yield of ~90%. The conversion was close to 100% on the basis of the NMR analysis. DTPA and SA was activated by using DCC and NHS, respectively; and then attached to the amine end of each PEG chain. In order to avoid the PEG coupling side-reaction, excessive DTPA or SA was added. The remaining DTPA or SA after the reaction was removed by dialysis against water, in which the NHS ester on the chain end was hydrolyzed to the carboxyl group. The yields of PEG-DTPA and PEG-SA were 65% and 71%,

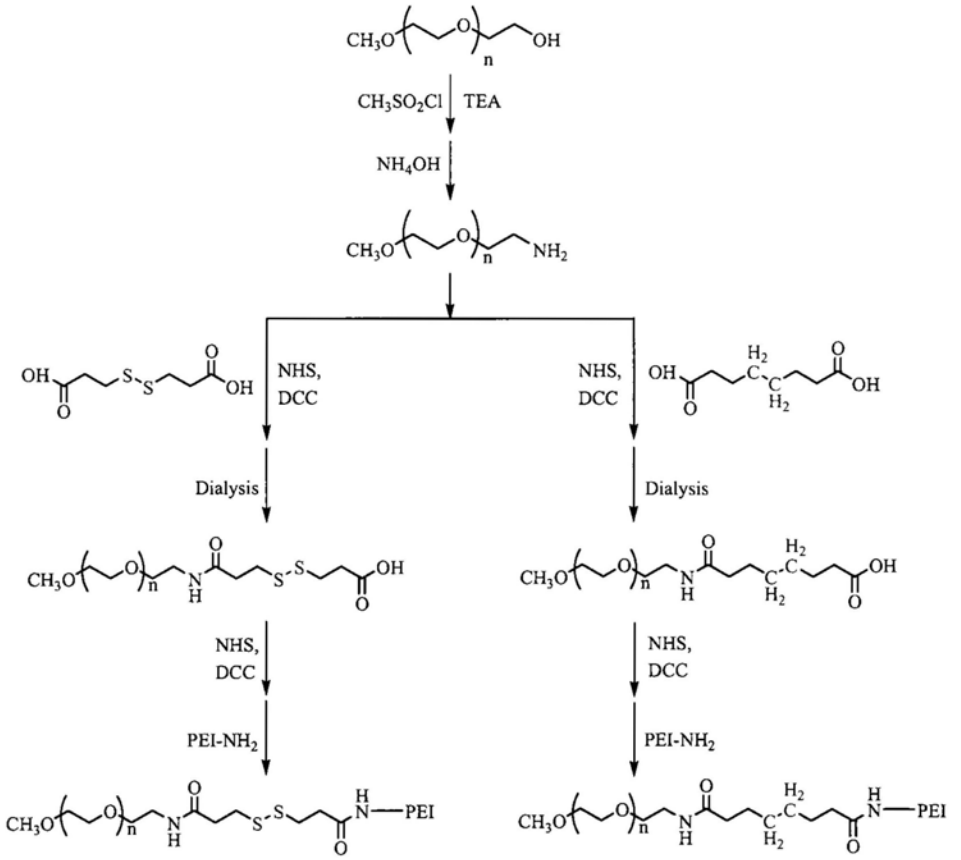

Scheme 4.1. Synthesis of two grafting copolymers: PEG-SS-PEI and PEG-CC-PEI.

respectively, because of some avoidable loss during the dialysis. The conversions were 90% and 96%, respectively, on the basis of the NMR results. Finally, the carboxyl end group was activated and conjugated to PEI with a molar ratio of $[-NH_2]$:[-COOH] = 1:1. The unreacted PEG chains were removed by dialyzed against a membrane ($M_{cut\text{-}off}$ ~2000 g/mol). Table 4.1 lists the feed and resultant PEG:PEI ratios of such prepared copolymers.

Table 4.1. Summary of molecular characters of two grating copolymers: PEG-SS-PEI and PEG-CC-PEI.

Copolymer	feed ratio	measured	dn/dc[b)]	DTT treatment	
	n_{PEG}: n_{PEI}	n_{PEG} : n_{PEI}[a)]	mL/g	$M_{w\ (before)}$ Kg/mol	$M_{w\ (after)}$ Kg/mol
PEG-SS-PEI	1.3:1.0	1.1:1.0	0.250	28.5 ± 0.6	25.5 ± 0.8
PEG-CC-PEI	1.2:1.0	1.0:1.0	0.248	27.8 ± 0.5	27.7 ± 0.9

a) Estimated from the ratio of the integrated -CH_2- signals on PEG and PEI in ^{1}H NMR.

b) Measured in PBS.

The absolute weight-average molar mass of each copolymer was characterized by static LLS, as shown in Table 4.1. The value of M_w(PEI25K) from the supplier was confirmed by our LLS measurements. M_w(PEG-SS-PEI) = 28.5 ± 0.6 g/mol, that was reduced to 25.5 ± 0.8 g/mol after a DTT treatment. In contrast, as expected, M_w(PEG-CC-PEI) remained a constant before and after the addition of DTT. Note that PEI25K is broadly distributed and shorter PEI chains are likely lost during the dialysis. Therefore, the calculated PEG-to-PEI composition on the basis of LLS results (M_w) was not very reliable, sometimes even higher than the feed ratio. Therefore, the PEG-to-PEI ratios from the NMR results (1.0:1.0 for PEG-SS-PEI and 1.1:1.0 for PEG-CC-PEI) are used thereafter, because a control experiment showed that the PEG ($M_w = 2.0\times10^3$ g/mol) can be completely removed by a 24-hr dialysis by using a dialysis membrane with $M_{cut\text{-}off}$ ~2,000 g/mol.

Formation of Polyplexes. Figure 4.2 shows that the relative scattering intensity of the PEI25K/DNA polyplexes decreases, but the average hydrodynamic radius (<R_h>) increase in the initial 15 min, indicating quick inter-chain aggregation, resulting in large polyplexes that precipitate out of the solution mixture under the high salt condition. The precipitation slows down and <R_h> remains ~600 nm afterwards, presumably because the concentration of those remaining polyplexes is too low. In contrast, the PEG-SS-PEI and PEG-CC-PEI polyplexes have an initial size of ~80

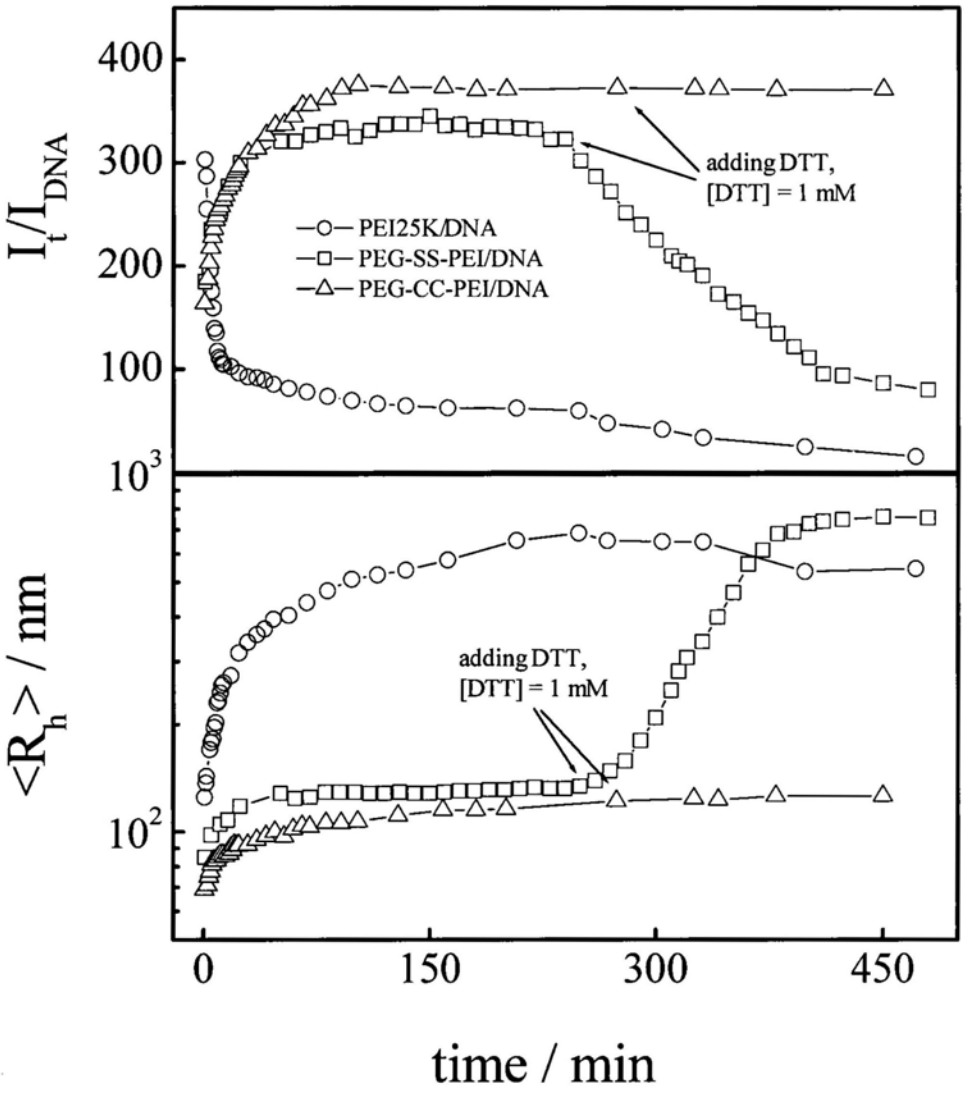

Figure 4.2. Time dependence of relative scattering intensity, defined as I_t/I_{DNA}, at $\theta = 90°$ and average hydrodynamic radius (<R_h>) of PEI/DNA, PEG-SS-PEI/DNA and PEG-CC-PEI/DNA polyplexes after the mixing of DNA and polymer solutions, where N:P = 10 and C_{DNA} = 2 μg/mL.

nm. Apparently, more DNA and polymer chains are incorporated into the polyplexes in PBS so that both the relative scattering intensity and $<R_h>$ increase, respectively approaching two plateaus after ~50 min, which reveals that one grafted PEG chain per PEI25K is sufficient to stabilize the polyplexes under the physiological salt condition. Therefore, we should be able to regulate the size of the polyplexes by adjusting the chain length of PEG and its grafting density on PEI.

The TEM images, as shown in Figure 4.3, support our LLS results: larger and flocculated morphology is observed for the PEI25K/DNA polyplexes formed in PBS, while individual particles with an average radius of ~90 nm are formed in the mixture of PEG-SS-PEI and DNA solutions, slightly smaller than $<R_h>$ measured from dynamic LLS. Figure 4.2 shows that the addition of reductive DTT into the PEI-g-PEI/DNA polyplexes dispersion at ~250 min leads to a decrease of the relative scattering intensity and an increase of $<R_h>$ of the PEG-SS-PEI/DNA polyplexes dispersion, further indicating that it is the cleavable PEG chains that stabilize the polyplexes in PBS. As expected, the addition of DTT has no influence on the PEG-CC-PEI/DNA polyplexes with a non-degradable -C-C- linkage between PEG and PEI.

Figure 4.4 shows that when N:P $\geq$ 3, the PEG-SS-PEI/DNA and PEG-CC-PEI/DNA polyplexes formed in PBS have similar M_w, $<R_h>$ and $<\rho>$, confirming that most of the DNA chains are complexed with the copolymer chains when N:P reaches 3 (*35, 36*), and the little difference in the PEG grafting density on

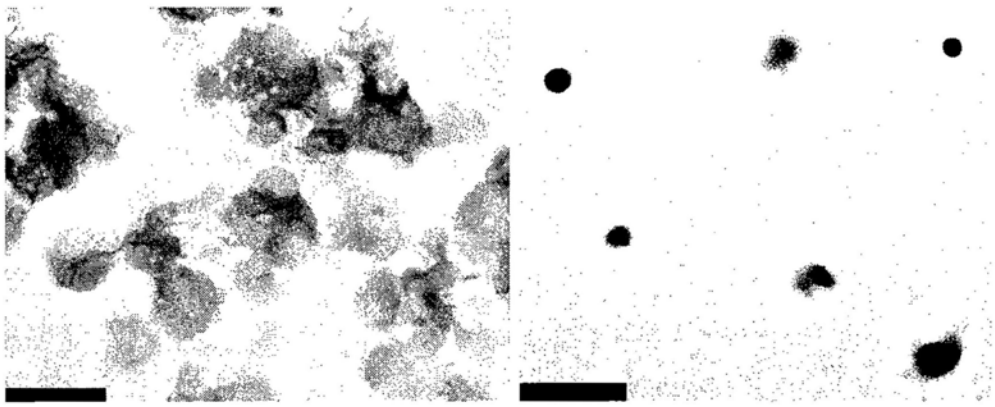

Figure 4.3. TEM images of PEI25K/DNA and PEG-SS-PEI/DNA polyplexes formed in PBS. Bar: 500 nm.

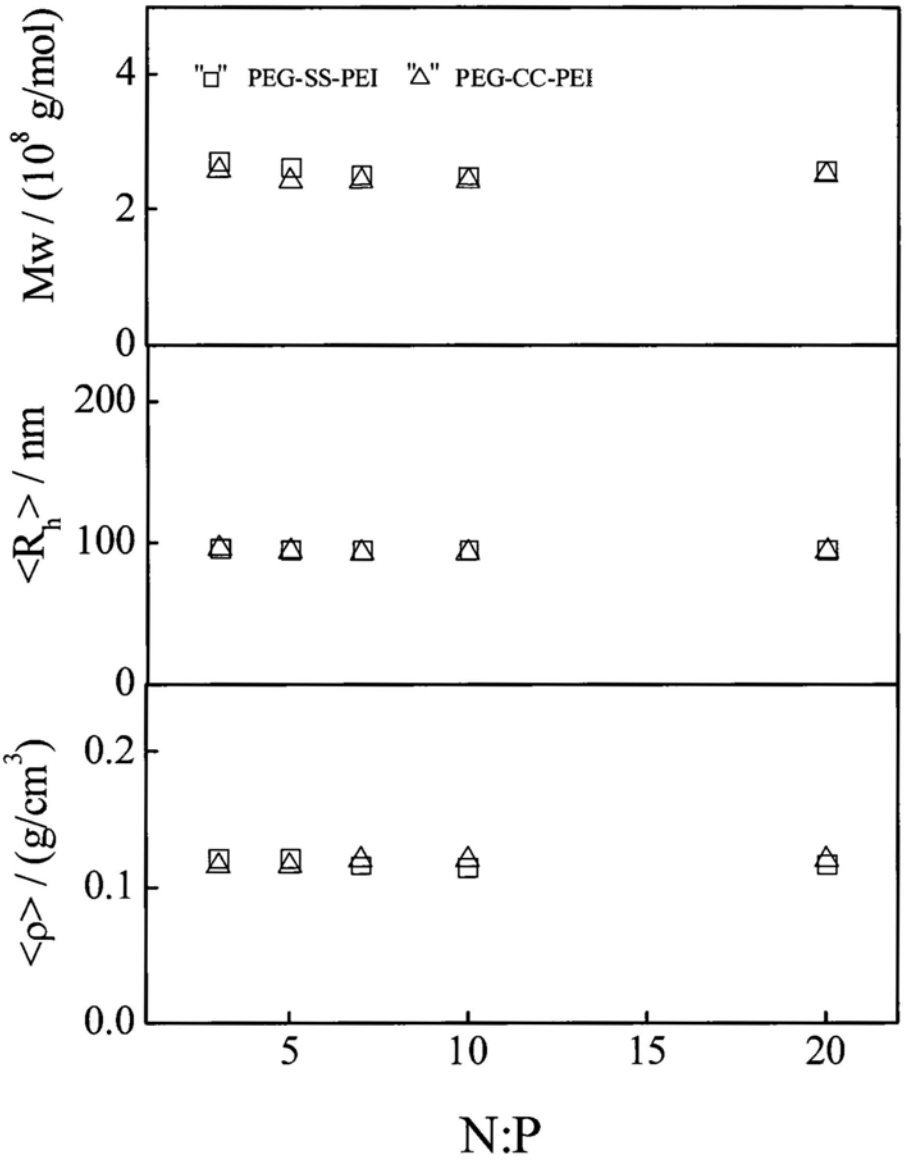

Figure 4.4. N:P ratio dependence of apparent weight-average molar mass (M_w), average hydrodynamic radius ($\langle R_h \rangle$) and average chain density ($\langle \rho \rangle \equiv M_w/N_A(4/3)\pi\langle R_h \rangle^3$) of PEG-SS-PEI/DNA and PEG-CC-PEI/DNA polyplexes in PBS.

the PEI25K (1.0 vs. 1.1) have no significant impact on the formation of the polyplexes. For a stable polyplex, M_w ~2.5 × 10^8 g/mol, revealing that each polyplex on average contains ~50 DNA and 5.6 × 10^3 PEG-g-PEI chains. The $\langle R_h \rangle$ for both PEG-SS-PEI and PEG-CC-PEI based polyplexes are 95 nm.

Further, Figure 4.5 shows that the addition of polymer reverses the ζ-potential at N:P ~2.5 and makes it to reach a plateau at N:P ~5; namely, +25 and +10 mV for the

PEI/DNA and PEG-g-PEI/DNA polyplexes, respectively, indicating that the PEG chains on the surface partially shield the cationic charge of PEI in the core. The addition of DTT removes the PEG shell so that the ζ-potential of the PEG-SS-PEI/DNA solution increases, but as expected, has no effect on the PEG-CC-PEI/DNA polyplexes. The gel retardation assay test is consistent with the ζ-potential measurements, i.e., DNA was completely complexed with polymer and retarded at N:P ~2.5. The results of the three polymers used are similar, indicating that the grafting PEG on PEI has little effect on the complexation between cationic

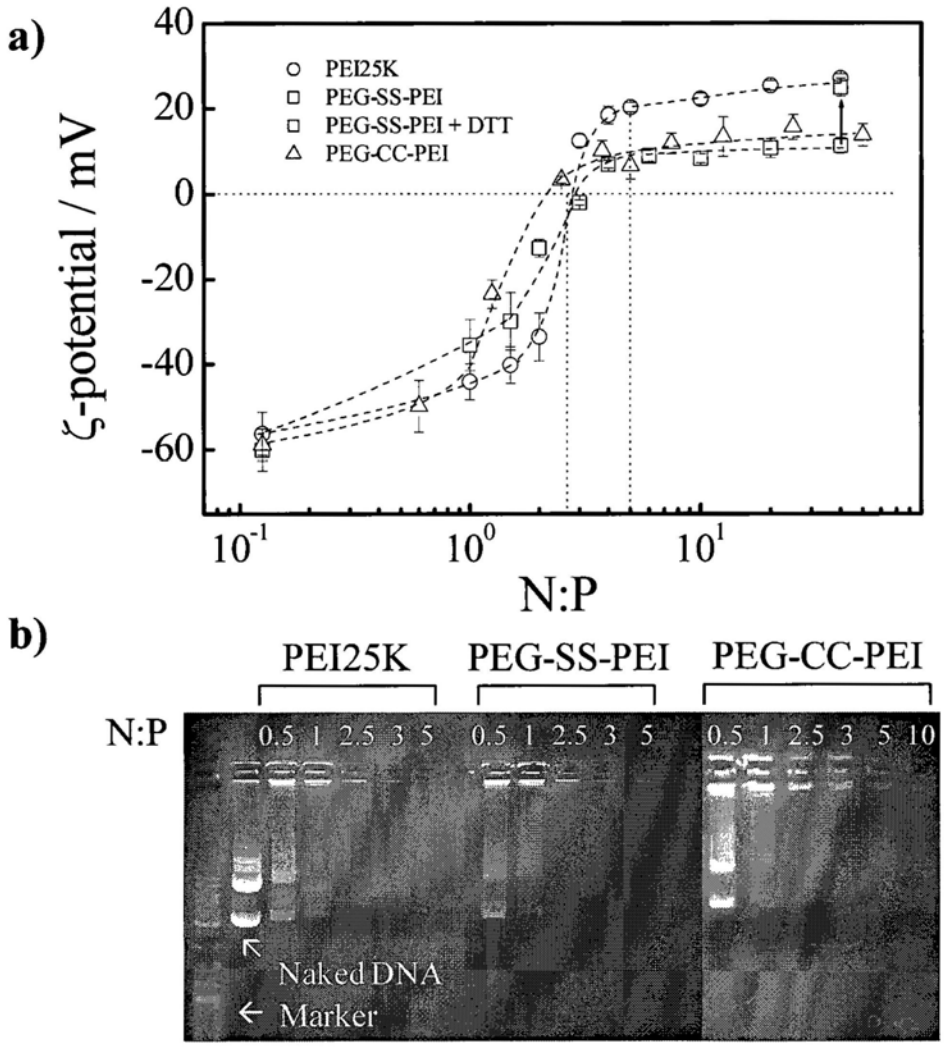

Figure 4.5. N:P ratio dependence of a) ζ-potential and b) gel retardation of different polymer/DNA polyplexes.

PEI with anionic DNA chains. This is reasonable because the complexation is mainly controlled by the charge neutrality.

It has been assumed that the intracellular release of DNA is due to its displacement by other polyanions, such as RNA and glycosaminoglycans (*7, 37*). Therefore, polyanionic heparin has been used as a model polymer to study the release of DNA from the polyplexes. Figure 4.6 shows that the addition of 1 unit heparin starts to displace DNA, reflecting in its migration, while 3 units of heparin are sufficient to displace most of the DNA chains from the polyplexes. The addition of DTT into the PEG-SS-PEI/DNA polyplexes dispersion reduces the required amount of heparin for the displacement of DNA to ~0.9 unit, but has no effect on the PEG-CC-PEI/DNA polyplexes, suggesting that the detachment of the cleavable PEG shell in the PEG-SS-PEI/DNA polyplexes in the reductive cytosol environment might be helpful to exfoliate PEI from the polyplexes and release DNA.

Cellular Uptake, Cytotoxicity and *in vitro* Transfection Efficiency. Figure 4.7 shows that the cellular uptake of each kind of the polyplexes form ed with the Cy5-labeled DNA in 150 mM PBS in terms of the cell-associated fluorescence after the incubation in serum-free or serum-containing transfection medium. T he PEI25K/DNA polyplexes clearly exhibit a higher cellular uptake level than the

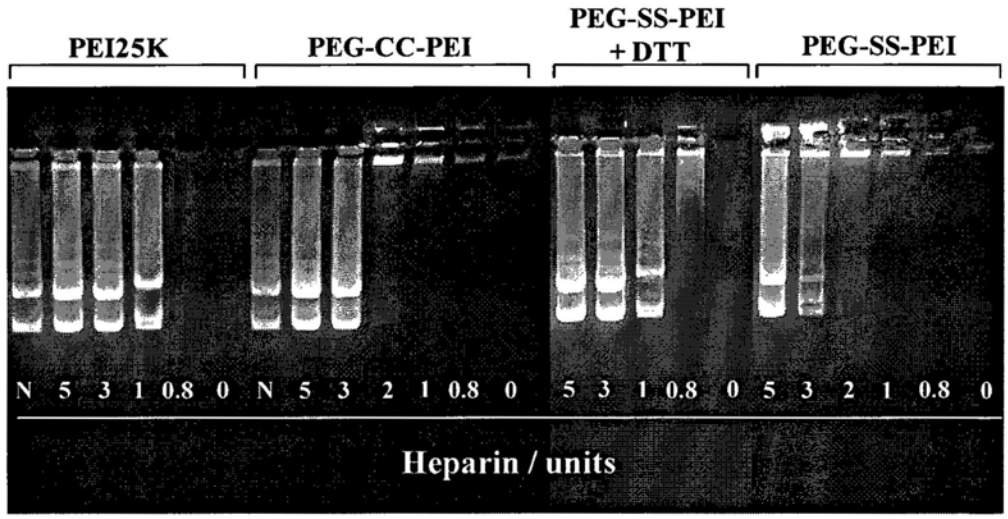

Figure 4.6. Test of displacement of DNA heparin, where polyplexes prepared with N:P = 10 are treated with different amounts of heparin for 20 min at the room temperature. N stands for the naked pDNA as a control.

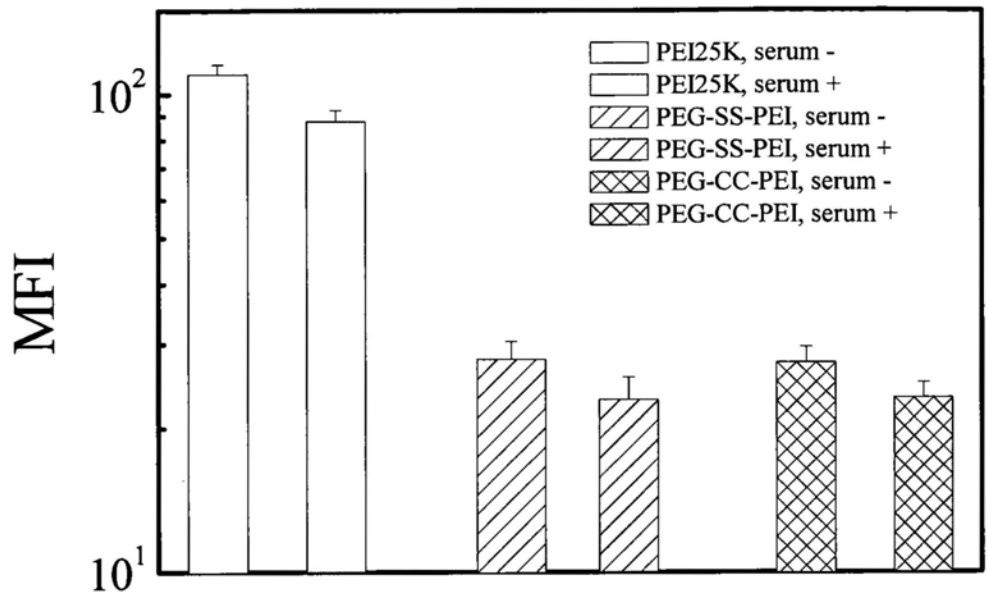

Figure 4.7. Cellular uptake of polyplexes prepared at N:P = 10 on 293T cells, where MFI is mean fluorescent intensity.

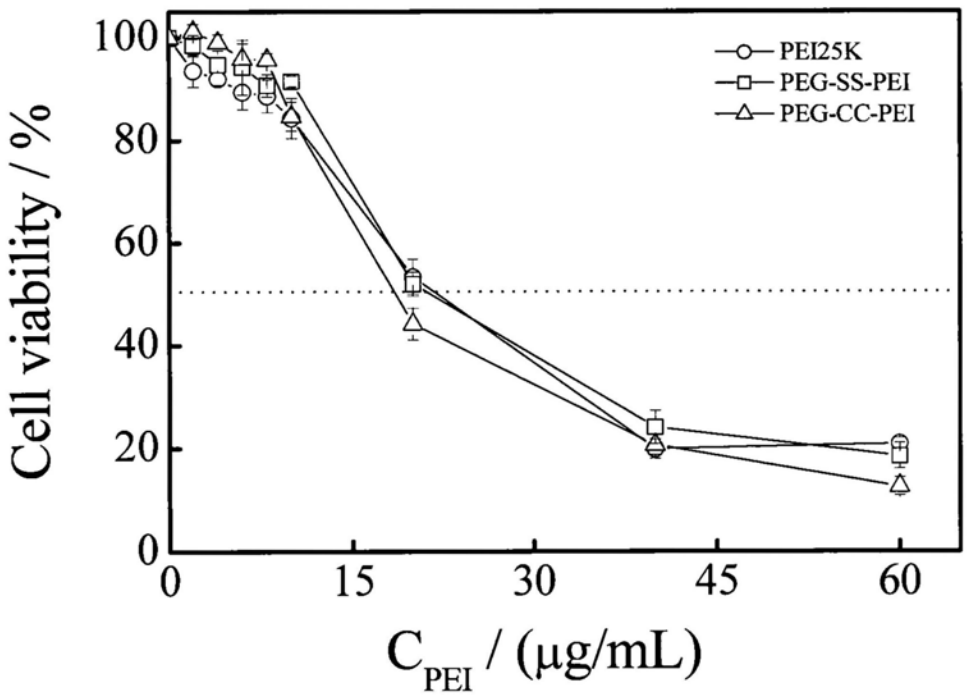

Figure 4.8. 293T cell viability of different polymers tested using MTT assay.

PEG-g-PEI/DNA polyplexes in the absence or presence of serum. Such a difference is attributed to a) the precipitation of the PEI25K/DNA polyplexes on the adherent cell surface; b) the steric shielding of PEG; and c) a less cationic charged surface of the PEG-g-PEI/DNA polyplexes. In each case, the presence of serum slightly reduces the cellular uptakes, presumably due to the adsorption of some negatively charged serum proteins on the positively charged polyplexes (*38, 39*). Figure 4.8 shows that PEI25K, PEG-SS-PEI and PEG-CC-PEI have a similar cytotoxicity profile with IC50 ~20 μg/mL, corresponding to N:P = 120 that will be too high to be used in any transfection experiment.

Figure 4.9 shows the *in vitro* transfection efficiencies of different polyplexes with 293T cells in the DMEM medium with or without 10% FBS. The polyplexes formed with higher N:P ratios are ~10^3 times more effective in the gene transfection than those formed with N:P = 3. All of those polymers show their optimum transgene efficiency at ca. N:P 10-20. And further increasing of N:P ratio lead to the decreased protein express, possibly due to the high cytotoxicity of PEI (data not shown).

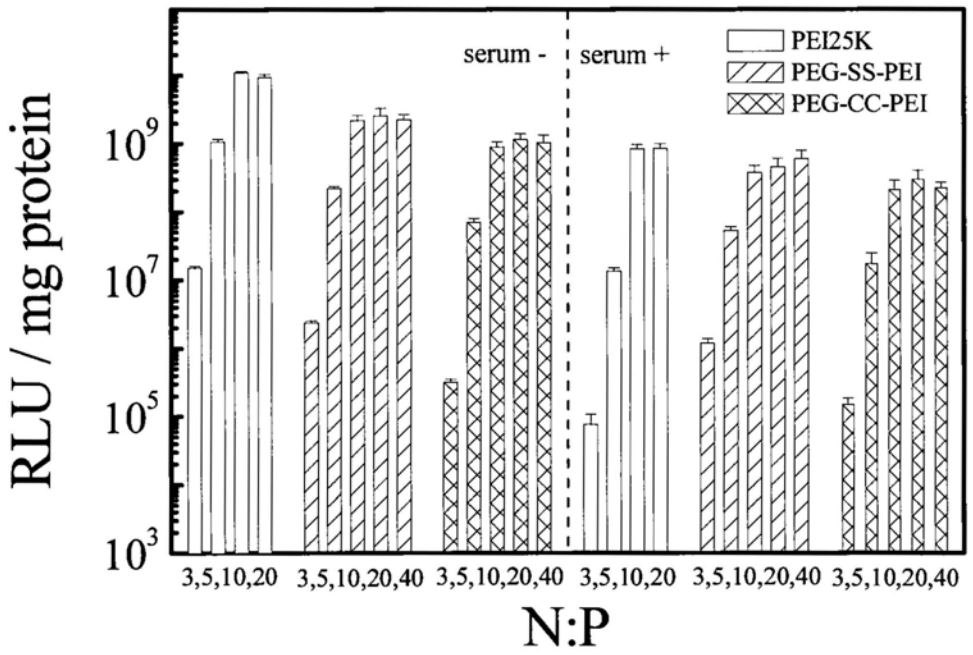

Figure 4.9. N:P ratio dependence of *in vitro* gene transfection efficiency of PEI25K, PEG-SS-PEI and PEG-CC-PEI in the serum-free (-) or serum (+) medium on 293T cells.

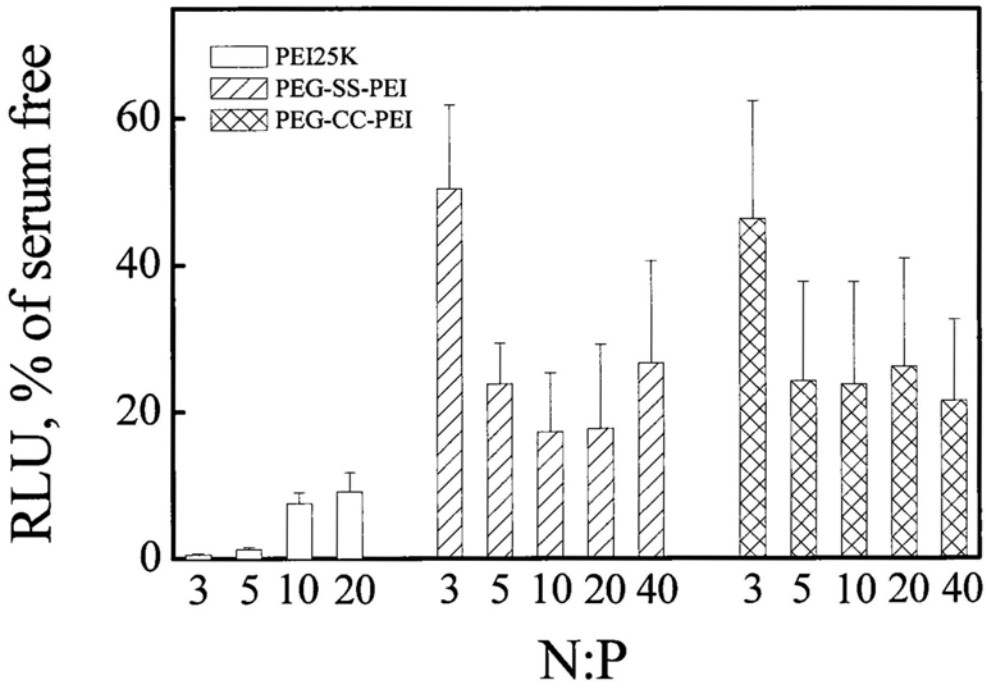

Figure 4.10. N:P ratio dependence of percentage of gene expression level in serum medium to that in serum-free medium for PEI25K, PEG-SS-PEI and PEG-CC-PEI, respectively.

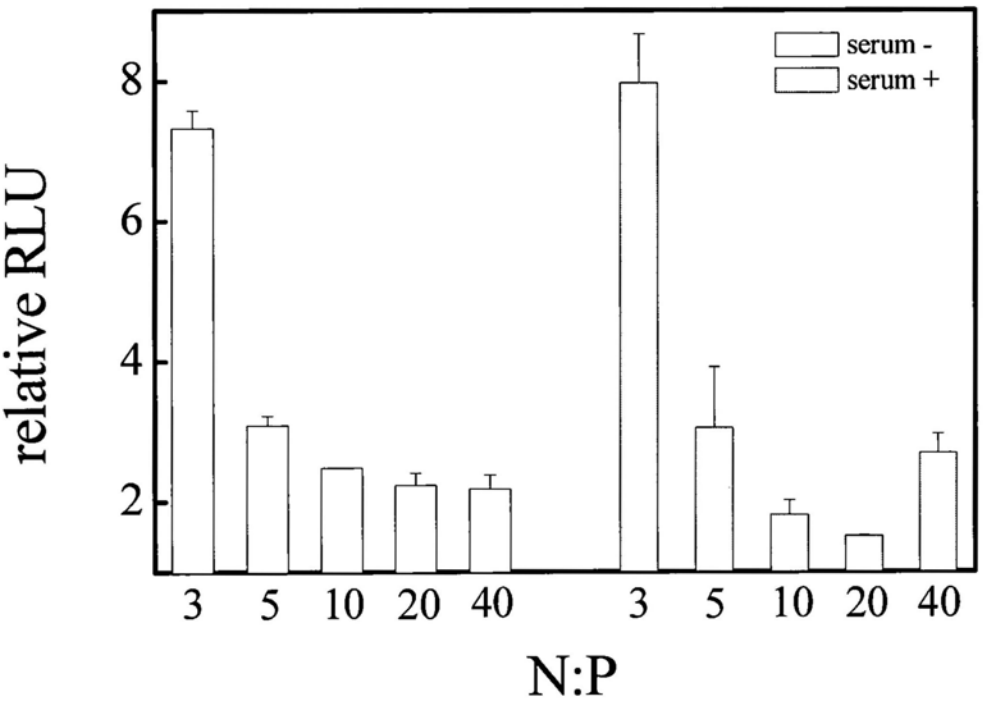

Figure 4.11. N:P ratio dependence of relative gene transfection efficiency of PEG-SS-PEI to PEG-CC-PEI in serum-free and serum mediums, respectively.

The presence of serum reduces the gene transfection efficiency, but has less effect on the PEG-g-PEI/DNA polyplexes (Figure 4.10). In the N:P range studied, PEI25K in the serum-containing medium is only 1%-9% efficient in comparison with that in a serum free medium, similar to those reported literature results (*40, 41*). The serum has a much less effect on the PEG-SS-PEI/DNA and PEG-CC-PEI/DNA polyplexes, due to the PEG-shielding.

Note that in the absence of serum, PEG-SS-PEI and PEG-CC-PEI are 4-6 and 8-40 times less efficient than PEI25K, respectively. The cellular uptake efficiencies based on the flow cytometry measurement shows that such a decrease is due to their lower cellular uptake. On the other hand, the flow cytometry measurements reveal that the cellular uptake of PEG-SS-PEI and PEG-CC-PEI are similar in the absence and presence of serum (Figure 4.7). However, PEG-SS-PEI is always 2-8 times more efficient than PEG-CC-PEI in the gene transfection (Figure 4.11). A combination of the results of the cytotoxicity test and heparin displacement shows that difference between PEG-SS-PEI and PEG-CC-PEI must be attributed to the breaking away of PEG from the PEG-SS-PEI/DNA polyplexes due to the disulfide linkages that are broken in the reductive cytosol, subsequently leading to an easier release of pDNA from the polyplexes (Figure 4.1).

4.4 Conclusion

Polyethylene glycol (PEG) and polyethyleneimine (PEI) can be coupled to form a graft copolymer (PEG-g-PEI) via either a reductive disulfide -S-S- or a non-degradable -C-C- bond. In comparison with the polyplexes formed between unmodified PEI and anionic pDNA, the polyplexes formed between PEG-g-PEI and pDNA via electrostatic interaction are stable under the physiological condition because the hydrophilic PEG chains form a stabilizing shell on their periphery. The polymer-conjugation has no effect on the polyplex formation; namely, most of pDNA are complexed with the copolymers when N:P = 3. PEGylation reduces the internalization of the polyplexes in *in-vitro* experiments. PEG-SS-PEI is 2-8 times more effective than its counterpart (PEG-CC-PEI) in the gene transfection,

presumably because the grafted PEG chains are cleaved in the reductive cytosol, promoting the release and translocation of DNA. Our results clearly demonstrate that using the disulfide linkage is a promising approach to overcome the PEGylation dilemma in the development of non-viral polymeric vectors for the gene or drug delivery.

References and Notes

(1) Pack, D. W., Hoffman, A. S., Pun, S., *et al. Nature Reviews Drug Discovery* **2005**, *4*, 581.

(2) Choi, Y. H., Liu, F., Kim, J. S., *et al. J. Controlled Release* **1998**, *54*, 39.

(3) Kwoh, D. Y., Coffin, C. C., Lollo, C. P., *et al. Biochimica Et Biophysica Acta-Gene Structure and Expression* **1999**, *1444*, 171.

(4) Neu, M., Fischer, D., and Kissel, T. *J. Gene Med.* **2005**, *7*, 992.

(5) Lungwitz, U., Breunig, M., Blunk, T., *et al. Eur. J. Pharm. Biopharm.* **2005**, *60*, 247.

(6) El-Aneed, A. *J. Controlled Release* **2004**, *94*, 1.

(7) Oliver Germershaus, Shirui Mao, Johannes Sitterberg, *et al. J. Controlled Release* **2008**, *125*, 145.

(8) Dufes, C., Uchegbu, I. F., and Schatzlein, A. G. *Adv. Drug Del. Rev.* **2005**, *57*, 2177.

(9) Petersen, H., Fechner, P. M., Martin, A. L., *et al. Bioconjugate Chem.* **2002**, *13*, 845.

(10) Wightman, L., Kircheis, R., Rossler, V., *et al. J. Gene Med.* **2001**, *3*, 362.

(11) Ogris, M., Steinlein, P., Kursa, M., *et al. Gene Ther.* **1998**, *5*, 1425.

(12) Dash, P. R., Read, M. L., Barrett, L. B., *et al. Gene Ther.* **1999**, *6*, 643.

(13) Roberts, M. J., Bentley, M. D., and Harris, J. M. *Adv. Drug Del. Rev.* **2002**, *54*, 459.

(14) Delgado, C., Francis, G. E., and Fisher, D. *Crit. Rev. Ther. Drug Carrier Syst.* **1992**, *9*, 249.

(15) Vinogradov, S. V., Bronich, T. K., and Kabanov, A. V. *Bioconjugate Chem.* **1998**, *9*, 805.

(16) Petersen, H., Fechner, P. M., Fischer, D., *et al. Macromolecules* **2002**, *35*, 6867.

(17) Blessing, T., Kursa, M., Holzhauser, R., *et al. Bioconjugate Chem.* **2001**, *12*, 529.

(18) Walker, G. F., Fella, C., Pelisek, J., *et al. Mol. Ther.* **2005**, *11*, 418.

(19) Knorr, V., Allmendinger, L., Walker, G. F., *et al. Bioconjugate Chem.* **2007**, *18*, 1218.

(20) Mishra, S., Webster, P., and Davis, M. E. *Eur. J. Cell Biol.* **2004**, *83*, 97.

(21) Schatzlein, A. G. *J. Biomed. Biotechnol.* **2003**, *2003*, 149.

(22) Kursa, M., Walker, G. F., Roessler, V., *et al. Bioconjugate Chem.* **2003**, *14*, 222.

(23) Fella, C., Walker, G. F., Ogris, M., *et al. Eur. J. Pharm. Sci.* **2008**, *34*, 309.

(24) Oishi, M., Nagasaki, Y., Itaka, K., *et al. J. Am. Chem. Soc.* **2005**, *127*, 1624.

(25) Li, W. J., Huang, Z. H., MacKay, J. A., *et al. J. Gene Med.* **2005**, *7*, 67.

(26) Takae, S., Miyata, K., Oba, M., *et al. J. Am. Chem. Soc.* **2008**, *130*, 6001.

(27) Saito, G., Swanson, J. A., and Lee, K. D. *Adv. Drug Del. Rev.* **2003**, *55*, 199.

(28) Manickam, D. S., and Oupicky, D. *J. Drug Targeting* **2006**, *14*, 519.

(29) Aronov, O., Horowitz, A. T., Gabizon, A., *et al. Bioconjugate Chem.* **2003**, *14*, 563.

(30) Chu, B. *Laser Lgiht Scattering*, 2nd ed,; Academic Press: New York, **1991**.

(31) Wu, C., and Xia, K. Q. *Rev. Sci. Instrum.* **1994**, *65*, 587.

(32) Berne, B., and Pecora, R. *Dynamic Light Scattering*; Plenum Press: New York, **1976**.

(33) Midoux, P., Breuzard, G., Gomez, J. P., *et al. Curr. Gene Ther.* **2008**, *8*, 335.

(34) Breunig, M., Lungwitz, U., Liebl, R., *et al. J. Gene Med.* **2005**, *7*, 1287.

(35) Boeckle, S., von Gersdorff, K., van der Piepen, S., *et al. J. Gene Med.* **2004**, *6*, 1102.

(36) Clamme, J. P., Azoulay, J., and Mely, Y. *Biophys. J.* **2003**, *84*, 1960.

(37) Ruponen, M., Ronkko, S., Honkakoski, P., *et al. J. Biol. Chem.* **2001**, *276*, 33875.

(38) Roufai, M. B., and Midoux, P. *Bioconjugate Chem.* **2001**, *12*, 92.

(39) Ogris, M., Brunner, S., Schuller, S., *et al. Gene Ther.* **1999**, *6*, 595.

(40) Christensen, L. V., Chang, C. W., Kim, W. J., *et al. Bioconjugate Chem.* **2006**, *17*, 1233.

(41) Tang, G. P., Zeng, J. M., Gao, S. J., *et al. Biomaterials* **2003**, *24*, 2351.

Chapter 5

Revisit the Complexation Between PEI-based Polycations and DNA – Free PEI Promotes Gene Transfection Efficiency

5.1 Introduction

Polyethylenimine (PEI) is a widely used non-viral gene transfection reagent both *in vitro* and *in vivo* because of its excellent transfection performance in most cultured cell lines (*1-4*), and it is often regarded as the "golden standard" to justify efficiency of other kinds of non-viral vectors (*5, 6*). The high efficiency of PEI is generally attributed to the high positive charge density on its backbone, as well as its good buffer capacity, which enable a so-called "proton sponge" effect in the endo/lysosome (*5-7*). Numerous chemical modifications have been applied on PEI in order to improve the gene delivery efficiency, including PEGylation to prolong *in vivo* circulation time and serum stability (*8-10*), introduction of intracellular biodegradable linkers to lower the cytotoxicity (*11-13*) and attachment of selective target ligands to improve cell or tissue specificity (*14-16*). However, little attention has been paid to the detailed complexation behavior between polycations and the negatively-charged DNA (*17, 18*).

The colloidal and physical characteristics of polymer/DNA polyplexes such as ζ-potential, size, and density, are important for an effective delivery of gene, but previous results were controversial and far from fully understanding (*19-22*). Therefore, it is necessary to revisit this complicated problem and understand the process in the microscopic level.

Clamme J. P. et al. studied the complexation of PEI and DNA by using two photon fluorescence correlation spectroscopy (*23*), and found that ~86% of the PEI molecules were in the free form in the solution when the PEI/DNA polyplexes was formed at N:P 10. Later, Boeckle S. et al. (*24*) used a size exclusion chromatography column to remove the free PEI from the PEI/DNA polyplexes and found that the remaining polyplexes has a N:P ratio of ~2.5. In addition, they found the existence of

free PEI substantially contributed to efficient gene expression, while the exact mechanism remained unknown.

Laser light scattering (LLS) and ζ-potential analysis are two most convenient and useful methods for the characterization of nanoparticle size, mass, and average surface potential. By using such methods, we have revisited the complexation between branched PEI with molecular weight 25kDa (PEI25K) and DNA, and we confirmed that most of anionic DNA chains are already complexed and condensed by cationic PEI25K chains at N:P ratio ~ 3 (*25*). In this chapter, we use such methods to investigate the complexation behavior between DNA and other three kinds of PEI-based vectors, i.e., PEI-7K-L, the disulfide-linked low molar mass PEI (details in Chapter 3), PEG-SS-PEI and PEG-CC-PEI, two PEG grafted PEIs with molar mass 25 kDa (details in Chapter 4).

5.2 Experimental Section

Materials and cell lines. Synthesis of PEI-7K-L, PEG-SS-PEI and PEG-CC-PEI were described in Chapter 3 and 4, respectively. Branched PEI with a weight-averaged molar mass of 25,000 g/mol (PEI25K) and 2,000 g/mol (PEI2K) were purchased from Sigma-Aldrich and used without further purification. Plasmid *p*GL3-control vector (5,256 bp) encoding modified firefly luciferase was provided by Promega (USA). Fetal bovine serum (FBS), Dulbecco's modified Eagle's medium (DMEM) and penicillin-streptomycin were purchased from GIBCO (NY, USA). 293T cells were grown at 37 °C, 5% CO_2 in DMEM supplemented with 10% FBS, penicillin at 100 units/mL and streptomycin at 100 μg/mL.

Formation and characterization of PEI/DNA polyplexes. Plasmid DNA was complexed with PEI-based polymers in PBS to form the PEI/DNA polyplexes as follows. PEI solutions (C_{PEI} = 3 × 10^{-4} g/mL) were added dropwise with different amounts into dilute DNA solutions (C = 14.5 μg/mL), resulting in samples with different molar ratios of nitrogen from PEI to phosphorus from DNA (N:P). Resultant solution mixtures with the polyplexes were incubated for 5 min at the room temperature before administration to the cell culture medium and other

characterizations.

Such prepared polyplexes were analyzed by the gel retardation assay, in which the polyplexes were mixed with a 6 × loading buffer (bromophenol blue/xylene cyanol) and loaded into an agarose gel well (0.8% agarose with 0.01% ethidium bromide in tris-borate EDTA buffer). The amount of DNA loaded into each well was 0.4 μg in a total volume of 10 μL. The electrophoresis was performed under 100 V for 30 min. DNA bands were visualized under UV.

The zeta-potential of the polyplexes dispersed in PBS (1×10^{-2} μg/mL pDNA) was measured by a commercial Brookhaven Zeta Plus spectrometer with two platinum-coated electrodes and a He-Ne laser as the light source. The current was fixed at 10 mA and at least 30 cycles were measured for each polyplexes dispersion.

To determine PEI concentrations, 900 μl/well 0.02M cupric acetate in 5% potassium acetate (pH 5.5) were added into a 100 μl of the sample or a PEI25K standard of known concentration in PBS. After mixing, the absorption at 630 nm was measured using an UV-Vis spectrometer (Hitachi, Japan), and concentrations were determined by comparing with the standard curve.

Laser light scattering. A commercial LLS instrument (ALV5000) with a vertically polarized 22-mV He-Ne laser (632.8 nm, Uniphase) was used. In dynamic LLS, the intensity-intensity time correlation function ($G^{(2)}(\tau)$) of PEI/DNA polyplexes solutions w ere measured at different scattering angles respectively. The Laplace inversion of each $G^{(2)}(\tau)$ can lead to a line-width distribution of $G(\Gamma)$ by the CONTIN program or by the double-exponential fitting, if there are only two relaxation modes, as

$$\{[G^{(2)}(q,\tau)-B]/B\}^{1/2}=A_1(q)e^{-\langle\Gamma\rangle_1\tau}+A_2(q)e^{-(\Gamma)_2\tau} \qquad (5\text{-}1)$$

where B is the measured baseline; $\langle\Gamma\rangle$ and A(q) are the average line-width and the normalized intensity contribution of each relaxation mode, respectively, and $A_1(q) + A_2(q) \equiv 1$; q is the scattering vector defined as $q \equiv (4\pi n/\lambda_0)\sin(\theta/2)$ with θ, λ_0 and n, the scattering angle, the incident wavelength in vacuum and the refractive index of solvent, respectively. $\langle\Gamma\rangle$ can be related to the average translational diffusion

coefficient <D> as <Γ> = <D>q^2. Using the Stokes-Einstein equation (*26*), <D> is further related to the average hydrodynamic radius (<R_h>) by <R_h> = $k_BT/(6\pi\eta$<D>), where η is the solvent viscosity. In this way, each G(Γ) can also be converted into a hydrodynamic radius distribution f(R_h).

In static LLS (*27*), we can obtain the weight-average molar mass (M_w) and the z-average root-mean square radius of gyration (<R_g>$_z$) of scattering objects in a dilute solution/dispersion from the angular and concentration dependence of the excess absolute scattering intensity (Rayleigh ratio $R_{vv}(q)$) as

$$\frac{KC}{R_{vv}(q)} \approx \frac{1}{M_w}\left(1+\frac{1}{3}q^2 < R_g >^2\right) \qquad (5\text{-}2)$$

where $K \equiv 4\pi^2n^2(dn/dC)^2/(N_A \lambda_0^4)$ and $q = (4\pi n\lambda_0)\sin(\theta/2)$ with N_A, dn/dC, n, and λ_0 being the Avogadro number, the specific refractive index increment, the solvent refractive index, and the wavelength of the light in a vacuum, respectively. A_2 is the second virial coefficient. $(dn/dC)_{632.8\ nm}$ of the PEI copolymer and DNA in water was determined by using the Jianke differential refractometer (*28*). $(dn/dC)_{632.8\ nm}$ of the polyplexes were calculated by using

$$(dn/dC)_{polyplex} = w_{DNA}(dn/dC)_{DNA} + w_{polymer}(dn/dC)_{polymer} \qquad (5\text{-}3)$$

where w_{DNA} and $w_{polymer}$ are weight fractions of DNA and PEI, respectively. The measurement angular range used was 20°-50° for the polyplexes. All of the measurements were carried out at 25.0 ± 0.1 °C.

***In vitro* gene transfection.** The *in vitro* gene transfection efficiency was quantified by using the luciferase transfection assays, in which plasmid *p*GL3 was used as an exogenous reporter gene. 293T cells were plated in the 48-well plate at an initial density of 50,000 cells per well, 24 h prior to the gene transfection. The PEI/DNA mixture with a desired N:P ratio was further diluted in serum-free medium and then administered to each well at a final concentration of 0.4 μg DNA/well. Complete DMEM medium (1 mL per well) was added 4 h after the gene transfection. Using a GloMax 96 microplate luminometer (Promega, USA) and the Bio-Rad protein assay reagent, the transgene expression level and corresponding protein concentration were determined in each well, 48 h after the polyplex administration. The gene

transfection efficiency is expressed as a relative luminescence unit (RLU) per cellular protein (mean ± SD of triplicates).

5.3 Results and Discussion

Figure 5.1 shows the N:P ratio dependence of hydrodynamic radius distribution

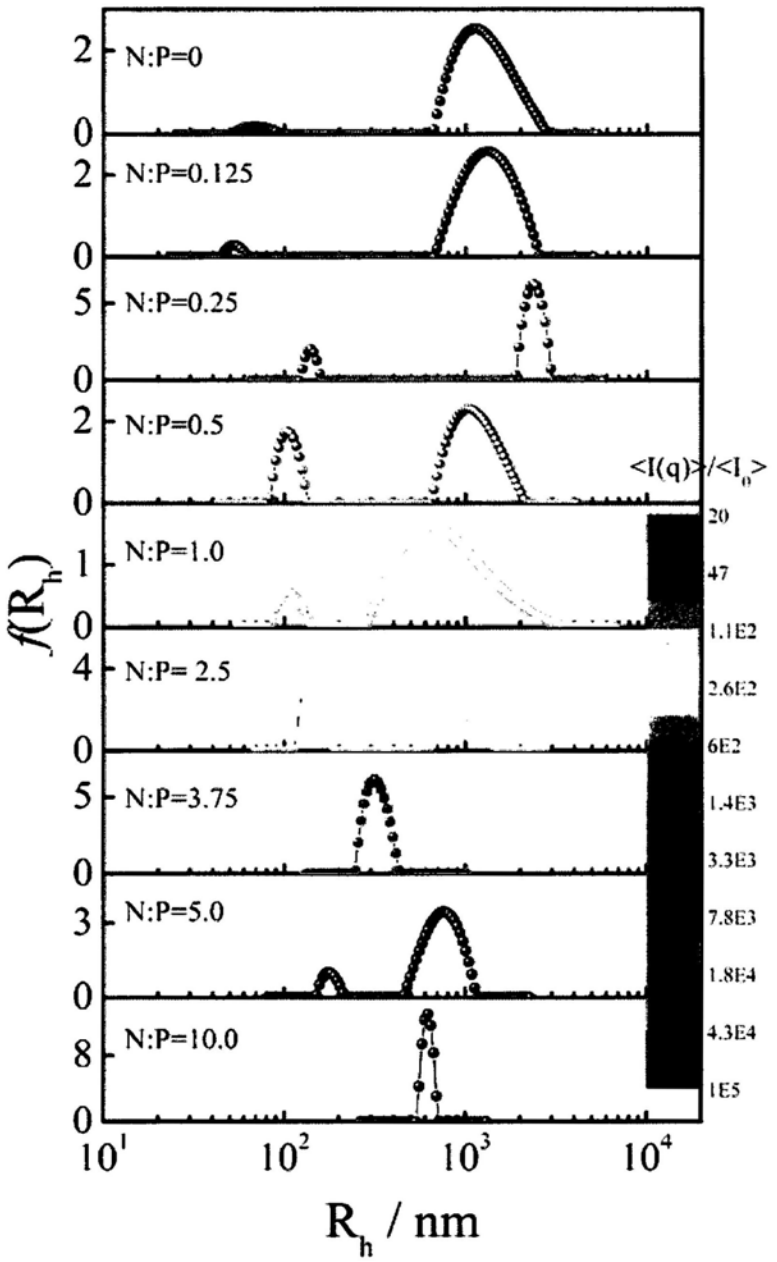

Figure 5.1 N:P ratio dependence of hydrodynamic radius distribution ($f(R_h)$) of PEI-7K-L/DNA polyplexes formed in PBS, where different colors represent variation of the normalized time-averaged scattering intensity of the solution mixture ($<I(q)>/<I>_0$).

($f(R_h)$) of *p*GL3 in PBS without and with the addition of different amounts of PEI-7K-L. In the pure *p*GL3 solution (N:P = 0.00), the peak located at ~1 μm represents the swollen and extended DNA chains. The addition of a small amount of PEI-7K-L (N:P = 0.25) leads to a new peak located at ~120 nm, presumably corresponding to the newly formed PEI/DNA polyplexes. Further addition of PEI results in more polyplexes with a larger size. When N:P reaches ~3.75, the DNA peak completely disappears, suggesting that most of the DNA chains are complexed with PEI-7K-L, i.e., almost no free DNA chains remain in the solution. The extent of

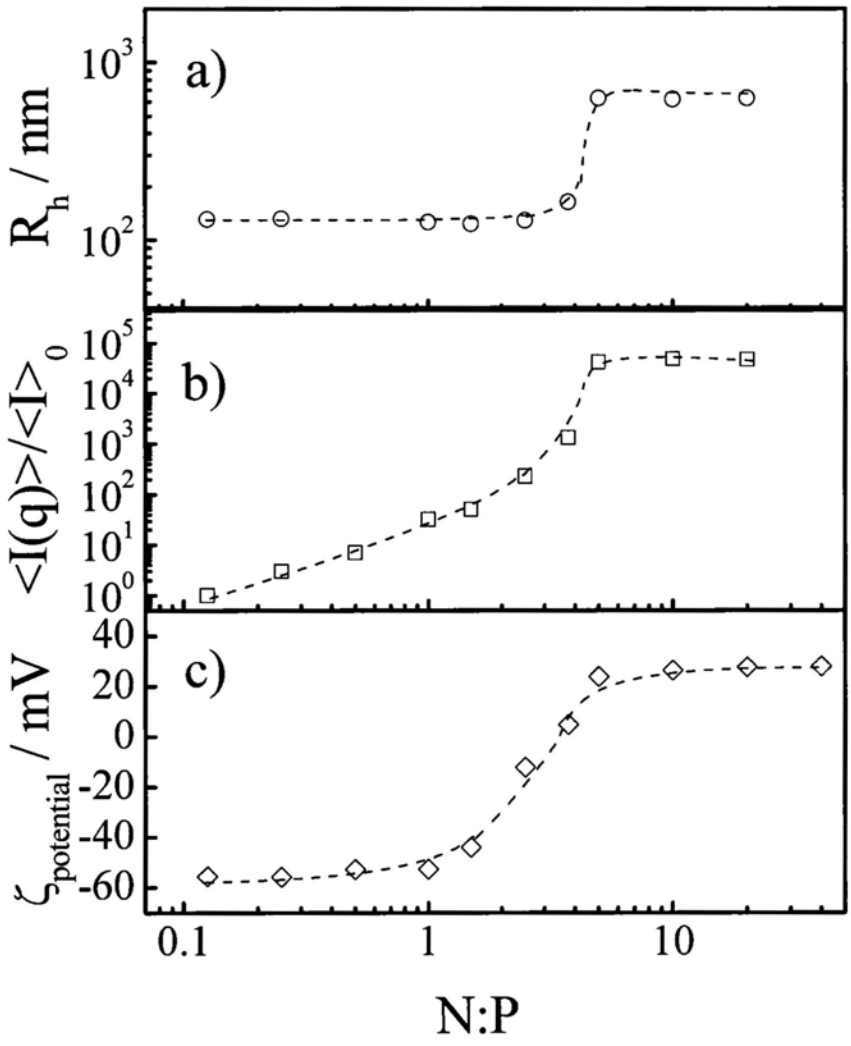

Figure 5.2 N:P ratio dependence of a) average hydrodynamic radius ($<R_h>$), b) normalized time-averaged scattering intensity ($<I(q)>/<I>_0$) and c) average zeta-potential ($\zeta_{potential}$) of PEI-7K-L/DNA polyplexes.

complexation was also evaluated by the gel-shift assay, as shown in Figure 3.10. The retarded mobility of the DNA bands and their reduced fluorescence intensity reveal a progressive condensation. Clearly, the two DNA bands (supercoiled and relaxed forms) disappear when N:P reaches ~ 3.5.

Figure 5.2 summaries the N:P ratio dependence of the average hydrodynamic radius ($<R_h>$), the normalized time-averaged scattering intensity at $\theta = 20^o$ ($<I(q)>/<I>_0$) and the zeta-potential ($\zeta_{potential}$) of the PEI-7K-L/DNA polyplexes formed in PBS. Wihtin the N:P range of 0.125-2.0, $<R_h>$ of the polyplexes remains constant while the scattering intensity and $\zeta_{potential}$ i ncrease gradually indicating that more and more negatively charged DNA chains are gradually complexed with the positively charged PEI chains. The $\zeta_{potential}$ of the polyplexes is inverted at N:P ~3. Meanwhile, both $<R_h>$ and scattering intensity sharply increased at N:P 2-5. These all reflect that a quick aggregation of initially formed small polyplexes might appear due to the weak $\zeta_{potential}$ of the colloid particles. Further addition of PEI in the range of N:P > 5 has nearly no effect on $<R_h>$, scattering intensity and $\zeta_{potential}$, clearly revealing that those further added PEI chains are free in the solution.

Similarly, Figure 5.3 shows the N:P ratio dependence of the average hydrodynamic radius ($<R_h>$), the weight-average molecular weight (M_w) and average chain density ($<\rho> \equiv M_w/N_A(4/3)\pi<R_h>^3$) of PEG-SS-PEI/DNA and PEG-CC-PEI/DNA polyplexes in PBS. Because of the PEG shielding, the polyplexes are stable in the physiological buffer (see Chapter 4), and we can obtain the absolute molecular weight due to the relatively smaller size by LLS ($qR_g < 1$). It is clear that when N:P $\geq$ 3, the PEG-SS-PEI/DNA and PEG-CC-PEI/DNA polyplexes formed in PBS have constant M_w, $<R_h>$ and $<\rho>$, as well as $\zeta_{potential}$ (see Figure 4.5), confirming that most of the DNA chains are complexed with the copolymer chains when N:P reaches 3. The additional PEI-based copolymers do not affect the physical characteristics of the polyplexes, which means that those additional PEG-g-PEI chains are also free in the solution mixture.

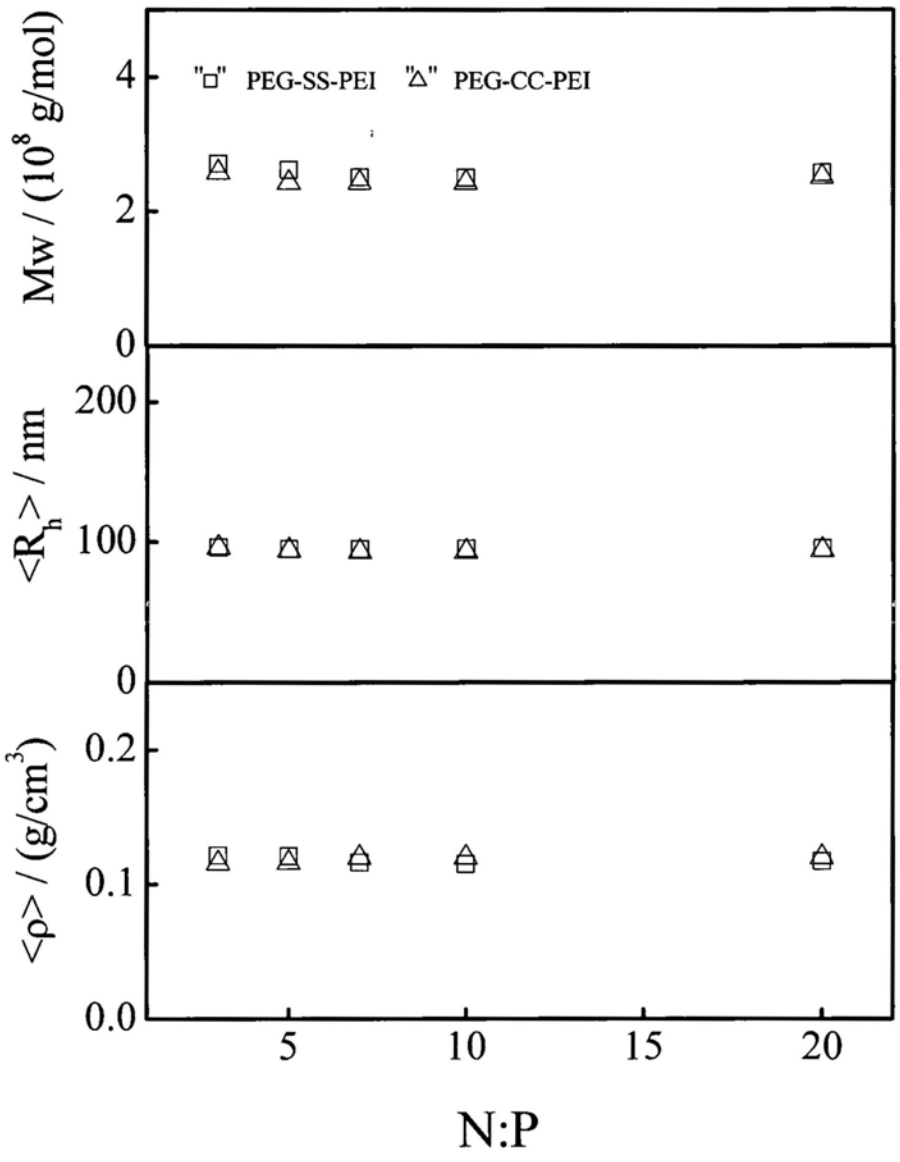

Figure 5.3 N:P ratio dependence of apparent weight-average molar mass (M_w), average hydrodynamic radius (< R_h>) and average chain density (<ρ> ≡ $M_w/N_A(4/3)\pi<R_h>^3$) of PEG-SS-PEI/DNA and PEG-CC-PEI/DNA polyplexes in PBS.

Only few previous studies noted the existence of free PEI, and measurements were made to determine the amount of free PEI in the PEI/DNA dispersion for a gene transfection. Clamme J. P. et al. found that, by using a two photon fluorescence correlation spectroscopy, there is ~86% free PEI when the polyplexes is prepared at N:P 10 (i.e., polyplexes is formed at N:P 1.4) (*23*), while Wagner and his coworkers

showed that the remaining PEI25K/DNA polyplexes has a N:P ratio ~2.5 after the polyplexes dispersion was passed through a size exclusion chromatography. However, from our LLS and zeta-potential results shown in Chapter 3 and this Chapter, we can see that negatively-charged DNA is not totally complexed by PEI25K at N:P 1.4 or 2.5, and zeta-potentials of the polyplexes were even not reversed to be positive.

Therefore, we try to use a simple filtration method to quantify the percentage of the free PEI here. Briefly, the polyplexes are prepared as described at N:P 10, which is considered as the optimum N:P ratio with the highest gene transfection efficiency in most of the cell lines (*29-31*). After 4-hrs incubation at RT in PBS, the polyplexes dispersion was centrifugated and the supernatant was carefully filtered with a 20-nm filter. The concentration of the free PEI in the filtrate was determined by a standard working curve (Figure 5.4). It is shown that the working curve is independent of the molar mass of the PEI used. Thus, we obtain that the percentages of free PEI are 70%, 65%, 71% and 70% for PEI25K/DNA, PEI-7K-L/DNA, PEG-SS-PEI/DNA and PEG-CC-PEI/DNA polyplexes at N:P 10, respectively. In other words, the polyplexes are formed at N:P 3.0, 3.5, 2.9 and 3.0, respectively.

After obtaining these N:P ratios, we compared their gene transfection efficiency

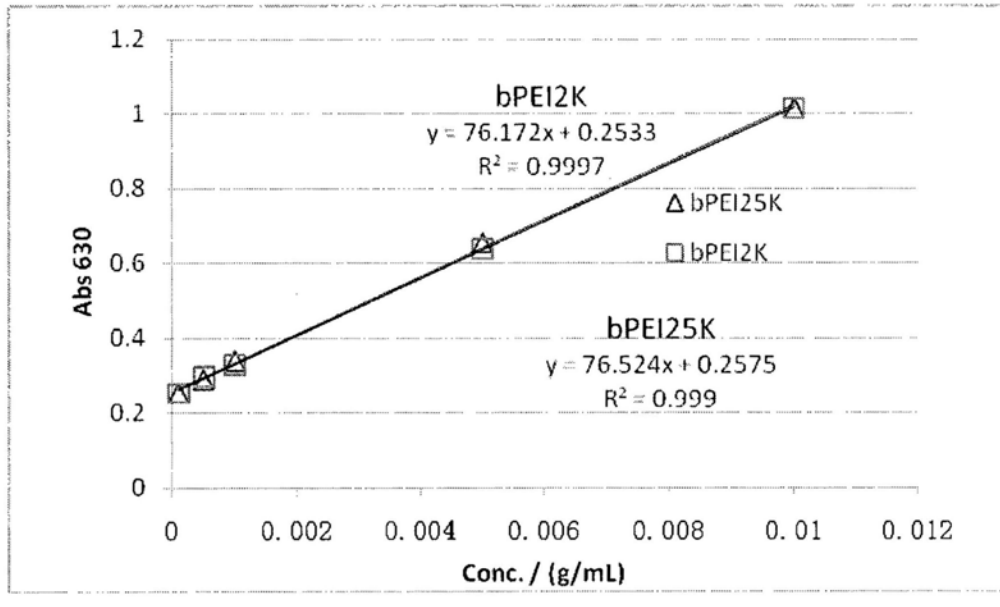

Figure 5.4 Standard working curves of PEI25K and PEI2K in PBS.

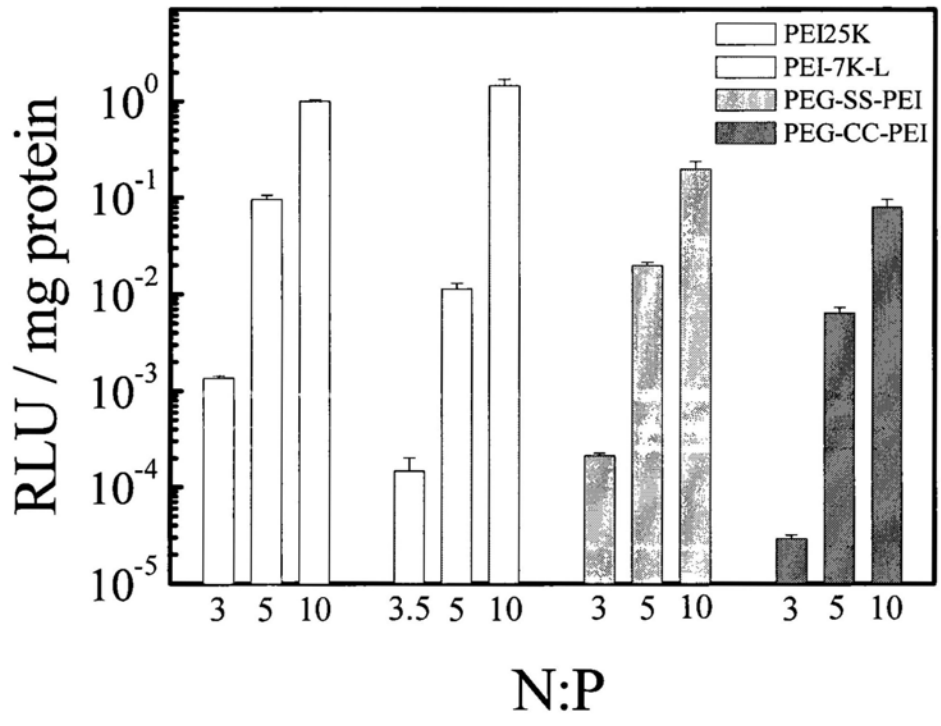

Figure 5.5 N:P ratio dependence of *in vitro* gene transfection efficiency of PEI25K, PEI-7K-L, PEG-SS-PEI and PEG-CC-PEI in the serum-free medium on 293T cells. The efficiencies are normalized by that of PEI25K at N:P 10.

with those at N:P 5 and N:P 10, as shown in Figure 5.5. It is obvious that the free PEIs greatly enhance the gene transfection efficiency by a factor of ~10^3. Next, one may ask an obvious but certainly overlooked question: what is the role of the free PEI in promoting the gene transfection efficiency? The possible reason could be the free PEI increases the cellular uptake, but our recent results show that the free PEI only marginally elevates the cellular uptake of the polyplexes (*25*). Therefore, the promoting mechanism must be downstream in the intracellular trafficking. One might argue that the decreased amount of PEI at low N:P ratio may lead to impaired ability of PEI to serve as a "proton sponge" reagent. It is true that the proton sponge hypothesis is a logical model for explaining why PEI is a successful vector for gene delivery, but some studies also showed contradictory data to such a hypothesis (*19, 22, 32*), or at least showed that buffer capacity may not be important or necessary (*33-35*). As shown in Figure 5.6, when additional 7 and 17 portions of PEI25K in a

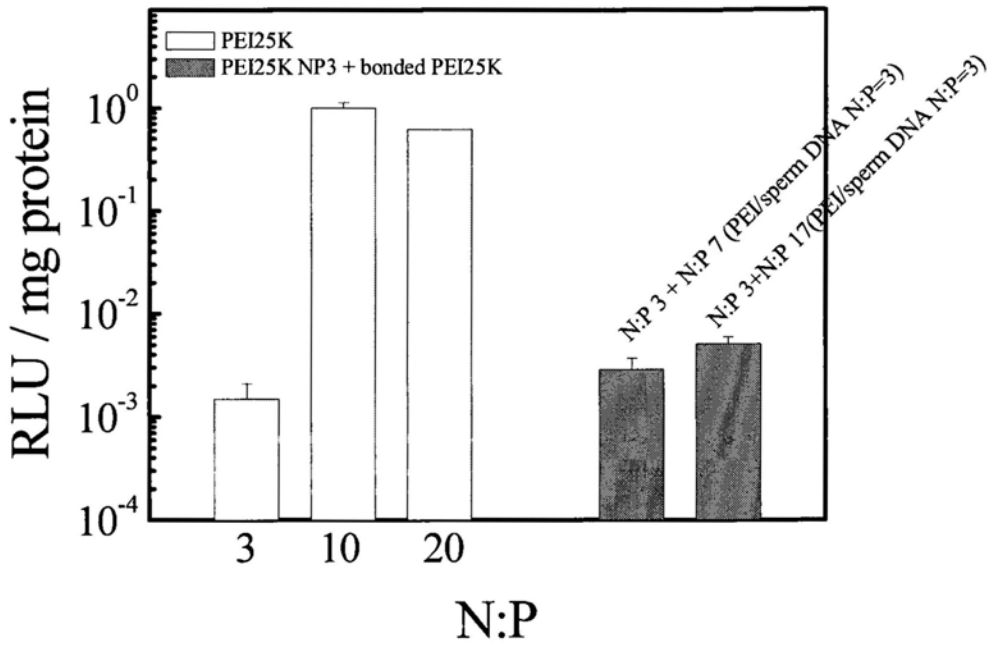

Figure 5.6 Gene transfection efficiency (normalized by PEI25K at N:P 10) of PEI25K at N:P 3, 10 and 20 (light gray bars) and PEI25K at N:P 3 supplemented by additional 7 and 17 portion of PEI25K but in complexed form with salmon sperm DNA (2000 bp, Invitrogen, USA) at N:P = 3 (dark gray bars).

complexed form with other inactive DNA are supplemented to the PEI25K/pGL3 polyplexes formed at N:P 3, the gene transfection of PEI25K at N:P 3 cannot be recovered to that of at N:P 10. Although this result may not exclude the possibility of free PEI as the "proton sponge", it at least indicates that the excess PEI must exist in the free form in promoting the gene transfection efficiency. The exact role(s) of free PEI for its promotion in gene transfection efficiency still need more experimental results and further detailed investigations. However, it already leads us a new way of thinking in the development of non-viral vectors.

5.4 Conclusions

A combination of laser light scattering (LLS) and a simple filtration results confirms that most of anionic DNA chains are complexed and condensed by cationic PEI-based polymer chains when the molar ratio of nitrogen from PEI to phosphorus from DNA (N:P) reaches ~ 3. In the solution with N:P > 3, there are two population

of PEI chains: bound to DNA and free in the solution. It's well known that the bound PEI chains inside the polyplexes provide a charge compensation so that DNA is condensed and protected. Nevertheless, our current study reveals that those free PEI chains also play a vital role in promoting gene transfection. The promotion mainly occurs inside the cell while we do not fully understand the detailed mechanism at this moment. Our finding leads to a different way in the development of non-viral vectors; namely, we might not need to invest much of our effort on the synthesis of different cationic polymers, but focus on a better understanding of the intracellular polyplexes trafficking. As for *in vivo* experiments, we should consider how to incorporate free chains together with polyplexes so that they can be simultaneously delivered to the targeted organs or cells.

References and Notes

(1) Lungwitz, U., Breunig, M., Blunk, T., *et al. Eur. J. Pharm. Biopharm.* **2005**, *60*, 247.

(2) Pack, D. W., Hoffman, A. S., Pun, S., *et al. Nature Reviews Drug Discovery* **2005**, *4*, 581.

(3) Neu, M., Fischer, D., and Kissel, T. *J. Gene Med.* **2005**, *7*, 992.

(4) Wong, S. Y., Pelet, J. M., and Putnam, D. *Prog. Polym. Sci.* **2007**, *32*, 799.

(5) Boussif, O., Lezoualch, F., Zanta, M. A., *et al. Proc. Natl. Acad. Sci. U. S. A.* **1995**, *92*, 7297.

(6) Kloeckner, J., Wagner, E., and Ogris, M. *Eur. J. Pharm. Sci.* **2006**, *29*, 414.

(7) Akinc, A., Thomas, M., Klibanov, A. M., *et al. J. Gene Med.* **2005**, *7*, 657.

(8) Roberts, M. J., Bentley, M. D., and Harris, J. M. *Adv. Drug Del. Rev.* **2002**, *54*, 459.

(9) Fella, C., Walker, G. F., Ogris, M., *et al. Eur. J. Pharm. Sci.* **2008**, *34*, 309.

(10) Tang, G. P., Zeng, J. M., Gao, S. J., *et al. Biomaterials* **2003**, *24*, 2351.

(11) Thomas, M., Ge, Q., Lu, J. J., *et al. Pharm. Res.* **2005**, *22*, 373.

(12) Lungwitz, U., and Goepferich, A. *J. Controlled Release* **2008**, *130*, 57.

(13) Breunig, M., Lungwitz, U., Liebl, R., *et al. Proc. Natl. Acad. Sci. U. S. A.* **2007**, *104*, 14454.

(14) Schatzlein, A. G. *J. Biomed. Biotechnol.* **2003**, *2003*, 149.

(15) Blessing, T., Kursa, M., Holzhauser, R., *et al. Bioconjugate Chem.* **2001**, *12*, 529.

(16) Walker, G. F., Fella, C., Pelisek, J., *et al. Mol. Ther.* **2005**, *11*, 418.

(17) Ikonen, M., Murtomaki, L., and Kontturi, K. *Colloids and Surfaces B-Biointerfaces* **2008**, *66*, 77.

(18) Nguyen, T. T., and Shklovskii, B. I. *J. Chem. Phys.* **2001**, *115*, 7298.

(19) Godbey, W. T., Wu, K. K., and Mikos, A. G. *J. Biomed. Mater. Res.* **1999**, *45*, 268.

(20) Ogris, M., Brunner, S., Schuller, S., *et al. Gene Ther.* **1999**, *6*, 595.

(21) Erbacher, P., Bettinger, T., Brion, E., *et al. J. Drug Targeting* **2004**, *12*, 223.

(22) Godbey, W. T., Barry, M. A., Saggau, P., *et al. J. Biomed. Mater. Res.* **2000**, *51*, 321.

(23) Clamme, J. P., Azoulay, J., and Mely, Y. *Biophys. J.* **2003**, *84*, 1960.

(24) Boeckle, S., von Gersdorff, K., van der Piepen, S., *et al. J. Gene Med.* **2004**, *6*, 1102.

(25) Yue, Y., Jin, F., Deng, R., *et al. J. Controlled Release* **2010**, *invited paper, submitted.*

(26) Berne, B., and Pecora, R. *Dynamic Light Scattering*; Plenum Press: New York, **1976**.

(27) Chu, B. *Laser Lgiht Scattering*, 2nd ed.; Academic Press: New York, **1991**.

(28) Wu, C., and Xia, K. Q. *Rev. Sci. Instrum.* **1994**, *65*, 587.

(29) Gosselin, M. A., Guo, W. J., and Lee, R. J. *Bioconjugate Chem.* **2001**, *12*, 989.

(30) Peng, Q., Zhong, Z. L., and Zhuo, R. X. *Bioconjugate Chem.* **2008**, *19*, 499.

(31) Manickam, D. S., and Oupicky, D. *Bioconjugate Chem.* **2006**, *17*, 1395.

(32) Gabrielson, N. P., and Pack, D. W. *J. Controlled Release* **2009**, *136*, 54.

(33) Brissault, B., Kichler, A., Guis, C., *et al. Bioconjugate Chem.* **2003**, *14*, 581.

(34) Yun-Xia Suna, Wang Xiaoa, Si-Xue Chenga, *et al. J. Controlled Release* **2008**, *128*, 171.

(35) Ou, M., Wang, X. L., Xu, R. Z., *et al. Bioconjugate Chem.* **2008**, *19*, 626.

Publications:

1 **Deng R.**, Yue Y., Jin F., Chen Y., Kung H.F., Lin C.M., Wu C., "Revisit the complexation of PEI and DNA — How to make low cytotoxic and highly efficient PEI gene transfection non-viral vectors with a controllable chain length and structure?", *Journal of Controlled Release*, 2009, *140*, 40.

2 **Deng R.**, Diao S., Yue Y., Ngai T., Wu C., Jin F., "Dynamic and structural scalings of the complexation between pDNA and bPEI in semidilute and low-salt solutions", *Biopolymers*, 2010, *93*, 571.

3 **Deng R.**, He N., Yue Y., Dai Z., Chen Y., Kung H.F., Lin C.M., Wu C., "Comparative study of non-degradable and reductive-degradable PEG-g-PEI copolymers in gene transfection", *Bioconjugate Chemistry*, submitted.

4 **Deng R.**, Jin F., Yue Y., Chen Y., Kung H.F., Lin C.M., Wu C., "Revisit the complexation of PEI and DNA — How the preparation of DNA/PEI polyplexes affect in-vitro gene transfection?", to be submitted.

5 Ranganathan K., **Deng R.**, Kainthan R.K., Wu C., Brooks D.E., Kizhakkedathu J.N., "Synthesis of thermoresponsive mixed arm star polymers by combination of RAFT and ATRP from a multifunctional core and its self assembly in water", *Macromolecules*, 2008, 41, 4226.

6 Yue Y., Jin F., **Deng R.**, Chen Y., Lin C.M., Kung H.F., Wu C., "Revisit the complexation of PEI and DNA — Effect of uncomplexed chains free in the solution mixture on gene transfection", *Journal of Controlled Release*, submitted.

7 Liu J., Zhang L., Lam W.Y., Jim K.W., Yue Y., **Deng R.**, Hong Y., Qin A., Sung H.Y., Williams D., Jia G., Tang B.Z., "Exploration of effective catalysts for diyne polycyclotrimerization, synthesis of an ester-functionalized hyperbranched polyphenylene, and demonstration of its utility as a molecular container with implication for controlled drug delivery", *Macromolecules*, 2009, 42, 7367.